

IMPLEMENTATION AND PERFORMANCE EVALUATION OF A
THREE ANTENNA DIRECTION FINDING SYSTEM

A THESIS SUBMITTED TO
THE GRADUATE SCHOOL OF NATURAL AND APPLIED SCIENCES
OF
MIDDLE EAST TECHNICAL UNIVERSITY

BY

ÖMER ÇAĞRI ARSLAN

IN PARTIAL FULFILLMENT OF THE REQUIREMENTS
FOR
THE DEGREE OF MASTER OF SCIENCE
IN
ELECTRICAL AND ELECTRONICS ENGINEERING

OCTOBER 2009

Approval of the thesis:

**IMPLEMENTATION AND PERFORMANCE EVALUATION OF A
THREE ANTENNA DIRECTION FINDING SYSTEM**

submitted by **ÖMER ÇAĞRI ARSLAN** in partial fulfillment of the requirements for the degree of **Master of Science in Electrical and Electronics Engineering Department, Middle East Technical University** by,

Prof. Dr. Canan Özgen
Dean, Graduate School of **Natural and Applied Sciences** _____

Prof. Dr. İsmet Erkmen
Head of Department, **Electrical and Electronics Engineering** _____

Prof. Dr. Temel Engin Tuncer
Supervisor, **Electrical and Electronics Engineering Dept., METU** _____

Examining Committee Members

Prof. Dr. Buyurman Baykal
Electrical and Electronics Engineering Dept., METU _____

Prof. Dr. Temel Engin Tuncer
Electrical and Electronics Engineering Dept., METU _____

Assoc. Prof. Dr. Özlem Aydın Çivi
Electrical and Electronics Engineering Dept., METU _____

Dr. Arzu Tuncay Koç
Electrical and Electronics Engineering Dept., METU _____

Dr. Bekir Ahmet Doğrusöz
ASELSAN _____

Date: 21.10.2009

I hereby declare that all information in this document has been obtained and presented in accordance with academic rules and ethical conduct. I also declare that, as required by these rules and conduct, I have fully cited and referenced all material and results that are not original to this work.

Name, Last name : Ömer Çağrı Arslan

Signature :

ABSTRACT

IMPLEMENTATION AND PERFORMANCE EVALUATION OF A THREE ANTENNA DIRECTION FINDING SYSTEM

Arslan, Ömer Çağrı

M. Sc., Department of Electrical and Electronics Engineering

Supervisor: Prof. Dr. Temel Engin Tuncer

October 2009, 104 pages

State of the art direction finding (DF) systems usually have several antennas in order to increase accuracy and robustness to certain factors. In this thesis, a three antenna DF system is built and evaluated. While more antennas give better DF performance, a three antenna system is useful for system simplicity and many of the problems in DF systems can be observed and evaluated easily. This system can be used for both azimuth and elevation direction of arrival (DOA) estimation. The system is composed of three monopole antennas, an RF front end, A/D converters and digital signal processing (DSP) units. A number of algorithms are considered, such as, three channel interferometer, correlative interferometer, LSE (least square error) based correlative interferometer and MUSIC (multiple signal classification) algorithms. Different problems in DF systems are investigated. These are gain/phase mismatch of the receiver channels, mutual coupling between antennas, multipath signals and multiple sources. The advantages and disadvantages of different algorithms are outlined.

Keywords: Three Channel Interferometer Algorithm, Correlative Interferometer Algorithm, LSE Based Correlative Interferometer Algorithm, MUSIC Algorithm, Phase Difference, Gain/Phase Mismatch, Mutual Coupling

ÖZ

ÜÇ ANTENLİ YÖN KESTİRME SİSTEM UYGULAMASI VE PERFORMANS ANALİZİ

Yüksek Lisans, Elektrik ve Elektronik Mühendisliği Bölümü

Tez yöneticisi: Prof. Dr. Temel Engin Tuncer

Ekim 2009, 104 sayfa

Yön kestirme sistemleri, doğruluk oranını belirli miktarda arttırmak için genellikle birden fazla antene sahiptir. Bu tezde, Üç Antenli Yön Kestirici yapılmış ve performans değerlendirmesi anlatılmıştır. Çok antenli yön kestirme sistemleri daha iyi performans göstermesine karşın, üç antenli yön kestirme sistemi, daha sade olması yönüyle kullanışlıdır ve bu sistem kullanılarak yön kestirme sistemlerinde görülen sorunlar kolayca gözlenip değerlendirilebilir. Bu sistem, geliş yönünün yanca ve yükseklik açılarının hesaplanması için kullanılabilir. Sistem üç monopol anten, RF bölümü, analog/sayısal çeviriciler ve sayısal sinyal işleme birimlerinden oluşmaktadır. Üç kanallı enterferometre, bağıntılı enterferometre, LSE tabanlı bağıntılı enterferometre ve MUSIC algoritmaları incelenmiştir. Yön kestirme sistemlerinde görülen çeşitli sorunlar araştırılmıştır. Bu sorunlar, alma kanallarının kazanç/faz uyumsuzluğu, antenler arasındaki karşılıklı bağlaşım etkisi, birden fazla sinyal yolu ve birden fazla sinyal kaynağıdır. Değişik algoritmaların avantaj ve dezavantajları belirlenmiştir.

Anahtar Kelimeler: Üç Kanallı Enterferometre Algoritması, Bağıntılı Enterferometre Algoritması, LSE Tabanlı Bağıntılı Enterferometre Algoritması, MUSIC Algoritması, Faz Farkı, Kazanç-Faz Uyumsuzluğu, Karşılıklı Bağlaşım Etkisi

To My Family

ACKNOWLEDGMENTS

I would like to thank to my supervisor Prof. Dr. Temel Engin Tuncer for his guidance and encouragement.

I also would like to thank to Tübitak for their financial support to this study.

TABLE OF CONTENTS

ABSTRACT	iv
ÖZ	vi
ACKNOWLEDGMENTS	viii
TABLE OF CONTENTS	ix
LIST OF TABLES	xi
LIST OF FIGURES	xii
LIST OF ABBREVIATIONS	xv
CHAPTERS	
1. INTRODUCTION.....	1
1.1 Scope of the Thesis	3
1.2 Outline of the Thesis	4
2. ALGORITHMS FOR DIRECTION FINDING.....	5
2.1 An Overview of DF Algorithms	5
2.2 Three Channel Interferometer Algorithm	6
2.2 Correlative Interferometer Algorithm	10
2.3 LSE Based Correlative Interferometer Algorithm	12
2.4 The MUSIC Algorithm	13
3. THREE ANTENNA DIRECTION FINDING SYSTEM.....	18
3.1 Hardware	18
3.1.1 Antenna	20
3.1.2 RF Front-End	25
3.1.3 Digital Baseband Processing.....	28
3.2 Software	39
3.2.1 DSP Software	39
3.2.2 FPGA Software	50
4. ANTENNA SYSTEM MEASUREMENTS	54
4.1 Mutual Coupling Between Antennas	54

4.2	Gain-Phase Mismatch of the Receivers	60
4.3	Cramer Rao Bound Calculation	61
5.	PERFORMANCE EVALUATION OF THE DIRECTION FINDING SYSTEM	63
5.1	Test Results of the Single Signal Transmitter Case	63
5.2	Test Results of Two Signal Transmitter Case.....	73
5.3	Test Results of Multipath Case	76
6.	CONCLUSION	85
6.1	Future Work	87
	REFERENCES.....	88
	APPENDICES	
A.	CIRCUIT DIAGRAMS OF THE PROCESSING BOARD	91
B.	LAYOUT AND ROUTING OF THE PROCESSING BOARD.....	99
C.	GRAPHICAL USER INTERFACE.....	102

LIST OF TABLES

TABLES

Table 4.1 – S-parameters of the antennas	58
Table 4.2 - The gain-phase mismatch of the system antennas.....	61
Table 5.1 – Angle RMSE versus number of samples test parameters	67
Table 5.2 – Angle RMSE versus DOA test parameters.....	69
Table 5.3 – Angle RMSE versus sample space angle step test parameters	71
Table 5.4 – Angle RMSE versus DOA test parameters for two transmitter case	75
Table 5.5 – Angle RMSE versus DOA test parameters for multi signal path case.....	78

LIST OF FIGURES

FIGURES

Figure 2.1 – Three Channel Interferometer Antenna Placement	7
Figure 3.1 – RF Front-End and the Processing Board	19
Figure 3.2 – Three Channel Direction Finding System Block Diagram.....	19
Figure 3.3 – Antenna of the Direction Finding System	20
Figure 3.4 – The VSWR Plot of the Antenna	21
Figure 3.5 – The Elevation Pattern for Phi is 90° and 270°	22
Figure 3.6 – The Elevation Pattern for Phi is 0° and 180°	23
Figure 3.7 – The Azimuth Pattern for Theta is 90°	24
Figure 3.8 – Antenna with the Ground Plane.....	25
Figure 3.9 – RF Front-End.....	26
Figure 3.10 – RF Amplifying-Filtering-Mixing Part.....	27
Figure 3.11 – AGC System of the RF Front-End	27
Figure 3.12 – RF Receiver	28
Figure 3.13 – The Processing Board Block Diagram	29
Figure 3.14 – Voltage Production.....	30
Figure 3.15 – Reset Controller.....	31
Figure 3.16 – Clock Circuit Block Diagram	32
Figure 3.17 – ADC and FPGA Data Interface	34
Figure 3.18 – FPGA and DSP Interface.....	35
Figure 3.19 –DSP - Flash ROM Interface.....	36
Figure 3.20 – DSP and UART Transceiver Interface	37
Figure 3.21 – UART Transceiver and Computer Interface.....	38
Figure 3.22 – The Processing Board.....	38
Figure 3.23 – Reading Algorithm Type Data Block Diagram	40
Figure 3.24 – Reading Data From FPGA Block Diagram	41
Figure 3.25 – Phase Calculation Block Diagram	42

Figure 3.26 – The Magnitude Response of the Digital Bandpass Filter	43
Figure 3.27 – The Impulse Response of the Digital Bandpass Filter.....	44
Figure 3.28 – In-phase and Quadrature Component Production.....	45
Figure 3.29 – The Magnitude Response of the Digital Lowpass Filter	46
Figure 3.30 – The Impulse Response of the Digital Lowpass Filter.....	47
Figure 3.31– DSP Software Block Diagram.....	50
Figure 3.32 – Dual Port RAM.....	51
Figure 3.33 – Write Process Block Diagram	52
Figure 3.34 – Read Process Block Diagram	53
Figure 4.1 – Illustration of the Mutual Coupling Effect	55
Figure 4.2 –Three Antenna Configuration	56
Figure 4.3 – Gain-Phase Mismatch Measurement Configuration.....	60
Figure 5.1 – Test Setup of the Three Antenna DF System	64
Figure 5.2 – Three Antenna DF System with Angle Measurement Apparatus	65
Figure 5.3 – Three Antenna Direction Finding System and Signal Transmitter	66
Figure 5.4 – RMSE of Azimuth Angle versus Number of Sample Graph.....	67
Figure 5.5 – RMSE of Elevation Angle versus Number of Sample Graph	68
Figure 5.6 – RMSE of Azimuth Angle versus DOA Graph	69
Figure 5.7 – RMSE of Elevation Angle versus DOA Graph	71
Figure 5.8 – RMSE of Azimuth Angle versus Sample Space Angle Step Graph.....	72
Figure 5.9 – RMSE of Elevation Angle versus Sample Space Angle Step Graph	73
Figure 5.10 – Illustration of Two Transmitters Test Setup.....	74
Figure 5.11 – RMSE of Azimuth Angle versus DOA Graph	75
Figure 5.12 – RMSE of Elevation Angle versus DOA Graph	76
Figure 5.13 – Metal Plate Placement Near the Antennas.....	77
Figure 5.14 – The Illustration of the Multipath Signal Test Setup	78
Figure 5.15 – RMSE of Azimuth Angle versus DOA Step-1 Graph.....	79
Figure 5.16 – RMSE of Elevation Angle versus DOA Step-1 Graph.....	80
Figure 5.17 – RMSE of Azimuth Angle versus DOA Step-2 Graph.....	81
Figure 5.18 – RMSE of Azimuth Angle versus DOA Step-2 Graph.....	81
Figure 5.19 – RMSE of Azimuth Angle versus DOA Step-3 Graph.....	82

Figure 5.20 – RMSE of Elevation Angle versus DOA Step-3 Graph.....	82
Figure 5.21 – RMSE of Azimuth Angle versus DOA Step-4 Graph.....	83
Figure 5.22 – RMSE of Elevation Angle versus DOA Step-4 Graph.....	84
Figure A.1 – First Voltage Production Circuit.....	91
Figure A.2 – Second Voltage Production Circuit	92
Figure A.3 – Reset Circuit	92
Figure A.4 – Clock Production Circuit	93
Figure A.5 – ADC and FPGA Data Interface Circuit	94
Figure A.6 – FPGA and DSP Interface Circuit.....	95
Figure A.7 – DSP and the Flashrom Interface Circuit.....	96
Figure A.8 – FPGA and the PROM Interface Circuit.....	97
Figure A.9 – DSP and UART Transceiver Interface Circuit	98
Figure B.1 – Front Side of the Processing Board	99
Figure B.2 – Back Side of the Processing Board	100
Figure B.3 – Clock Buffer and ADC’s.....	101
Figure C.1 – GUI of the DF System	103
Figure C.2 – View of the GUI During the Program Run-Time	104

LIST OF ABBREVIATIONS

DF	: Direction Finding	FIR	: Finite Impulse Response
DSP	: Digital Signal Processor	UART	: Universal Asynchronous Receive Transmit
MUSIC	: Multiple Signal Classification	CSL	: Chip Support Library
RF	: Radio Frequency	ROM	: Read Only Memory
LOB	: Line of Bearing	RAM	: Read Access Memory
TDOA	: Time Difference of Arrival	AGC	: Automatic Gain Controller
DOA	: Direction of Arrival	PCB	: Printed Circuit Board
LSE	: Least Square Error	VSWR	: Voltage Standing Wave Ratio
IF	: Intermediate Frequency	GPIO	: General Purpose Input Output
ADC	: Analog to Digital Converter	LSB	: Least Significant Bit
SNR	: Signal to Noise Ratio	FPGA	: Field Programmable Gate Array
RMS	: Root Mean Square	PROM	: Programmable Read Only Memory
SINAD	: Signal to Noise Plus Distortion	PLL	: Phase Locked Loop
THD	: Total Harmonic Distortion		
RMSE	: Root Mean Squared Error		
ENOB	: Effective Number of Bits		

CHAPTER 1

INTRODUCTION

Direction finding (DF) has been an important issue since the directional property of radio waves was discovered. During the twentieth century, the area of the direction finding has grown and evolved. Today, direction finding plays a major role in the broader areas of radiolocation and radio navigation. Numerous techniques have been formulated, and many operational systems have been developed to satisfy a wide variety of technical and operational requirements. The practical applications of direction finding systems are numerous such as; radio navigation, search and rescue services, signal direction finding and location systems, homing systems, warning systems, radio astronomy and smart antennas.

There are several direction finding systems that have been developed last century. Pseudo-Doppler, Watson-Watt, Brueninger and Interferometer direction finding systems are the examples of various direction finding systems. Moreover, new generation DF systems which use superresolution methods become popular recent years. MUSIC algorithm can be classified as one of the superresolution DF methods.

The Pseudo-Doppler direction finding system is a phase measurement system and it is sometimes described in terms of rotating antenna and the Doppler effect [1]. This system measures signal phase changes using commutated sequential elements located on the circumference of a circle [1]. The direction of arrival of a signal can be determined by moving an antenna in the circle in the horizontal plane and noting the phase change that results [2]. Phase change at a rate of 2π radians per second is equivalent to a Doppler frequency shift of one Hertz. When the antenna is moving directly toward or away from the target the rate of the phase change is maximum and

will produce a maximum frequency increase (toward) or decrease (away), with zero frequency shift when the antenna is moving tangential to the wave equiphase lines [2].

The Watson-Watt direction finding system is a simple amplitude comparison scheme using two orthogonal Adcock beamforming arrays. Each Adcock array is made of two dipole elements that are phase reversed to create a figure “8” beam pattern. The optimal array spacing is about $\lambda/8$ with relatively short dipole element lengths [1]. The Watson-Watt Adcock DF process uses two orthogonal Adcock arrays nicknamed the “sine” and “cosine” receiver channels, where the angle of arrival is estimated by taking the arctangent of the voltages from these two RF channels. The Watson-Watt DF process has two fundamental problems: first, the correct quadrant of the azimuth cannot be determined uniquely, and second, the arctangent approximation deviates as the array diameter to signal wavelength ratio changes [1].

The Brueninger direction finding system corrects the deficiencies of Watson-Watt direction finding system [1]. In the Brueninger direction finding system, a sense antenna is used to distinguish signal phase that resolves line of bearing (LOB) quadrant ambiguities. The omni antenna may be a separate antenna or can be formed from the sum of all four Adcock elements [1]. Moreover explicit phase-amplitude correlation methods are used instead of taking arctangent of voltages [1].

The interferometer DF system makes a direct measurement of the phase differences between two or more points on the wavefront and converts the phase information into angle of arrival [2]. Interferometer direction finding systems investigate the time differences of arrival of the signals by calculating the phases of the channel signals which are received at different antennas. The phase information of the distinct channels are processed by using various direction finding algorithms to find the direction of arrival. Literature survey shows that direction finding performance of the interferometer direction finding system is affected by mutual coupling between the antennas [3]. The performance of a multi channel direction finding system is considerably affected by the electromagnetic characteristics of the antenna array [4]. The

effects of the mutual coupling among antenna elements are significant and become more drastic as the interelement spacing drops below half a wavelength [5]. The performance of a multi-channel direction finding system may be degraded significantly when the effect of the mutual coupling is ignored [6]. The effects of mutual coupling should be investigated and taken into account when direction of arrival calculations are conducted.

One of the widely used interferometers is the correlative interferometer. This interferometer compares the measured phase differences of the receive channel signals with pre-measured sample space of signal phase differences for possible direction of arrivals [7]. Maximum correlation between the phase measurements and the sample space reveals the DOA [7]. In the correlative DF systems, the effects of mutual coupling and gain/phase mismatch are automatically included in the DF calculations by using pre-measurement method so that the DF performance of correlative interferometers is better than the standard interferometers. Consequently, correlative interferometers have become one of the most preferred commercial DF systems because of their sufficient accuracy.

MUSIC algorithm, forms a spectral estimator by using eigen analysis of the received signals. In this superresolution method, the DOA is obtained from the characteristics of the spectral estimator. Maximum value of the spectral estimator corresponds to the DOA of the incident signal. Moreover, the MUSIC algorithm makes it possible to determine the DOA of the multiple signals. In this case, the estimator has more than one peak which correspond to DOA of different signals. However, the MUSIC algorithm breaks down in the case of coherent signals [8].

1.1 Scope of the Thesis

The main purpose of this study is to design and implement a three antenna direction finding system. It is aimed to implement various direction finding algorithms and evaluate the DF performance of the system for different algorithms. It is also aimed

to investigate the mutual coupling, gain/phase mismatch, multipath signals and multiple signal effects on the three antenna direction finding system.

The implementations of three channel interferometer algorithm, correlative interferometer algorithm, LSE based correlative interferometer algorithm and MUSIC algorithm are accomplished. Root mean square error (RMSE) of DOA estimations are determined for each DF algorithm under the cases of single signal transmitter, multi signal transmitter and multipath signals. In addition, the effect of mutual coupling on the three antenna system is examined when the element distances are λ and $\lambda/2$ and when there is a signal reflection near the antennas.

1.2 Outline of the Thesis

The direction finding algorithms are given in Chapter 2. Hardware and software design of the three antenna system is explained in Chapter 3. The effects of mutual coupling and gain phase mismatch are given in Chapter 4. The performance evaluation of the system is described in Chapter 5.

CHAPTER 2

ALGORITHMS FOR DIRECTION FINDING

In this chapter, implemented direction finding algorithms in the system are investigated. Three channel interferometer algorithm, correlative interferometer algorithm, LSE based correlative interferometer algorithm and MUSIC algorithm are explained.

The organization of this chapter is as follows: In Section 2.1, implemented DF algorithms in the three antenna DF system are briefly described. In Sections 2.2, 2.3, 2.4 and 2.5 these algorithms are explained in detail.

2.1 An Overview of DF Algorithms

In the three antenna DF system, different DF algorithms are implemented to acquire information about the DOA of the incident source signal. The algorithms are based on determining the relation between the phase differences of the channel signals and the direction of the signal. When the antennas of the system are located at different points with respect to the signal transmitter, the arrival time of the source signal differs for each antenna. Time difference of the signal arrival causes phase differences for the receive channels and DF algorithms use this fact to obtain the DOA. Three channel interferometer algorithm uses the relation between the phase difference information of each channel signal with the antenna spacing. The correlative and the LSE based correlative interferometer algorithms depend on the comparison of the measured phase differences with a sample space that is constructed in an ideal field. In the MUSIC algorithm, the spectral analysis of the channel signals that are received from each of the

antennas is realized to find the DOA of the source signal. Moreover two source signals can be determined in the three antenna DF system by using MUSIC algorithm.

The constructed DF system is adjusted to receive signals at 446MHz frequency and the antennas of the system are located at the $\lambda/2$ equal distances with respect to each other.

Received input signal model is,

$$\mathbf{x}(t) = \mathbf{A}\mathbf{s}(t) + \mathbf{v}(t) , \quad (2.1)$$

where $\mathbf{x}(t)$ is the received input signal vector, \mathbf{A} is the steering matrix, $\mathbf{s}(t)$ is the incident signal vector and $\mathbf{v}(t)$ is the noise vector at the antennas. It is assumed that signals and noise are uncorrelated and the elements of the noise vector are zero mean and they have variance value of σ^2 .

2.2 Three Channel Interferometer Algorithm

Three channel interferometer algorithm determines the DOA information by direct phase comparison of the subject signal received by separate, disposed antennas [9]. When the antennas are located at different points, phase difference emerges between receiver channels. In other words, the phase differences between each received signals are related to the direction of the signal transmitter. Three channel interferometer measures the DOA by using the relationship between phase difference of channel signals and DOA. Three antennas are located in the x-y plane and x-z plane as illustrated in Figure 2.1.

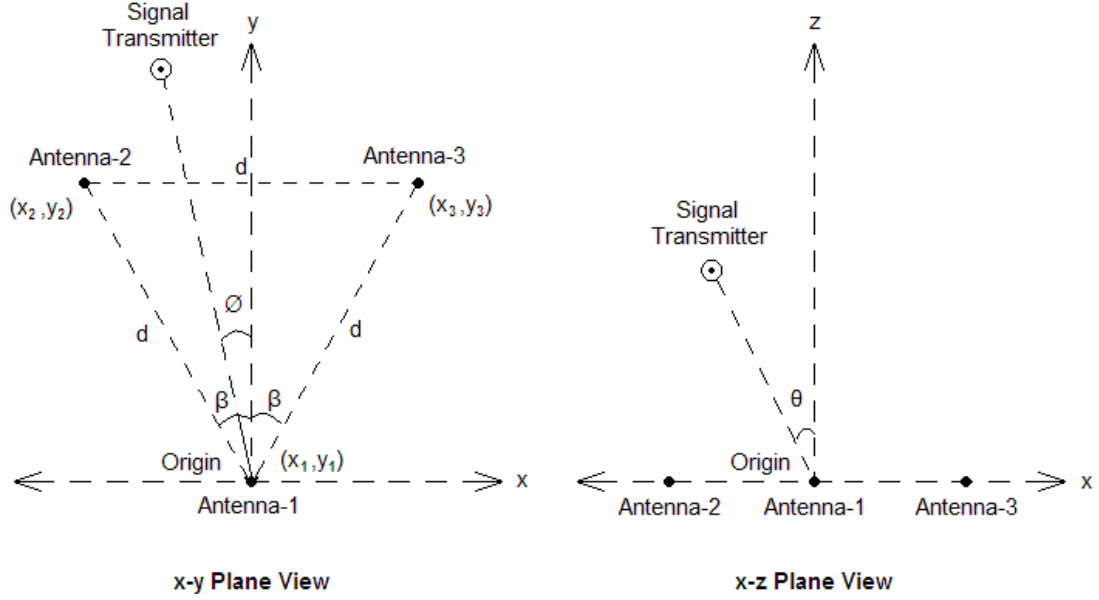


Figure 2.1 – Three Channel Interferometer Antenna Placement

In Figure 2.1, d is the distance between the antennas, ϕ is the azimuth angle of the DOA. The angle between the y -axis and the second antenna is β and similarly the angle between the y -axis and the third antenna is β and β is equal to 30° . The coordinates of the second and the third antenna are (x_2, y_2) and (x_3, y_3) , respectively. The first antenna is located at the origin of the interferometer system and θ represents the elevation angle of the DOA.

If the first antenna is at the origin, and there is only one signal, the received signals for the antennas can be written as,

$$\mathbf{x}(t) = \begin{bmatrix} x_1(t) \\ x_2(t) \\ x_3(t) \end{bmatrix} = \begin{bmatrix} s(t) \\ s(t) \exp(j \frac{2\pi}{\lambda} (-d \cos \phi \sin \theta \sin \beta + d \sin \phi \sin \theta \cos \beta)) \\ s(t) \exp(j \frac{2\pi}{\lambda} (d \cos \phi \sin \theta \sin \beta + d \sin \phi \sin \theta \cos \beta)) \end{bmatrix}, \quad (2.2)$$

where $\mathbf{x}(t)$ is the received signal vector, $x_1(t)$, $x_2(t)$ and $x_3(t)$ are the signals on Antenna-1, Antenna-2 and Antenna-3 respectively.

When the phase of the first antenna signal, $x_1(t)$, is taken as a reference, the phases of the antenna signals can be written as,

$$\mathbf{\Phi} = \begin{bmatrix} \Phi_1 \\ \Phi_2 \\ \Phi_3 \end{bmatrix} = \begin{bmatrix} 0 \\ \frac{2\pi}{\lambda}(-d \cos \phi \sin \theta \sin \beta + d \sin \phi \sin \theta \cos \beta) \\ \frac{2\pi}{\lambda}(d \cos \phi \sin \theta \sin \beta + d \sin \phi \sin \theta \cos \beta) \end{bmatrix}, \quad (2.3)$$

where $\mathbf{\Phi}$ is the signal phase vector, Φ_1 , Φ_2 and Φ_3 are the phases of the signals on Antenna-1, Antenna-2 and Antenna-3 respectively.

The signal phase difference of the Antenna-2 and the Antenna-1 can be calculated as,

$$\Phi_2 - \Phi_1 = \frac{2\pi}{\lambda} d \sin \theta (\sin \phi \cos \beta - \cos \phi \sin \beta). \quad (2.4)$$

The signal phase difference of the Antenna-3 and the Antenna-1 can be calculated as,

$$\Phi_3 - \Phi_1 = \frac{2\pi}{\lambda} d \sin \theta (\sin \phi \cos \beta + \cos \phi \sin \beta). \quad (2.5)$$

The ratio of the sum and difference of the expressions (2.4) and (2.5) can be written as,

$$\frac{(\Phi_3 - \Phi_1) + (\Phi_2 - \Phi_1)}{(\Phi_3 - \Phi_1) - (\Phi_2 - \Phi_1)} = \frac{\frac{4\pi}{\lambda}(d \sin \theta \sin \phi \cos \beta)}{\frac{4\pi}{\lambda}(d \sin \theta \sin \beta \cos \phi)}. \quad (2.6)$$

A new parameter, Ψ , can be defined by using the expression, (2.6), as,

$$\Psi = \frac{(\Phi_3 - \Phi_1) + (\Phi_2 - \Phi_1)}{(\Phi_3 - \Phi_1) - (\Phi_2 - \Phi_1)} = \frac{\cos \beta \sin \phi}{\sin \beta \cos \phi}. \quad (2.7)$$

It is clear that the azimuth angle of the DOA, ϕ , can be derived from the expression, (2.7), as,

$$\phi = \arctan(\Psi \tan(\beta)). \quad (2.8)$$

The three channel interferometer algorithm calculates the azimuth angle of the DOA by using the expression, (2.8), which shows the relationship between the azimuth angle and the signal phase differences.

A parameter, P , can be defined by using the signal phase differences as,

$$P = \{((\Phi_2 - \Phi_1) + (\Phi_3 - \Phi_1)) \sin(\beta)\}^2 + \{((\Phi_3 - \Phi_1) - (\Phi_2 - \Phi_1)) \cos(\beta)\}^2. \quad (2.9)$$

The parameter, P , is equal to,

$$P = \left(\frac{4\pi}{\lambda} d \sin \theta \cos \beta \sin \phi \sin \beta \right)^2 + \left(\frac{4\pi}{\lambda} d \sin \theta \sin \beta \cos \phi \cos \beta \right)^2. \quad (2.10)$$

The expression, (2.10), can be modified as,

$$P = \left(\frac{4\pi}{\lambda} d \sin \theta \cos \beta \sin \beta \right)^2 (\sin^2 \phi + \cos^2 \phi) = \left(\frac{4\pi}{\lambda} d \sin \theta \cos \beta \sin \beta \right)^2. \quad (2.11)$$

It is clear that the elevation angle, θ , of the DOA can be derived from (2.11) as,

$$\theta = \arcsin \frac{\sqrt{P}}{\frac{4\pi}{\lambda} d \cos \beta \sin \beta}. \quad (2.12)$$

The three channel interferometer algorithm calculates the elevation angle of the DOA by using the expression, (2.12), which shows the relationship between the elevation angle and the signal phase differences.

2.2 Correlative Interferometer Algorithm

The correlative interferometer algorithm is based on comparing the measured signal phase differences with a sample space which contains the set of phase differences of channel signals for the possible signal directions [7]. Maximum correlation between the sample space and the phase measurement indicates the corresponding DOA of the signal. The sample space is created by recording phase differences of the channel signals in a matrix whose columns represent different DOA's in an ideal field. Measured phase difference vector is compared with the columns of the sample space matrix. The column which has maximum correlation with the measured phase difference vector is designated to find the DOA [7].

A particular signal phase difference vector of the sample space is represented as,

$$\Phi(\phi_i, \theta_j) = \begin{bmatrix} \Phi_{1-2}(\phi_i, \theta_j) \\ \Phi_{1-3}(\phi_i, \theta_j) \\ \Phi_{2-3}(\phi_i, \theta_j) \end{bmatrix}, \quad (2.13)$$

where $\Phi(\phi_i, \theta_j)$ is signal phase difference vector, $\Phi_{k-m}(\phi_i, \theta_j)$ is the signal phase difference of channel k and m at ϕ_i azimuth angle and θ_j elevation angle. $k = 1, 2$ and $m = 2, 3$.

The sample space is measured in an ideal field with an azimuth angle interval of $\Delta\phi$ covering 360° degrees [7] and with an elevation angle interval of $\Delta\theta$ covering 180° degrees. $\Delta\phi$ and $\Delta\theta$ indicate the resolution of the sample space. When the values of $\Delta\phi$ and $\Delta\theta$ decrease, the resolution of the sample space and the DF accuracy of the correlative interferometer algorithm increase. In this work, $\Delta\phi=5^\circ$ covering 360° and $\Delta\theta=7.5^\circ$ covering 15° . For each elevation angle 72 different channel signal phase difference vector set is obtained. Totally 216 different signal phase difference vectors are obtained. In other words, measured sample space has 216 signal phase difference vector sets.

In order to improve the DF accuracy, measured sample space can be expanded by an interpolation method. In this work, cubic spline interpolation is used. The azimuth and elevation angle accuracy of the sample space is increased by the interpolation method so that new sample space covers more signal phase difference vector sets than the measured sample space. Consequently, the measured signal phase differences can be compared with more sample space vector sets by using interpolation method and the DOA calculation accuracy is increased.

For the three channel direction finding system the measured signal phase difference vector is represented as,

$$\Phi_T(\phi, \theta) = \begin{bmatrix} \Phi_{1-2}(\phi, \theta) \\ \Phi_{1-3}(\phi, \theta) \\ \Phi_{2-3}(\phi, \theta) \end{bmatrix}, \quad (2.14)$$

where Φ_T is measured channel signals phase difference vector, $\Phi_{k-m}(\phi, \theta)$ is the signal phase difference of channel k and m at ϕ azimuth angle and θ elevation angle. $k = 1, 2$ and $m = 2, 3$.

Correlation of the measured phase difference vector, $\Phi_T(\phi, \theta)$, and a sample space vector is obtained by using the expression (2.15),

$$R_{i,j} = \frac{(\Phi_T(\phi, \theta))^T \Phi(\phi_i, \theta_j)}{\sqrt{(\Phi_T(\phi, \theta))^T \Phi_T(\phi, \theta) (\Phi(\phi_i, \theta_j))^T \Phi(\phi_i, \theta_j)}}, \quad (2.15)$$

where $R_{i,j}$ is the normalized correlation of $\Phi_T(\phi, \theta)$ and $\Phi(\phi_i, \theta_j)$.

Maximum value of $R_{i,j}$ is equal to the maximum correlation of the measured phase difference vector and a sample space vector. The azimuth and the elevation angle values which cause maximum correlation in (2.15), corresponds to the DOA of the signal.

2.3 LSE Based Correlative Interferometer Algorithm

In the LSE based method, the DF algorithm computes the vector difference (i.e., vector error), and searches for the LSE between the measured vector and each of the sample space vectors [10].

For the LSE based correlative interferometer algorithm sample space of the correlative interferometer algorithm is used and error vector set is obtained by subtracting columns of the sample space from the measured vectors as,

$$\Phi_E(\phi_i, \theta_j) = \Phi_T(\phi, \theta) - \Phi(\phi_i, \theta_j), \quad (2.16)$$

where $\Phi_E(\phi_i, \theta_j)$ is error vector, $\Phi_T(\phi, \theta)$ is the measured phase difference vector and $\Phi(\phi_i, \theta_j)$ is the sample space vector.

The least square cost function for the LSE based correlative interferometer [10] is,

$$G(\phi_i, \theta_j) = (\Phi_E(\phi_i, \theta_j))^T R_{LSE}^{-1} \Phi_E(\phi_i, \theta_j). \quad (2.17)$$

Maximum value of the least square cost objective is searched to identify the DOA [10], i.e.,

$$G(\phi_M, \theta_M) = \arg \max_{\phi_i, \theta_j} G(\phi_i, \theta_j), \quad (2.18)$$

where $G(\phi_M, \theta_M)$ is the maximum value of the least square cost objective at ϕ_M azimuth and θ_M elevation angles which are considered as DOA of the signal.

2.4 The MUSIC Algorithm

The MUSIC algorithm is based on eigenvalue decomposition, which is also called a subspace-based method [11]. MUSIC is a superresolution direction finding algorithm. The main difference between MUSIC and the previous methods is the fact that MUSIC algorithm can be used to find the DOA of the multiple signals.

For an M element array with D incident signals, the received signal model can be represented as,

$$\mathbf{x}(t) = \mathbf{A}\mathbf{s}(t) + \mathbf{n}(t) \quad t=1, 2, \dots, N, \quad (2.19)$$

where $\mathbf{x}(t)=[x_1(t), \dots, x_M(t)]^T$ is the received input data vector, \mathbf{A} is the steering matrix, $\mathbf{s}(t)=[s_1(t), \dots, s_D(t)]^T$ is the incident signal vector, $\mathbf{n}(t)=[n_1(t), \dots, n_M(t)]^T$ is the noise vector and N is the number of samples.

If the mutual coupling between antennas is taken into account, the received signal model can be represented as,

$$\mathbf{x}(t)=\mathbf{CAs}(t)+\mathbf{n}(t) \quad t=1,2, \dots, N, \quad (2.20)$$

where \mathbf{C} is the mutual coupling matrix.

The steering matrix, \mathbf{A} , is $M \times D$ and it is composed of D steering vectors. The steering matrix can be written as,

$$\mathbf{A}=[\mathbf{a}(\phi_1, \theta_1) \quad \mathbf{a}(\phi_2, \theta_2) \quad \dots \quad \mathbf{a}(\phi_j, \theta_j) \quad \dots \quad \mathbf{a}(\phi_D, \theta_D)], \quad (2.21)$$

where $\mathbf{a}(\phi_j, \theta_j)$ is the steering vector for the j -th incident signal.

The steering vector, $\mathbf{a}(\phi, \theta)$, can be represented as,

$$\mathbf{a}(\phi, \theta)=\begin{bmatrix} e^{-j\left(\frac{2\pi}{\lambda}(x_1 \sin \theta \cos \phi+y_1 \sin \phi \sin \theta+z_1 \cos \theta)\right)} \\ e^{-j\left(\frac{2\pi}{\lambda}(x_2 \sin \theta \cos \phi+y_2 \sin \phi \sin \theta+z_2 \cos \theta)\right)} \\ \vdots \\ e^{-j\left(\frac{2\pi}{\lambda}(x_M \sin \theta \cos \phi+y_M \sin \phi \sin \theta+z_M \cos \theta)\right)} \end{bmatrix}, \quad (2.22)$$

where λ is the wavelength of the signals, x_i , y_i and z_i are the coordinates of the array elements for $i=1, \dots, M$.

The covariance matrix of the received signal [12] is,

$$\mathbf{R}_{xx} = E\{\mathbf{x}(t) \mathbf{x}(t)^H\} = \mathbf{A} \mathbf{R}_{ss} \mathbf{A}^H + \sigma^2 \mathbf{I}, \quad (2.23)$$

under the assumption that signals and noise are uncorrelated. Also noise is zero mean with a variance of σ^2 [11]. \mathbf{I} is identity matrix and \mathbf{R}_{ss} is the correlation matrix of the incident signals. It is assumed that \mathbf{R}_{ss} is of full rank D [12].

Covariance matrix can be expressed in terms of its eigenvalues, λ_m , and eigenvectors, e_m , [12] as,

$$\mathbf{R}_{xx} = \sum_{m=1}^M \lambda_m e_m e_m^H = \mathbf{V} \mathbf{A} \mathbf{V}^H, \quad (2.24)$$

where $\mathbf{A} = \text{diag}\{\lambda_1, \dots, \lambda_M\}$ is the eigenvalue matrix and \mathbf{V} is the eigenvector matrix. The eigenvalues of the covariance matrix are real and positive, arranged in descending order [12].

The eigenvalues λ_m of the covariance matrix [12] are,

$$\lambda_m > \sigma^2 \text{ for } m = 1, \dots, D, \text{ and } \lambda_m = \sigma^2 \text{ for } m = D+1, \dots, M. \quad (2.25)$$

As given in (2.25), the $M-D$ smallest eigenvalues of \mathbf{R}_{xx} are equal to σ^2 , and the eigenvectors e_m , $m=D+1, \dots, M$ corresponding to these eigenvalues span the noise subspace. The D steering vectors that make up \mathbf{A} lie in the signal subspace and are hence orthogonal to the noise subspace [8], [12].

The number of incident signals can therefore be determined by inspection of the magnitudes of the eigenvalues [11].

Consequently, the covariance matrix can be partitioned into D -dimensional subspace spanned by the incident signal mode vectors and $M-D$ dimensional subspace spanned by the $M-D$ noise eigenvectors [12], i.e. ,

$$\mathbf{R}_{xx} = \mathbf{V}_s \mathbf{A} \mathbf{V}_s^H + \mathbf{V}_n \mathbf{A} \mathbf{V}_n^H, \quad (2.26)$$

where \mathbf{V}_s is the $M \times D$ signal subspace and \mathbf{V}_n is the $M \times (M-D)$ noise subspace [12].

The MUSIC algorithm uses following steps to find the DOA. First, the covariance matrix given in (2.24), is computed and the minimum eigenvalue of the covariance matrix of the observations as well as the number of eigenvalues equal to this value are determined. Second, the noise subspace of the eigenvectors associated with this minimum eigenvalue is formed, and then the spectrum, $P(\phi, \theta)$, of the incident signals is estimated by using noise subspace and steering vectors [8], [12].

The spectrum, $P(\phi, \theta)$, of the incident signals is,

$$P(\phi, \theta) = \frac{1}{\mathbf{a}^H(\phi, \theta) \mathbf{V}_n \mathbf{V}_n^H \mathbf{a}(\phi, \theta)}, \quad (2.27)$$

where $\mathbf{a}(\phi, \theta)$ is the steering vector and \mathbf{V}_n is the matrix that contains the noise eigenvectors [12].

The DOA of signal sources is determined by finding the values of ϕ and θ that gives the maximum $P(\phi, \theta)$ result [11]. The number of the peaks of the spectrum, $P(\phi, \theta)$, gives the number of the incident signals [8], [12].

When the mutual coupling effect is considered, the expression of the spectrum estimation becomes,

$$P(\phi, \theta) = \frac{1}{a^H(\phi, \theta) C^H V_n V_n^H C a(\phi, \theta)} . \quad (2.28)$$

The compensation of the mutual coupling effect can be realized in the MUSIC algorithm by using (2.28). This new spectrum estimation takes into account the mutual coupling and it is expected that this estimator improves the accuracy of the DOA estimation.

CHAPTER 3

THREE ANTENNA DIRECTION FINDING SYSTEM

In this chapter, hardware and software design of the three antenna direction finding system are explained. The hardware is described in three main parts; antenna, RF front-end and digital baseband processing. In the software part, DSP and FPGA program codes are presented.

This chapter is organized as follows: In Section 3.1, the hardware of system is explained. The software of the system is discussed in Section 3.2.

3.1 Hardware

The hardware of the three antenna direction finding system is composed of three antennas, an RF front-end and a digital baseband processing part. RF front-end part is responsible for converting the input RF signals received by antennas to IF signals which are sent to digital baseband processing part. To produce the IF signal, the combination of amplifiers, filters and mixers are used in the RF front-end. In the digital baseband processing part, analog to digital conversion and digital signal processing are realized. The RF front-end is connected onto the processing board by using PCB (printed circuit board) connectors as shown in Figure 3.1. The block diagram of the system hardware is shown in Figure 3.2.

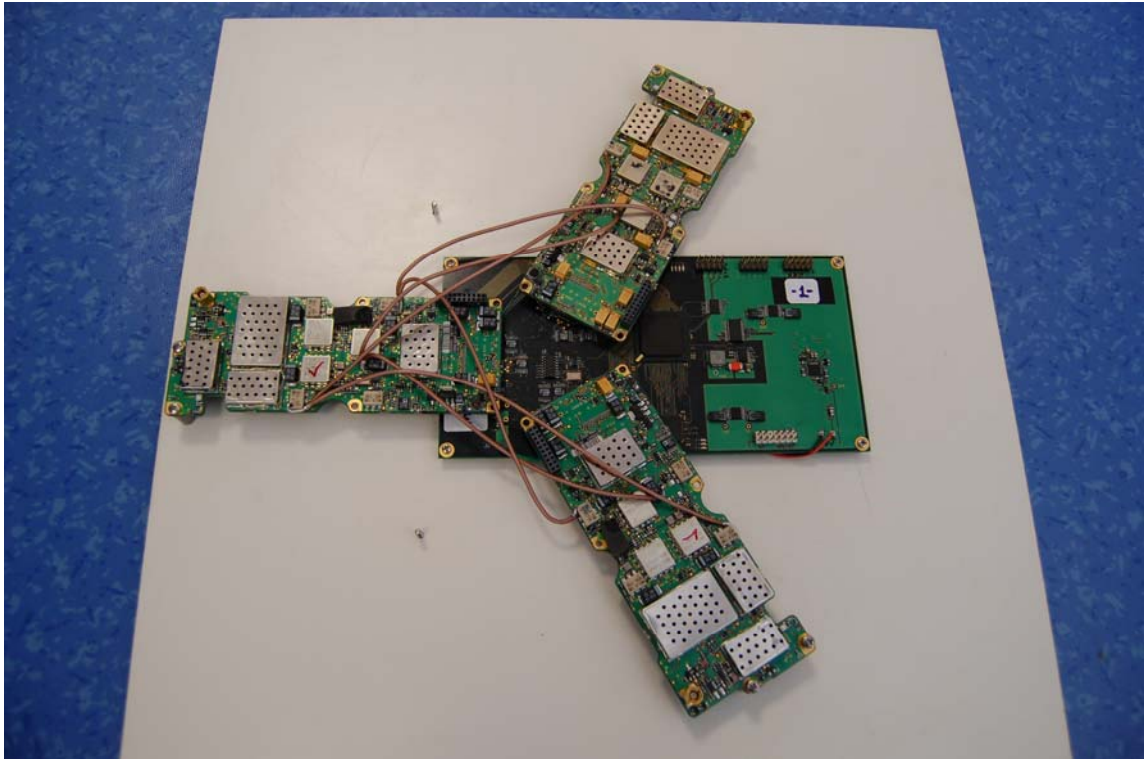


Figure 3.1 – RF Front-End and the Processing Board

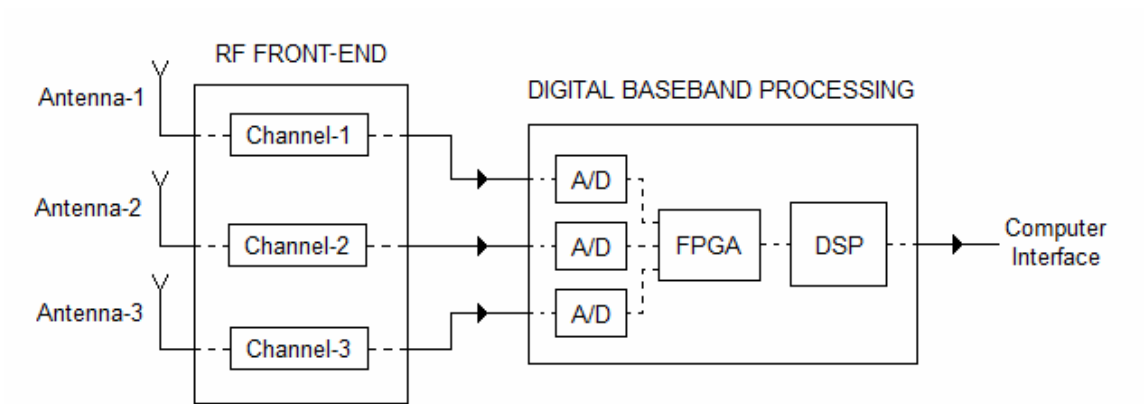


Figure 3.2 – Three Channel Direction Finding System Block Diagram

3.1.1 Antenna

In the DF system, AC MARINE ZS-C-0320 normal mode helical antennas are used. The helical antenna can be considered as a vertical array of loops, at least for the case when the diameter of the helix is small compared to a wavelength [13]. The result is normal mode radiation with higher gain than a single loop, providing an omnidirectional antenna with compact size and reasonable efficiency [13]. Moreover the normal mode helical antennas are useful as short, vertically polarized radiators, similar to the monopoles and they are widely used in portable systems, primarily because it can be shorter than $\lambda/4$ monopole [14], [15]. The antenna can be seen in Figure 3.3.



Figure 3.3 – Antenna of the Direction Finding System

The length of the antennas are 70 ± 2 mm and their polarization is vertical. The antennas can operate properly at 435MHz-470MHz frequency range and their impedances are 50Ω .

In the datasheet of the antenna AC MARINE ZS-C-0320, it is claimed that the antenna has a VSWR (voltage standing wave ratio) value which is smaller than 2 at 446MHz operating frequency. The VSWR characteristics of the antenna is given in Figure 3.4.



Figure 3.4 – The VSWR Plot of the Antenna

The antenna is simulated in the CST Microwave Studio simulation tool to observe the antenna radiation pattern characteristics. The radiation pattern of the antenna

is investigated in elevation pattern and azimuth pattern parts. The elevation pattern is shown in Figure 3.5 and in Figure 3.6, for the theta values of 0° to 90° at phi is equal to 90° and 270° and at phi is equal to 0° and 180° respectively. The simulations are conducted with infinite ground plane.

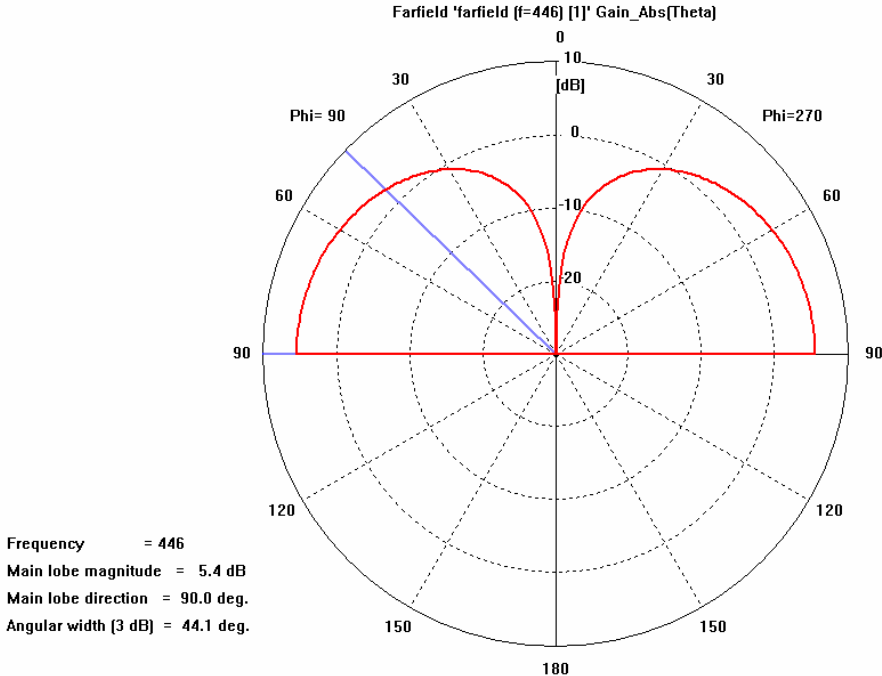


Figure 3.5 – The Elevation Pattern for Phi is 90° and 270°

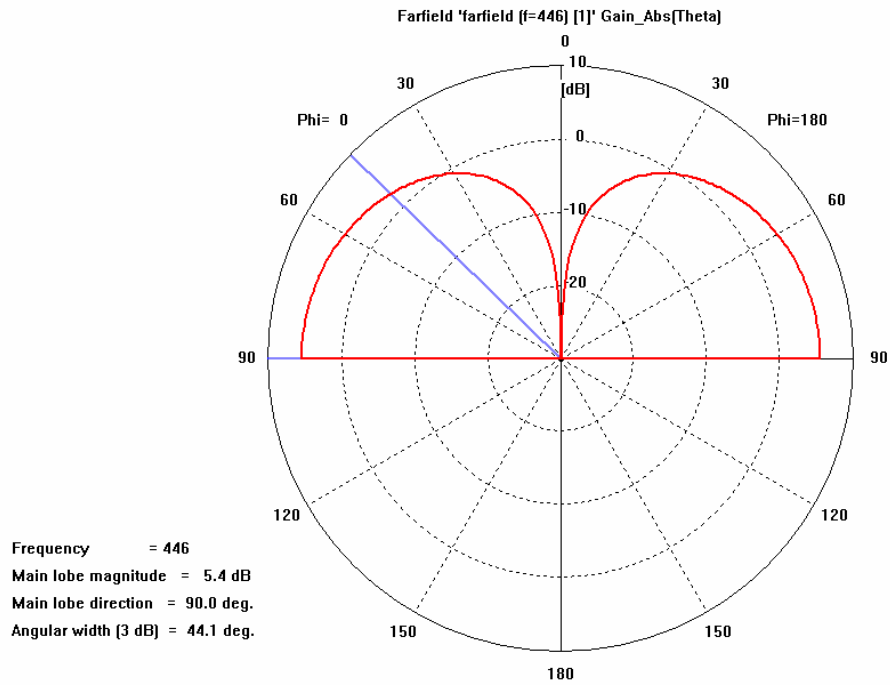


Figure 3.6 – The Elevation Pattern for Phi is 0° and 180°

The azimuth radiation pattern of the antenna for the phi values of 0° to 360° at theta is equal to 90° is shown in Figure 3.7.

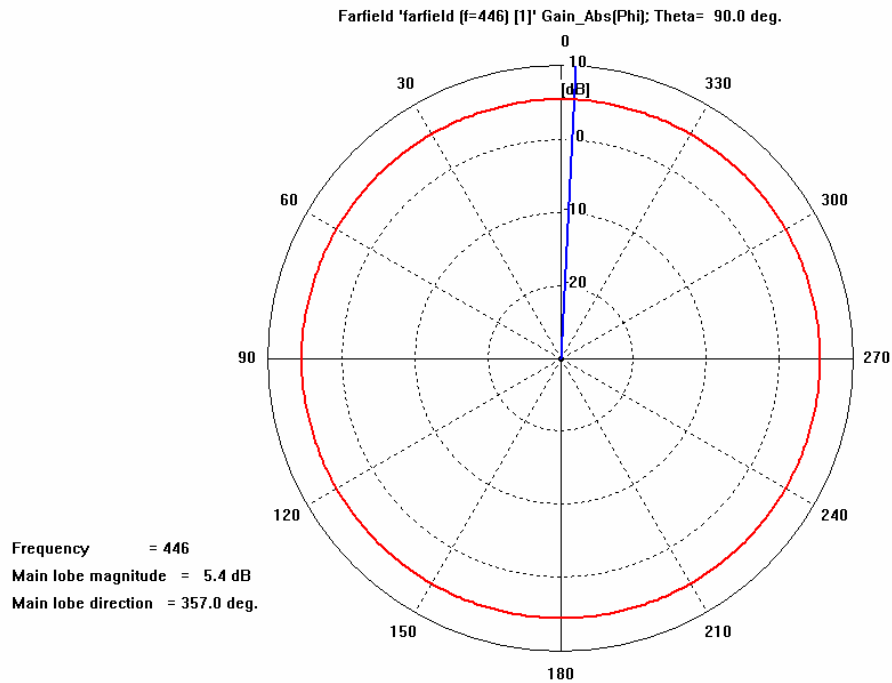


Figure 3.7 – The Azimuth Pattern for Theta is 90°

The helical antenna behaves more like a dipole or monopole with a ground plane antenna [16]. By using a ground plane, the image theory can be applied to the antenna with a length of l . It can be considered to be equivalent to dipole with length $2l$ in free space [17]. The current distribution along the pole is the same as the dipole, thus the radiation pattern is the same above the ground plane [16]. The ground plane which is used in the system is 25cm x 25cm metal plate. The antenna with the ground plane is shown in Figure 3.8.

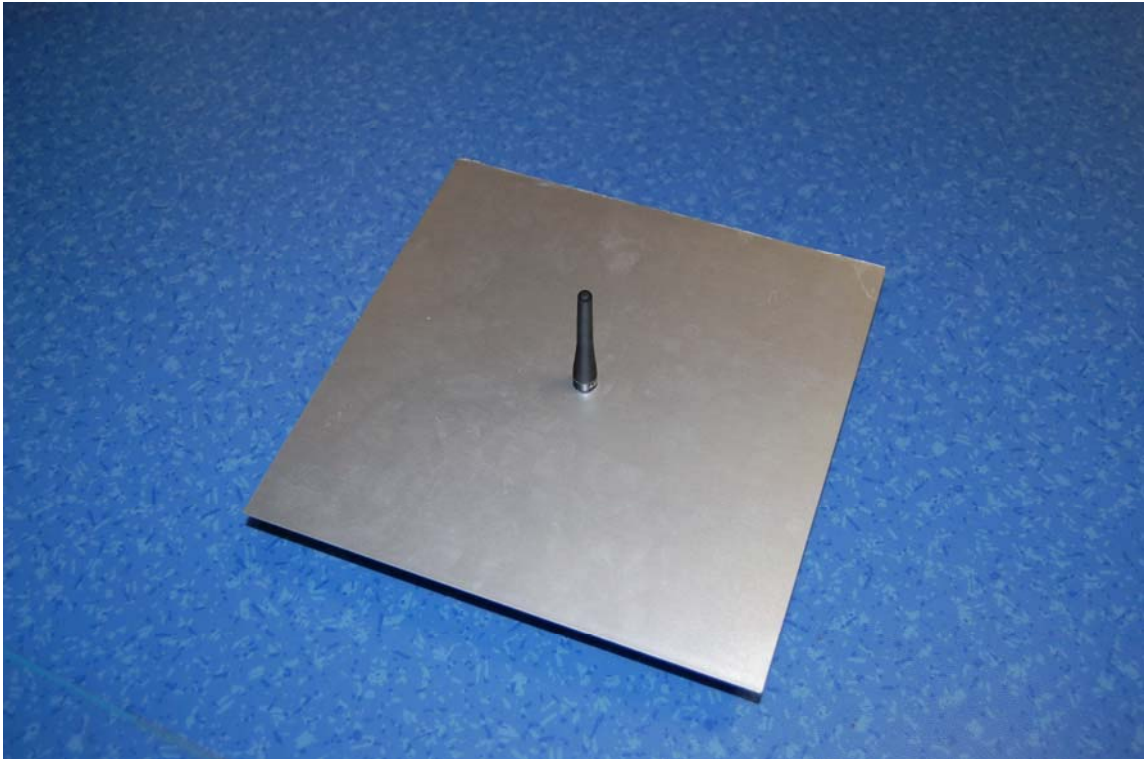


Figure 3.8 – Antenna with the Ground Plane

3.1.2 RF Front-End

RF signal is received and converted to IF in the RF front-end part. The RF front-end has three receive channels each of which is connected to distinct antennas. Receive channels are calibrated to receive 446MHz channel signals and to obtain 21.4MHz IF signals. In each receive channels, signal amplifying, filtering and mixing processes are realized for the RF to IF conversion and each receive channel uses the same clock source to obtain phase matching. The RF front-end block diagram is shown in Figure 3.9.

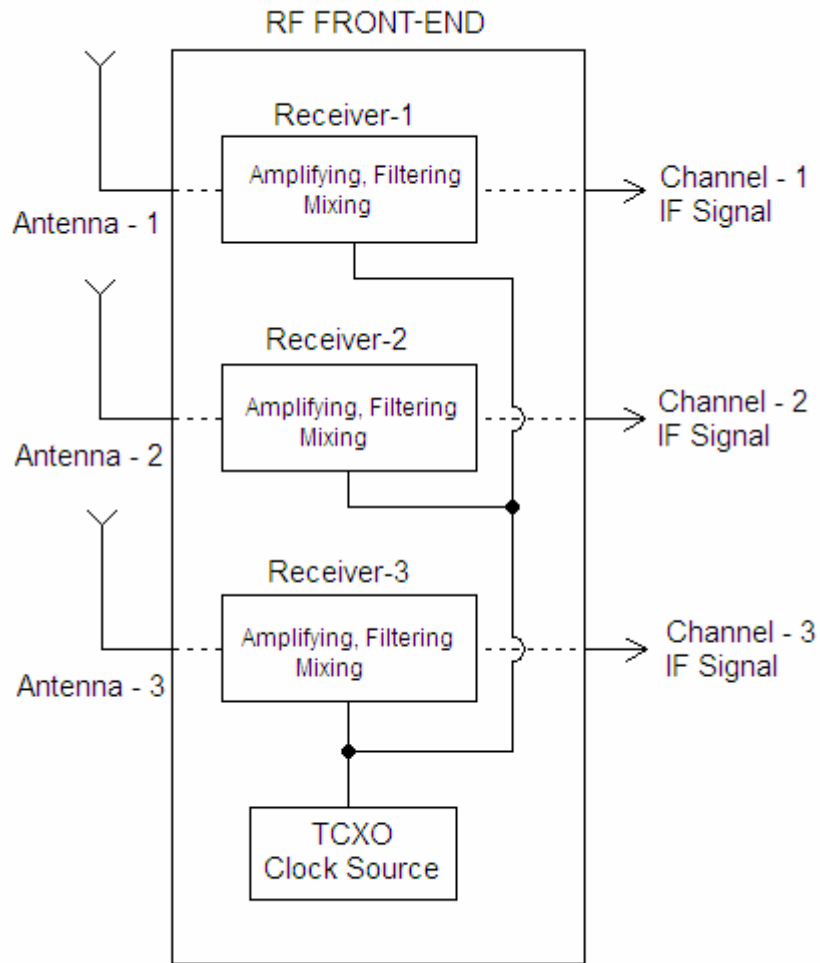


Figure 3.9 – RF Front-End

In receive channels, the input signal is amplified by a low noise amplifier which gives 20dB gain to the signal with a noise factor of 8dB. Amplified signal is then filtered by a filter which passes the signals between 438MHz and 454Mhz. The output of the filter is connected to a mixer to decrease the frequency of the signal to 21.4MHz. The signal is multiplied by 467.4MHz for obtaining 21.4MHz IF signal. This part can be seen in Figure 3.10.

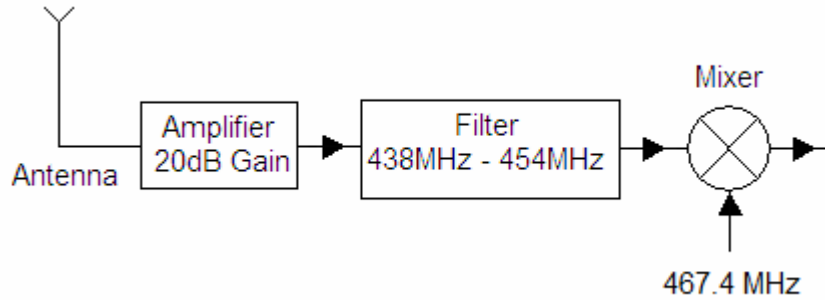


Figure 3.10 – RF Amplifying-Filtering-Mixing Part

The output of the mixer is connected to the second part which is composed of an attenuator, amplifier, narrow band filter and AGC (automatic gain controller) combinations. In this part, the amplitude of the signal is controlled by the AGC and the signal is filtered by a narrow band filter which passes the signals between 21.35MHz and 21.45MHz. The AGC system holds the magnitude of the IF signal output at the value of -6.47dBm by using attenuator and amplifier combination. The AGC system can attenuate the IF signal by 40dB or amplifies the signal by 100dB to hold the signal constant at -6.47dBm magnitude value. The narrow band filter which has 100KHz 3dB bandwidth is used at the end of this part. The block diagram of AGC and narrowband filtering part is shown in Figure 3.11.

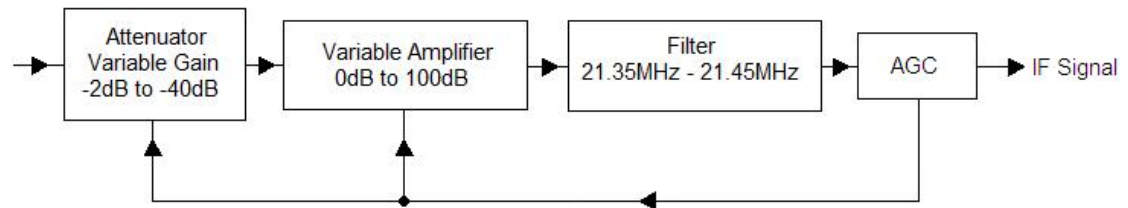


Figure 3.11 – AGC System of the RF Front-End

The RF front-end is sensitive to RF signals which have minimum magnitude value of -115dBm . The overall dynamic range of the RF front-end is -115dBm to $+15\text{dBm}$. The signals which are in the dynamic range of the RF front-end can be held at the magnitude value of 6.47dBm .

One of the receivers in the RF front-end part is shown in Figure 3.12.

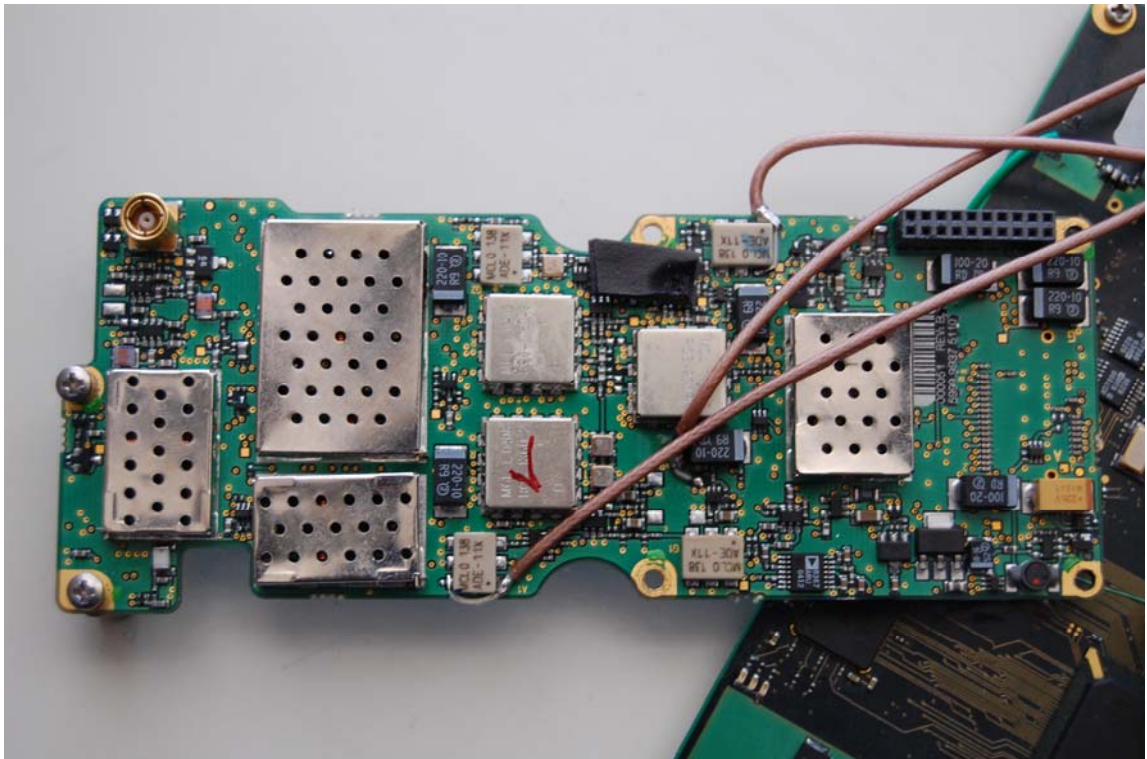


Figure 3.12 – RF Receiver

3.1.3 Digital Baseband Processing

In the digital baseband processing part, analog IF signals are digitized and processed to obtain phase differences of channel signals. Digital baseband processing is realized in a DSP based board which is mainly composed of ADC's, FPGA, DSP and UART transceiver. The processing board has connection with a computer to monitor the

process results and to send commands which determine the direction finding algorithm type.

In the processing board, three identical MAXIM MAX1449EHJ ADC's simultaneously digitize the incoming analog IF signals and send digital data to XILINX XC3S1000 FPGA. Three ADC's and the FPGA have parallel interfaces for transferring the data from ADC's to FPGA so that data is accumulated in the internal dual port RAM of the FPGA. As a signal processor TEXAS INSTRUMENTS TMS5509A Fixed Point DSP is used in the board. Digitized signal is read by the DSP from the FPGA's dual port RAM when DSP is ready to process the data. After signal processing is completed, results are sent to TEXAS INSTRUMENTS TL16C750CIPM UART transceiver. The UART transceiver has an external interface with a computer via MAXIM MAX3237 RS232 driver so that the processing results can be monitored on the computer screen. The processing board block diagram is shown in Figure 3.13.

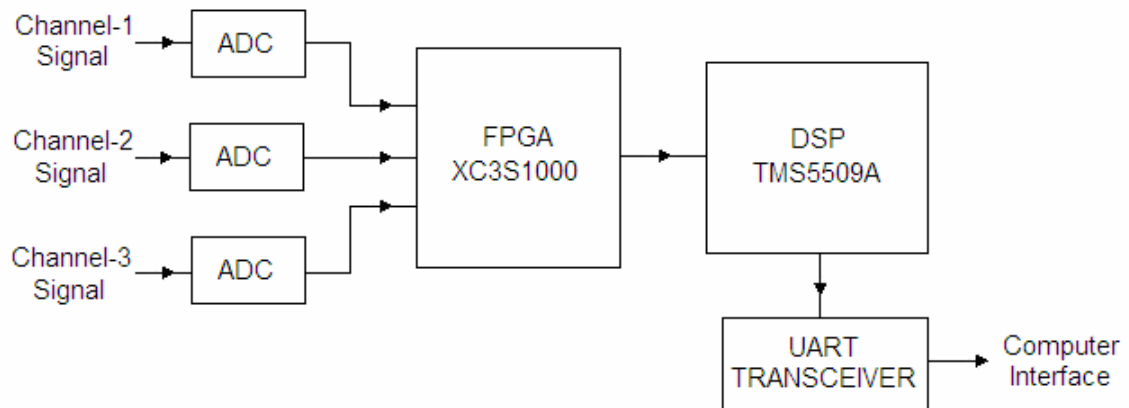


Figure 3.13 – The Processing Board Block Diagram

Required voltages for the processing board are 3.3V, 2.5V, 1.6V and 1.2V. These voltages are produced by using six different voltage regulators whose inputs are 5V input voltage. 3.3V is produced by MAXIM MAX1904ETJ, 2.5V and 1.8V are

produced by MAXIM MAX1793EUE-33 regulators whereas 1.2V is produced by MAX1830EEE regulator. The input voltage of the MAX1793EUE-33 regulators and MAX1830EEE regulator is also 5V input voltage. The production of the board voltages is shown in Figure 3.14.

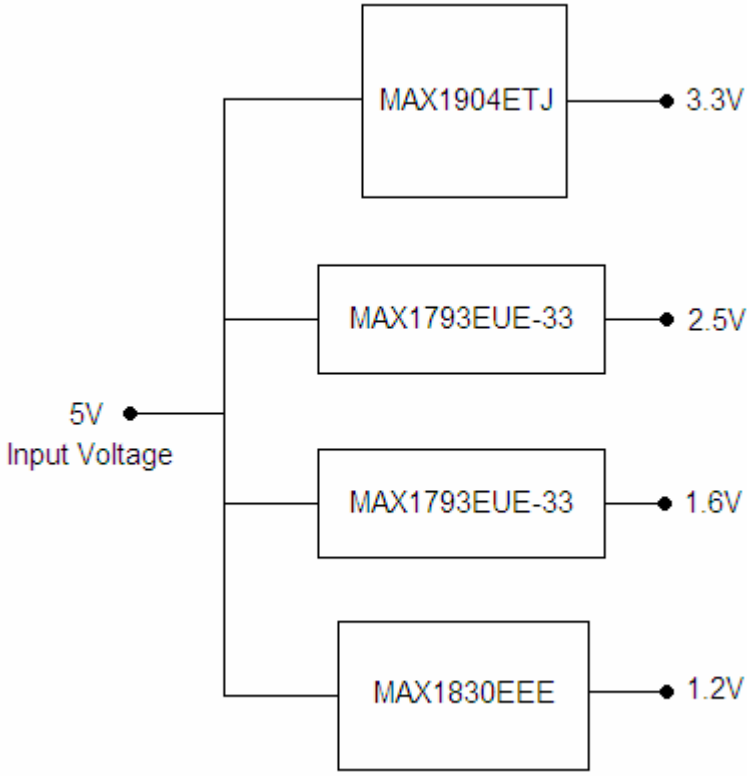


Figure 3.14 – Voltage Production

The reset signal for the DSP is produced by MAXIM MAX6707KA-T reset controller. DSP operating voltages 3.3V and 1.6V are monitored at the reset controller's input. If these voltages drop below the 3.08V and 1.4V, reset signal is produced at the controller output so that DSP software is restarted. Moreover during the power up period, reset signal is sent to the DSP and the FPGA by the reset controller for

initializing the software in the chips. Connections of the reset controller can be seen in Figure 3.15.

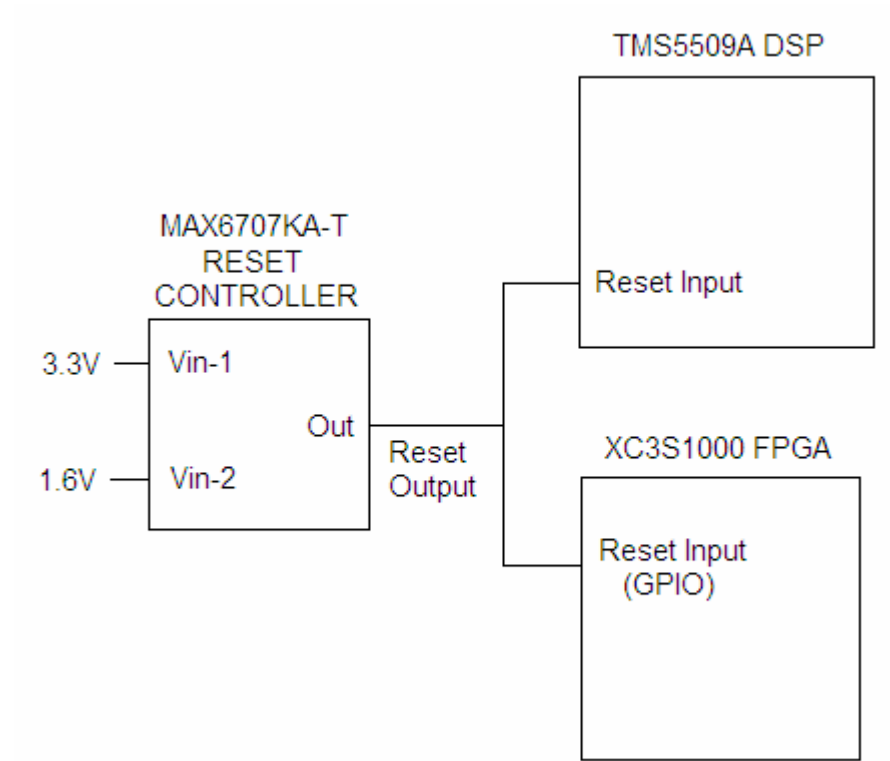


Figure 3.15 – Reset Controller

The clock of the board is supplied by 24MHz EC54 SMX7 clock oscillator and LINEAR TECHNOLOGY LT1719 square wave generator. 24MHz clock signal is obtained from the output of the square wave generator which is connected to AMI FS6377-01 PLL to produce clocks for DSP, UART transceiver and clock buffer. Output clock signals of the PLL are 24MHz DSP clock signal, 3.072MHz UART transceiver clock signal and 24MHz clock buffer input signal. Clock buffer output of the PLL is connected to a zero delay buffer CYPRESS CY2308SI to feed each ADC's and FPGA with the same clock. Since the clock buffer is zero delay, it does not cause any undesired phase skew between the ADC's clock signal. Moreover the clock signal routes of each ADC on the PCB are designed identical in length, in shape and in thickness to obtain

clock phase matching between all of three ADC's. In other words ADC's are all matched in terms of the clock source. CY2308SI clock buffer doubles the clock signal frequency which means that clock frequency of ADC's and the FPGA is 48MHz. The block diagram of the clock circuit is shown in Figure 3.16.

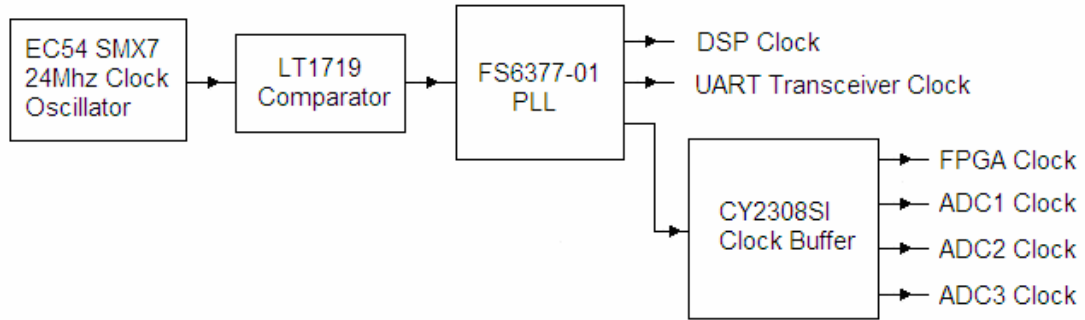


Figure 3.16 – Clock Circuit Block Diagram

The analog IF signals are digitized by three identical 10-Bits MAX1449EHJ ADC's which are working with 48MHz sampling frequency [18]. The operating voltages of ADC's are 3.3V and the clock signals of each ADC are obtained from the zero delay clock buffer CYPRESS CY2308SI.

The SINAD (signal to noise plus distortion) value of the DF system, including the RF front-end and processing parts, is 52dB. The ENOB (enable number of bits) value is calculated by using the SINAD as,

$$ENOB = \frac{SINAD - 1.76}{6.02}. \quad (3.1)$$

The required ENOB value for the DF system is calculated as 8.345 bits by using (3.1). 10-Bits MAX1449EHJ ADC's are used in the system because they have ENOB values of 9.358 at 21.4MHz input frequency [18].

Analog IF signals which have center frequency of 21.4MHz are sampled at 48MHz which is over the Nyquist rate so that problem of aliasing is prevented [19].

According to the Nyquist theorem [20],

$$\frac{f_s}{2} > f_c , \quad (3.2)$$

where f_s is sampling frequency and f_c is maximum frequency of the analog IF signal.

A parallel data interface is used to transfer digital data from ADC's to FPGA. Since the FPGA is using the same 48MHz clock source with the ADC's, it can simultaneously store all of the three channel's digital data. At each clock cycle 10-Bit data is received by the FPGA. For storing the data, FPGA's internal dual port RAM is used. The total size of the internal dual port RAM is 432-Kbits which is adequate to buffer the data before it is received by the DSP [21]. ADC and FPGA data interface is shown in Figure 3.17.

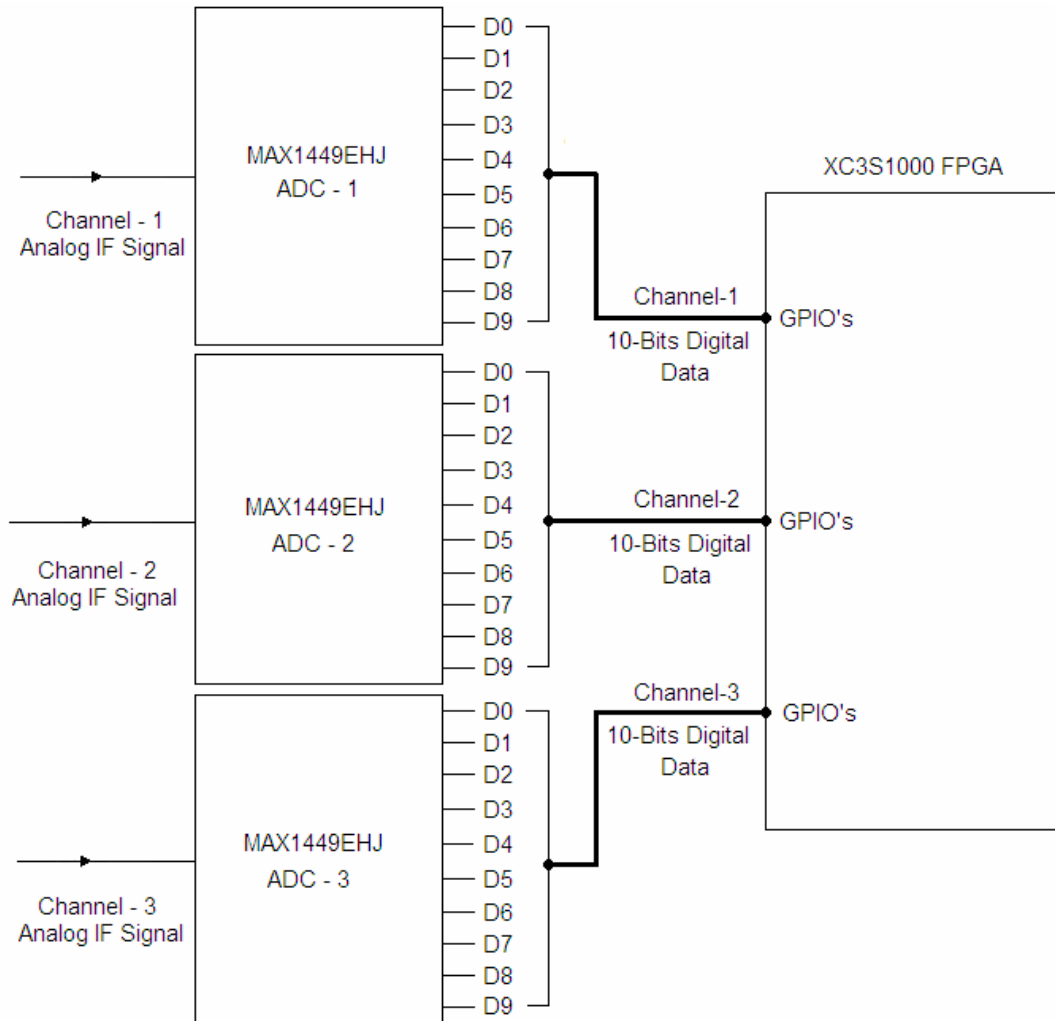


Figure 3.17 – ADC and FPGA Data Interface

For each processing cycle, 250 samples of the analog IF signal is used in the DSP. When DSP is ready to process, stored data is sent to DSP by using the parallel interface of the DSP and the FPGA. The interface has 10-Bits length data bus, 20-Bits length address bus, a chip enable (CE) signal, an output enable (OE) signal and a write enable (WE) signal. The interface of the DSP and the FPGA can be seen in Figure 3.18.

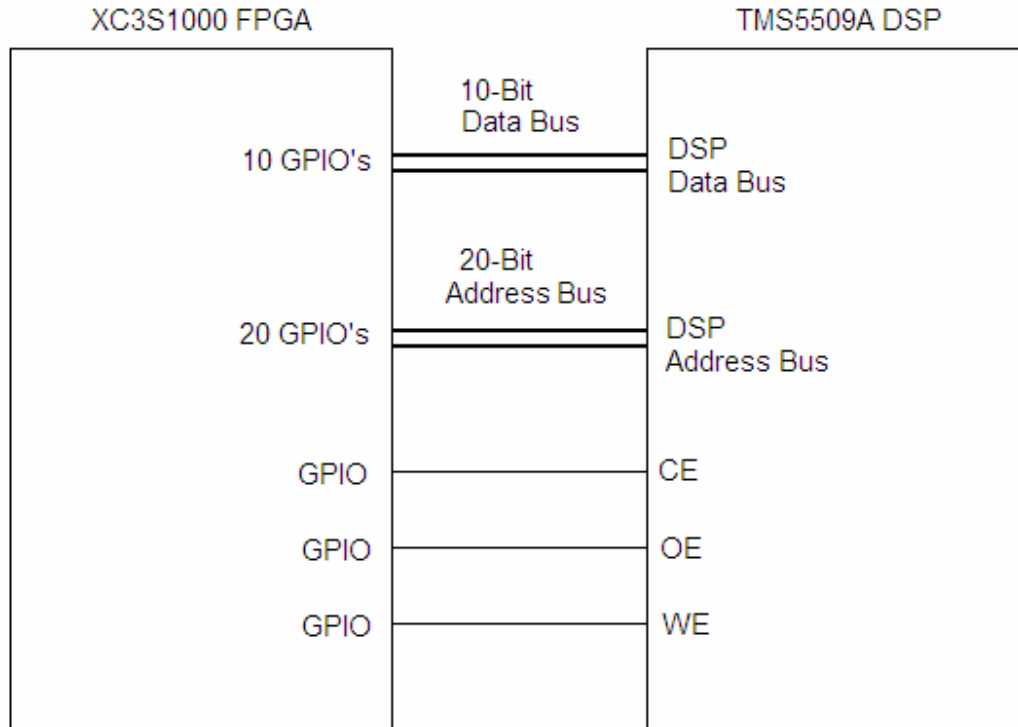


Figure 3.18 – FPGA and DSP Interface

The operating voltages of the FPGA are 3.3V, 2.5V and 1.2V. I/O's (Inputs/Outputs) of the FPGA are fed with 3.3V, whereas, the core of the FPGA operates with 2.5V and 1.2V. For loading the software to the FPGA, XILINX XCF04SVO20 PROM is used. The software of the FPGA is loaded to PROM. When the board is powered on, FPGA is booted by the PROM.

Signal processing operations are realized in the fixed point DSP TMS5509A. The DSP has a parallel interface with AMD AM29LV160DT-90EI Flash ROM as shown in Figure 3.19. The interface has 16-Bits length data bus, 20-Bits length address bus, a chip enable (CE) signal, an output enable (OE) signal and a write enable (WE) signal. By using the parallel interface the software of the DSP is loaded from the flash ROM when the board is powered on.

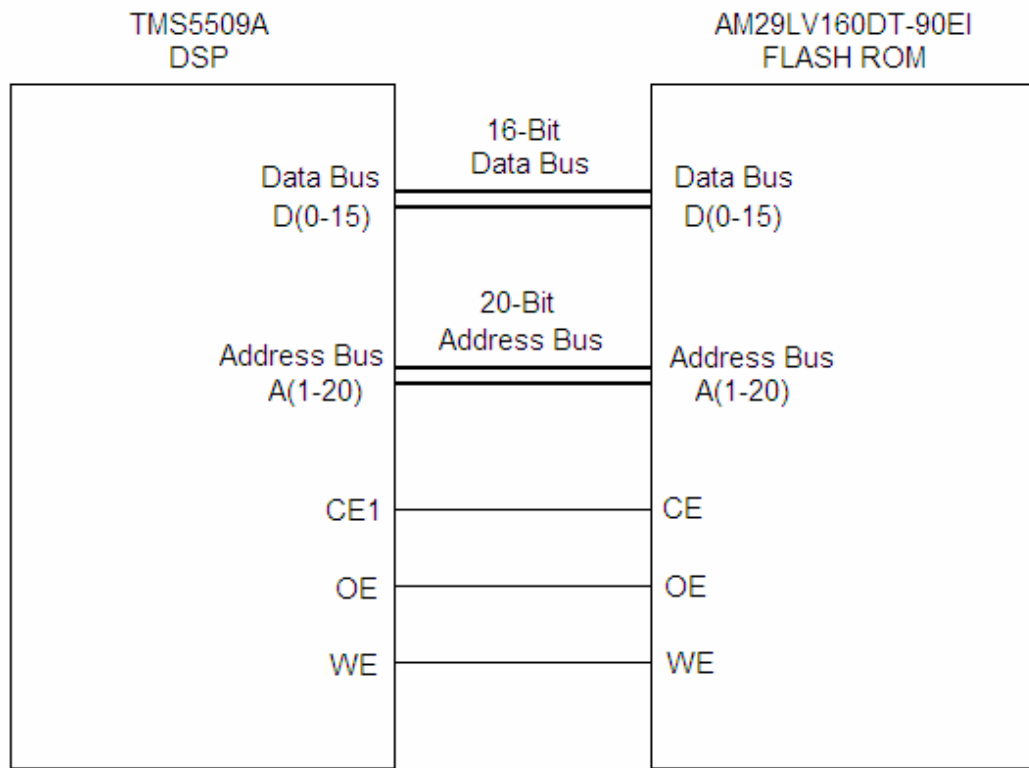


Figure 3.19 –DSP - Flash ROM Interface

DSP has a parallel interface with TL16C750CIPM UART transceiver to send DOA (direction of arrival) information and to receive commands from the computer. The interface has 8-Bits length data bus, 3-Bits length address bus, a chip enable (CE) signal, an output enable (OE) signal and a write enable (WE) signal as shown in Figure 3.20.

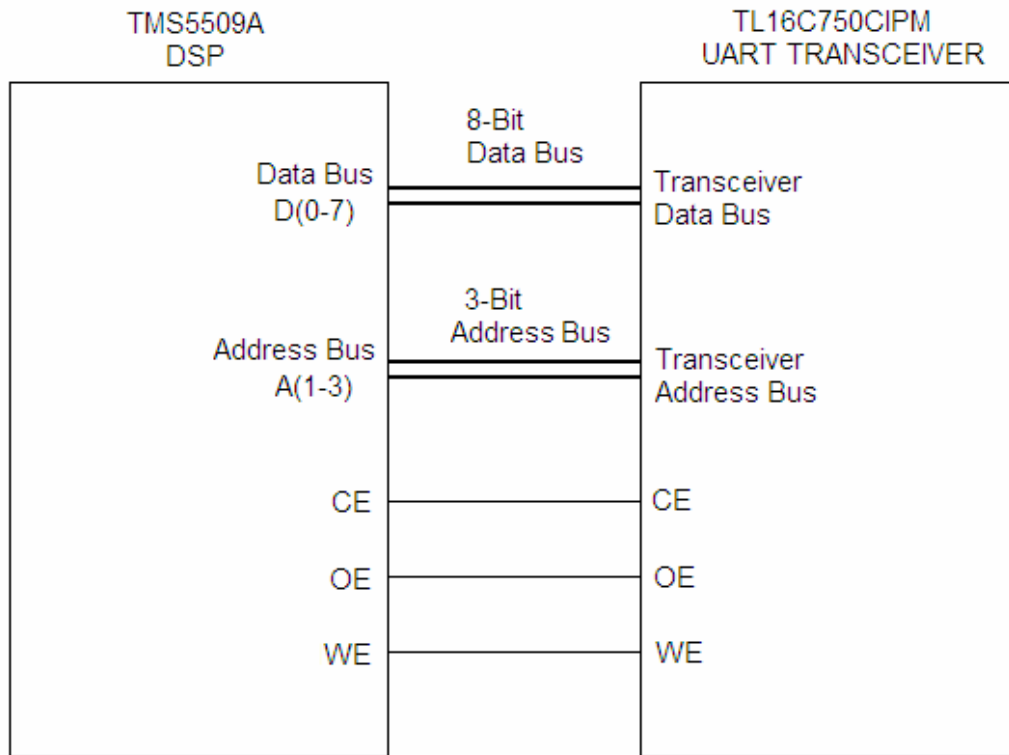


Figure 3.20 – DSP and UART Transceiver Interface

The UART transceiver has an external interface with a computer via MAX3237 RS232 driver. The computer and the UART transceiver can communicate using RS232 (recommended standard 232) communication standard. In other words, output data is received from the UART transceiver and sent to RS232 connector over the RS232 driver. A computer is connected to RS232 connector so that an external interface is established between the processing board and the computer. The external interface is used for monitoring the output data on the computer screen and to receive commands that determine the algorithm type from the computer. The interface of the UART transceiver and the computer is shown in Figure 3.21 and the processing board is shown in Figure 3.22.

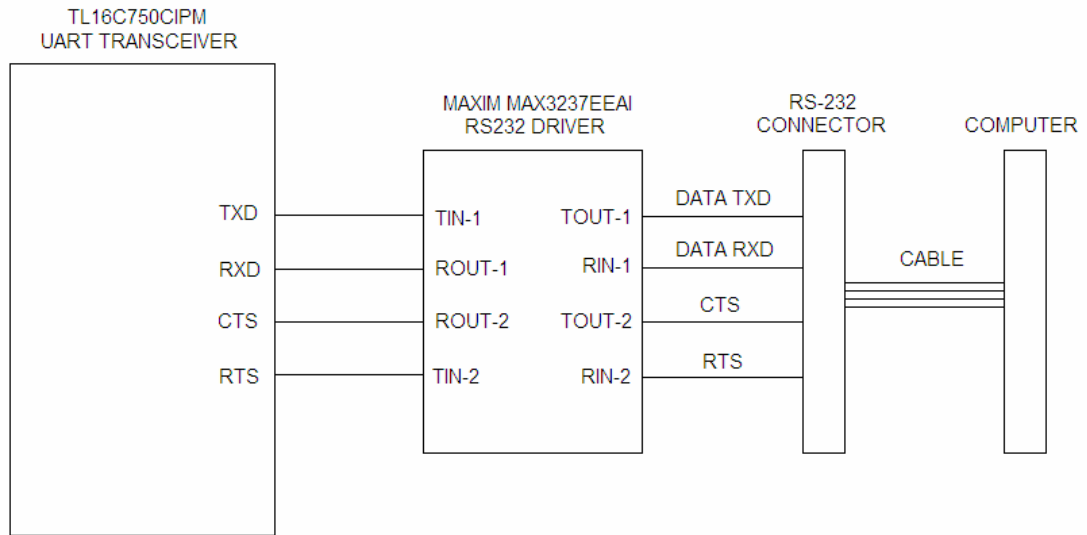


Figure 3.21 – UART Transceiver and Computer Interface

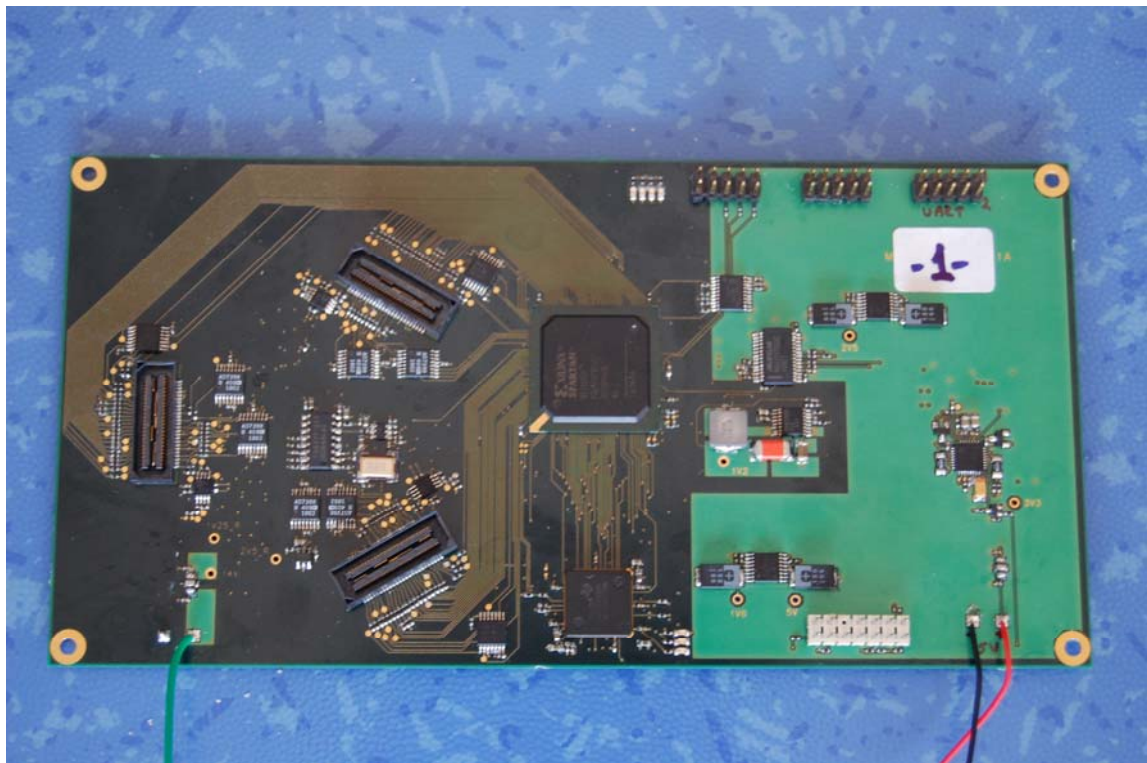


Figure 3.22 – The Processing Board

3.2 Software

The software of the three channel direction finding system is composed of two parts, TMS5509A DSP software and XC3S1000 FPGA software. Digital signal processing is realized by the DSP software whereas buffering the digitized signal data is controlled by the FPGA software.

3.2.1 DSP Software

Reading channel signal data from the dual port RAM of the FPGA, calculating channel signal phase differences, implementing DF algorithms and sending DF results to UART transceiver are conducted by the DSP software. The implemented algorithms in the DSP software are three channel interferometer algorithm, correlative interferometer algorithm and least square error based correlative interferometer algorithm.

DSP program code starts to run by checking which direction finding algorithm is going to be used. The information of the algorithm type is written to the internal data register of the UART transceiver by using external computer interface. When the computer sends the algorithm type data, the internal data ready register in the UART transceiver is refreshed and data is written to the internal data register of the UART transceiver. DSP software continuously polls the internal data ready register of the UART transceiver to determine the computer accesses to the processing board. When the data ready register of the UART transceiver indicates that the computer sends algorithm type information to the processing board, DSP program reads the internal data register of the UART transceiver to designate the algorithm type. The block diagram of this process is shown in Figure 3.23.

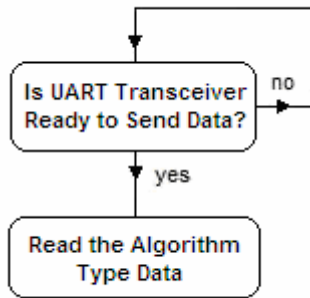


Figure 3.23 – Reading Algorithm Type Data Block Diagram

After the algorithm type is designated, START command is sent to the FPGA. START command is used for starting the data buffering in the FPGA. When the FPGA sends data buffering completed response, DSP sends READ command to the FPGA. READ command is sent to read the buffered data from the FPGA. DSP reads 250 data each of which is 10-Bit long. When all of the 250 data are read, DSP sends STOP command to the FPGA. STOP command indicates the end of the reading process. The block diagram of this process can be seen in Figure 3.24.

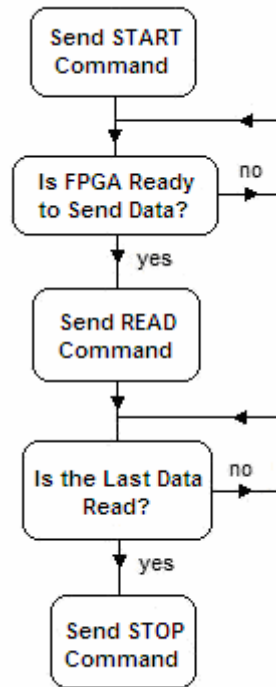


Figure 3.24 – Reading Data From FPGA Block Diagram

After digital signal data are read from the FPGA, DSP starts to find the phase differences of each channel signals by using the correlation matrix. At this part, the processes of digital signal filtering, in-phase and quadrature signal component production and calculations of channel signals phase differences are realized. The block diagram of phase calculation part is shown in Figure 3.25.

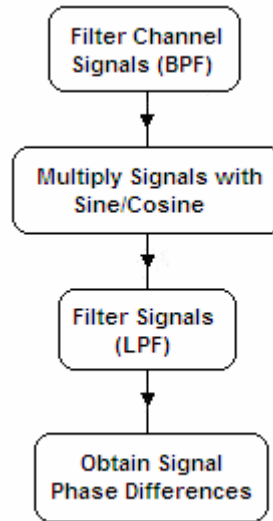


Figure 3.25 – Phase Calculation Block Diagram

To filter the digitized IF signal, a digital bandpass filter is used for each receive channels. For bandpass filtering, a linear phase FIR (finite impulse response) type filter is designed. FIR filters are less sensitive to finite wordlength effects such as coefficient quantization errors and roundoff noise, they have a highly regular structure which is advantageous for the implementation and they are stable [22], so that this type of filter is preferred. Moreover linear phase FIR filters can have exact linear phase response, resulting in a constant group delay over the frequency range of interest. Therefore, no phase distortion is introduced by the filter [23]. The filter is linear phase and type-I which means that the filter coefficients are symmetric and hence the number of the multipliers is reduced by half [24], [25].

The bandpass filter has 95 coefficients and the filter is center at 0.891 normalized frequency value which corresponds to 21.4MHz. The 3dB bandwidth of the bandpass filter is 200KHz. The magnitude response of the digital bandpass filter is shown in Figure 3.26.

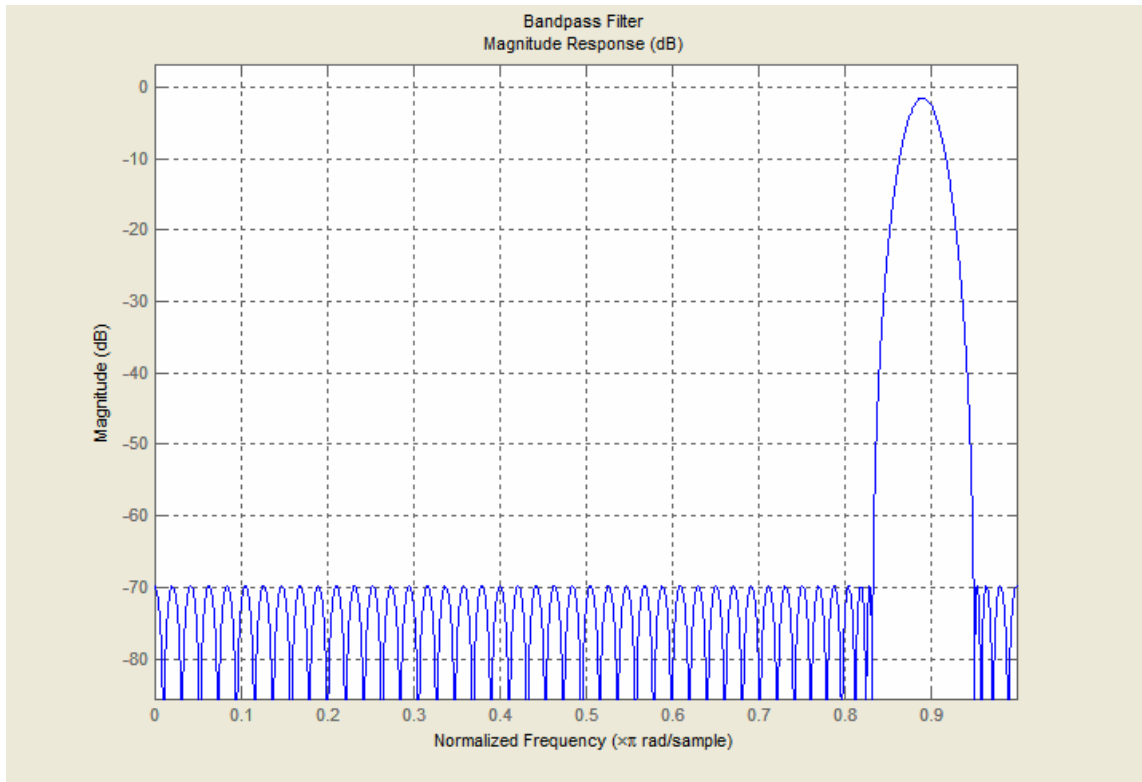


Figure 3.26 – The Magnitude Response of the Digital Bandpass Filter

The impulse response of the digital bandpass filter is shown in Figure 3.27.

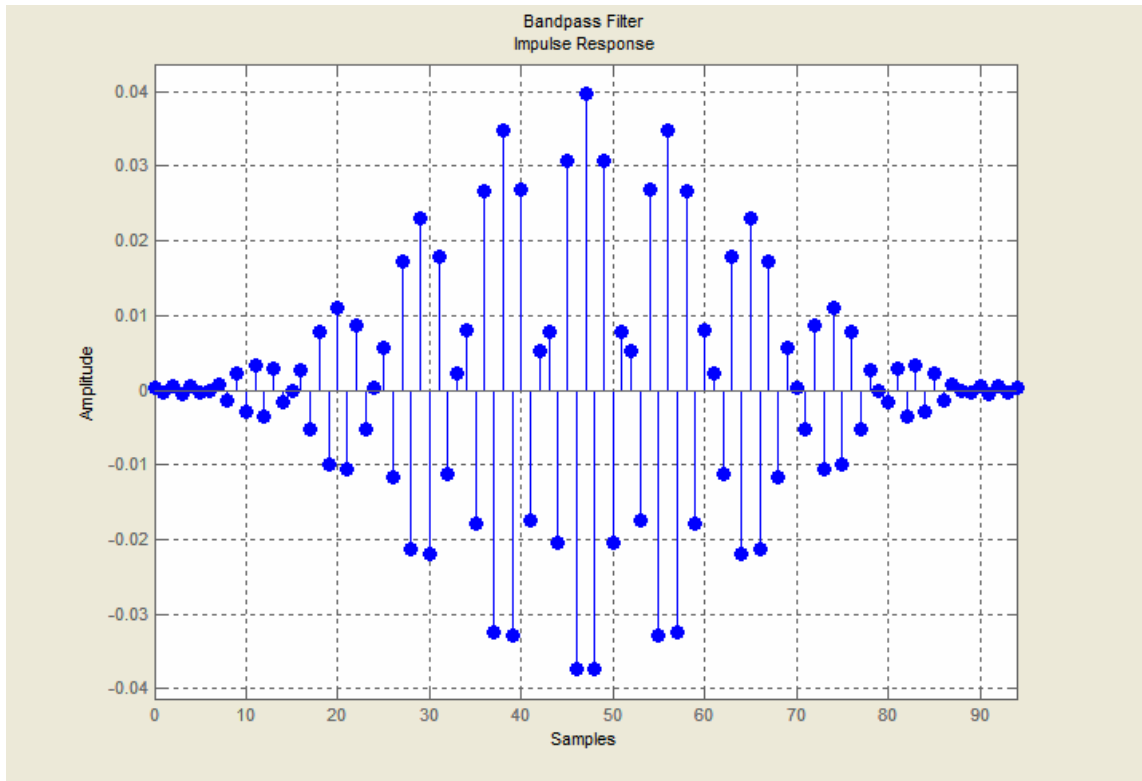


Figure 3.27 – The Impulse Response of the Digital Bandpass Filter

The equation for an FIR filter of length L can be expressed as [23]

$$y(n) = b_0x(n) + b_1x(n-1) + \dots + b_{L-1}x(n-L+1) = \sum_{i=0}^{L-1} b_i x(n-i), \quad (3.3)$$

where $y(n)$ is the filter output, $x(n)$ is the input signal, b_i is the i -th filter coefficient.

Bandpass filtering is realized in DSP software by multiplying filter coefficients with IF signal samples as given in (3.3) [26]. The convolution operation is conducted for all of the three channel signals separately.

For each three channels, the outputs of the bandpass filtering process are divided into in-phase and quadrature components. To obtain in-phase and quadrature components, the signals are multiplied by sine and cosine signals having frequency equal to the center frequency of the signals. After that the outputs of the multiplication are filtered by a digital low-pass filter. The block diagram of this technique can be seen in Figure 3.28.

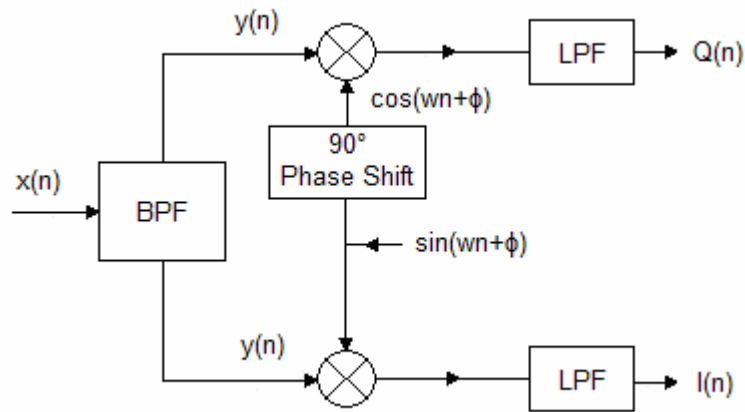


Figure 3.28 – In-phase and Quadrature Component Production

- $x(n)$: the digitized IF signal
- $y(n)$: output of the bandpass filter
- $Q(n)$: quadrature component
- $I(n)$: in-phase component

Each of the bandpass filtered channel signal is multiplied with $\sin(2\pi fn)$ and $\cos(2\pi fn)$ signals whose frequency, f , is 21.4Mhz.

By using the digital filter design tool of the MATLAB, equiripple, type I, linear phase digital lowpass filter is designed [27]. The lowpass filter has 123 coefficients and the magnitude response of the digital lowpass filter is shown in Figure 3.29.

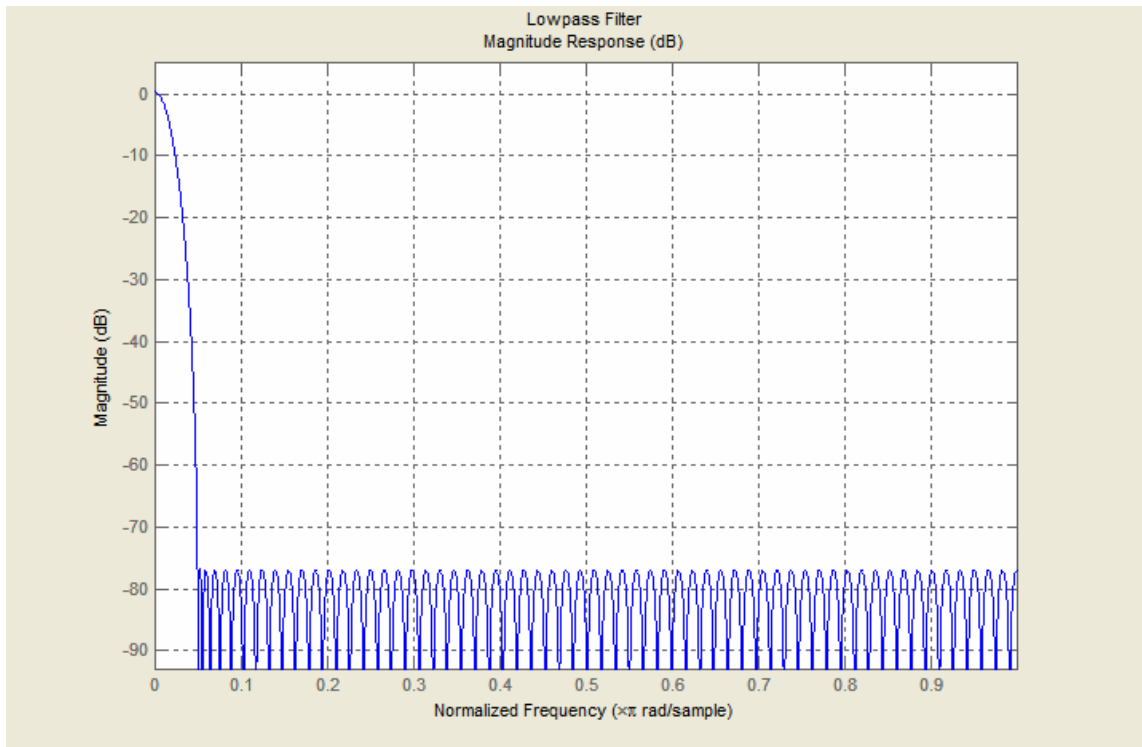


Figure 3.29 – The Magnitude Response of the Digital Lowpass Filter

The impulse response of the digital lowpass filter is shown in Figure 3.30.

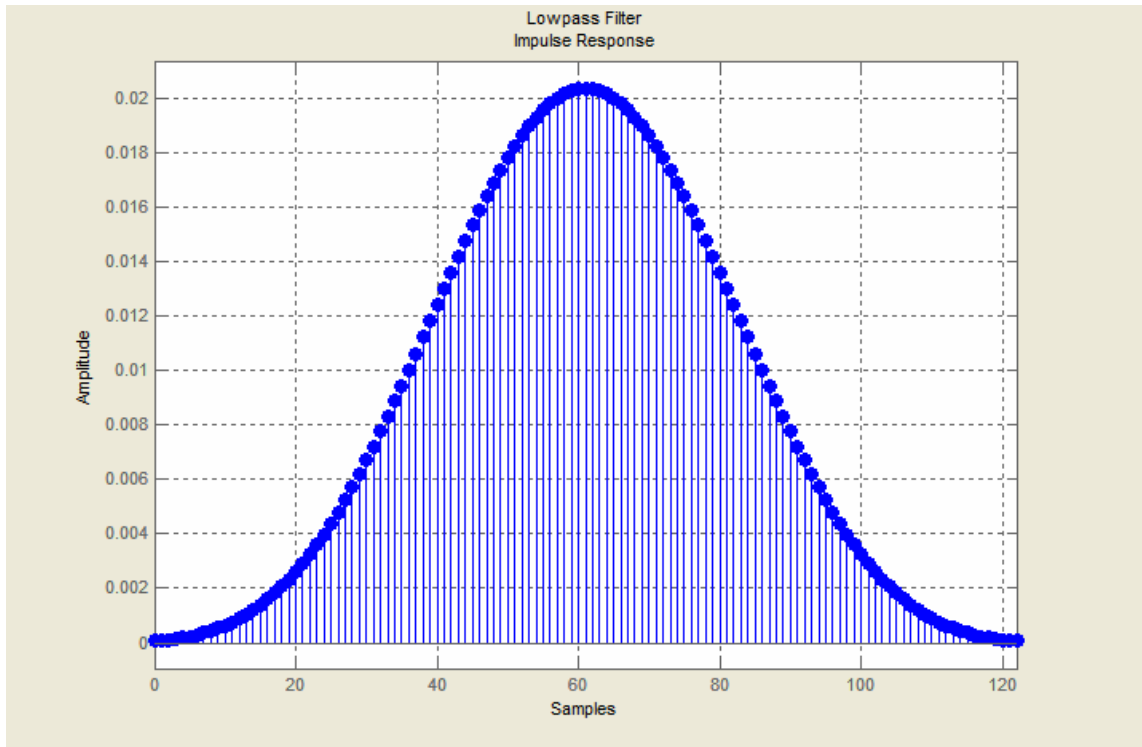


Figure 3.30 – The Impulse Response of the Digital Lowpass Filter

Lowpass filtering is realized in DSP software by using (3.3) and is conducted for all of the three channel signals separately.

After in-phase and quadrature parts of the signals are obtained for each three channels, phase differences between the channel signals can be found by using the autocorrelation matrix of the channel signals.

Produced in-phase and quadrature components are used to represent the receive channel signals as,

$$y_k(t) = I_k(t) + jQ_k(t), \quad (3.4)$$

where $y_k(t)$ is complex data for k th channel, $I_k(t)$ is in-phase component data for k th channel, $Q_k(t)$ is quadrature component data for k -th channel, N is the number of samples, $t = 1, 2, 3, \dots, N$ and $k = 1, 2, 3$.

The array output, $\mathbf{y}(t)$, can be written as,

$$\mathbf{y}(t) = \begin{bmatrix} y_1(t) \\ y_2(t) \\ y_3(t) \end{bmatrix}, \quad t = 1, 2, 3, \dots, N, \quad (3.5)$$

where N is equal to 250.

The output samples can be stacked in a 3×250 output matrix, \mathbf{Y} . The sample covariance matrix of \mathbf{Y} gives the information of channel phase differences.

$$\mathbf{R} = \frac{1}{N} \mathbf{Y} \mathbf{Y}^H, \quad (3.6)$$

where \mathbf{R} is 3×3 sample covariance matrix.

The sample covariance matrix, \mathbf{R} , can be written as

$$\mathbf{R} = \begin{bmatrix} r_{11} & r_{12} & r_{13} \\ r_{21} & r_{22} & r_{23} \\ r_{31} & r_{32} & r_{33} \end{bmatrix}, \quad (3.7)$$

where r_{12} , r_{13} and r_{23} are complex numbers and their phases are equal to phase difference of channel-1 and channel-2 signals, channel-1 and channel-3 signals, channel-2 and channel-3 signals respectively.

Phase differences of the channel signals are calculated by

$$\varphi(i, j) = \arctan\left(\frac{\text{Im}\{r_{ij}\}}{\text{Re}\{r_{ij}\}}\right), \quad (3.8)$$

where the $\varphi(i, j)$ is the phase difference of i -th and the j -th channel signals, r_{ij} is the i -th row and the j -th column element of the sample autocorrelation matrix, R .

After phase calculations are completed, the software starts to implement desired DF algorithm. By using the phase difference information as an input in the algorithm, software finds the DOA of the signal.

Finally the DOA information is sent to UART transceiver for monitoring the result on a computer screen. The block diagram of the whole DSP software can be seen in Figure 3.31.

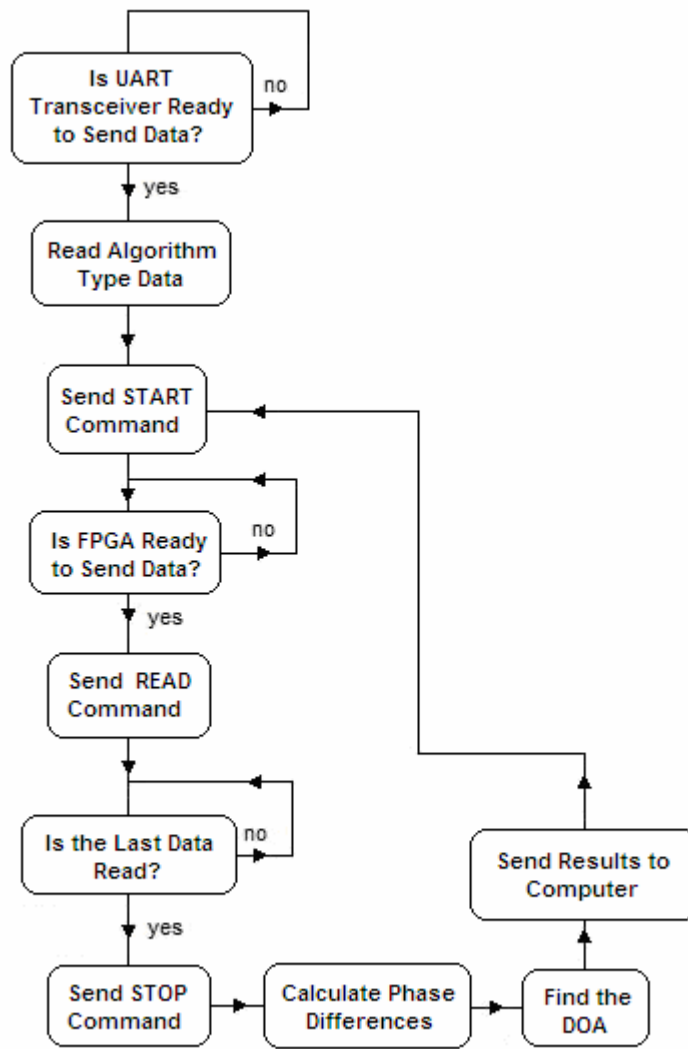


Figure 3.31– DSP Software Block Diagram

3.2.2 FPGA Software

In the FPGA software, the processes of buffering the digitized signal data and transferring the data to DSP are controlled. Digitized signal data are written to internal dual port RAM by using the write process and stored data are sent to the DSP by using the read process. One side of the internal dual port RAM has 10-Bits wide data bus, 13-Bits wide address bus, a clock input, an enable input and a write enable input. Internal

dual port RAM inputs and outputs are connected to write and read processes as shown in Figure 3.32.

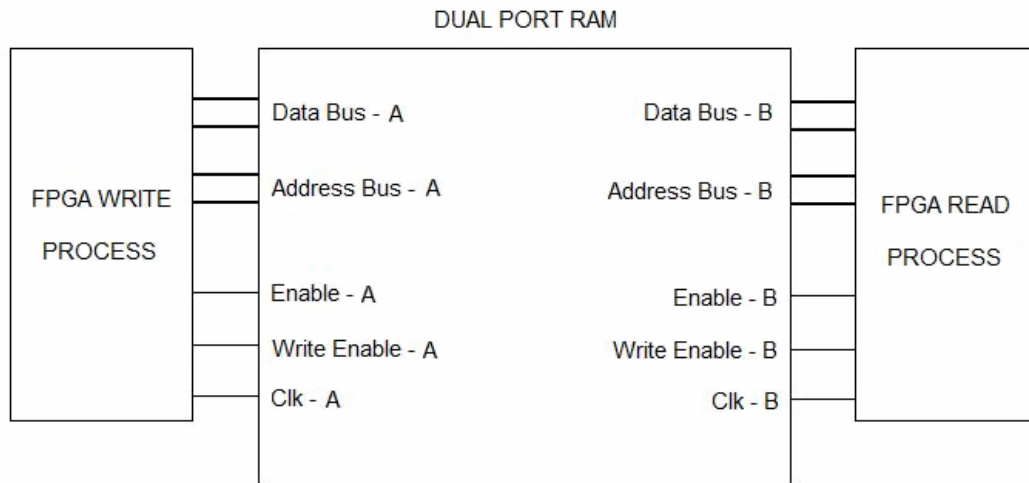


Figure 3.32 – Dual Port RAM

When DSP sends START command, data is written to dual port RAM until the last address of the memory location is reached. The clock input of the dual port RAM is equated to input clock signal of the FPGA so that write process operating clock is equal to the ADC clocks. At every rising edge of the dual port RAM clock, 10-Bits data is written to register which is pointed by dual port RAM address bus. Totally 8192 of 10-Bits data are written to internal registers of the dual port RAM. At the end of the process a ready to send flag is sent to DSP. Ready to send flag indicates that data are stored in the FPGA and they are ready to be sent. The block diagram of the write process is shown in Figure 3.33.

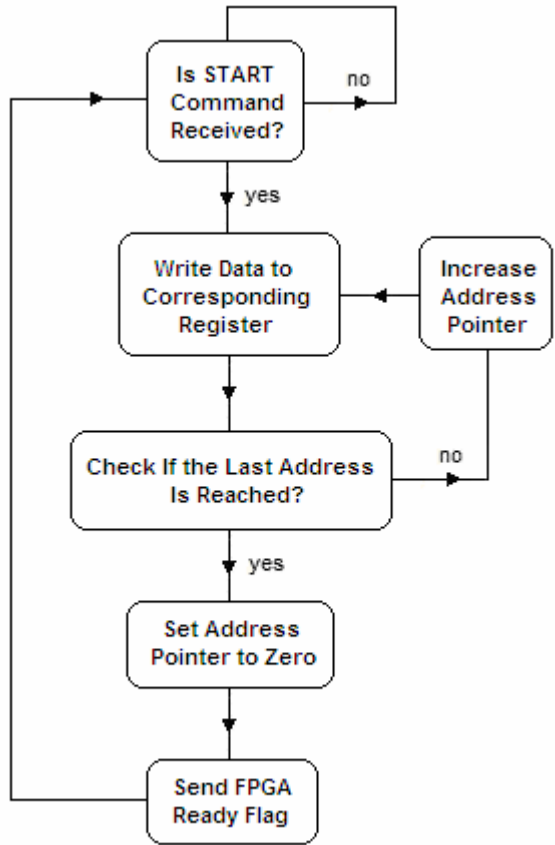


Figure 3.33 – Write Process Block Diagram

When the DSP sends READ command, stored 10-Bits long data are sent to the output of the FPGA. Starting from the address zero, 10-Bits long data are sent to FPGA output until the address 250 is reached. When the last data word is received by the DSP, it sends STOP command which causes dual port RAM to stop sending data. The block diagram of the read process can be seen in Figure 3.34.

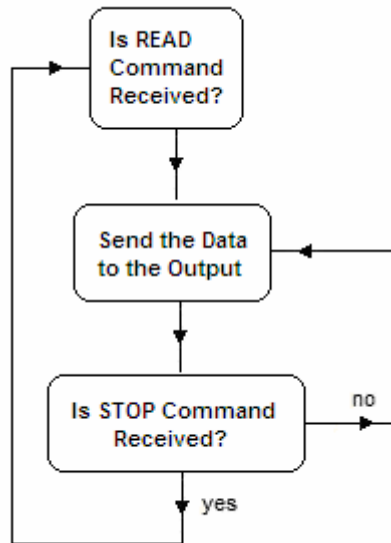


Figure 3.34 – Read Process Block Diagram

To summarize, at every processing cycle DSP reads 250 data which are sampled at 48MHz, for each receive channel. Received data is processed in the DSP and the DOA information is obtained. Then next 250 data for each channel is read and processed by the DSP and a new DOA information is obtained for these 250 samples and the cycle goes on continuously like this. In this method, every 250 data of the channel signals are considered as one sample of the DF system. Consequently, this method is advantageous in that at one moment high number of data is processed.

CHAPTER 4

ANTENNA SYSTEM MEASUREMENTS

In this chapter, the effects of mutual coupling and gain-phase mismatch are considered. Scattering parameters (S-parameters) of three antenna system are determined to understand the mutual coupling effect on the system. Moreover Cramer Rao Bound for the experiment scenario is calculated to determine the limit for DOA accuracy.

In Section 4.1, the mutual coupling effect is studied. The gain/phase mismatch is determined in Section 4.2, the Cramer Rao Bound calculations are given in Section 4.3.

4.1 Mutual Coupling Between Antennas

In a real array, the antennas interact with each other and alter the currents from that which would exist if the elements were isolated. This interaction, called mutual coupling, changes the current magnitude, phase and distribution on each element [28]. Mutual coupling arises due to the interaction of two or more antennas as a result of the elements being in close proximity to each other. This effect is observed during transmission or reception of elements in the array [29]. The effects of the mutual coupling on the performance of a multi antenna system depend upon the antenna type, antenna design parameters, relative positioning of the antennas in the system and radiation characteristics of the antennas [30].

The mutual coupling effect between two antennas is illustrated in Figure 4.1. Assume that a plane wave (θ_0) is incident, and it strikes antenna m first where it causes

current flow. Part of the incident wave will be rescattered into space as (2), the other will be directed toward antenna n as (3) where it will add vectorially with the incident wave (0), and part will travel into its feed as (1). It is then evident that the amount of energy received by each element of an antenna array is the vector sum of the direct waves and those that are coupled to it parasitically from the other element [30].

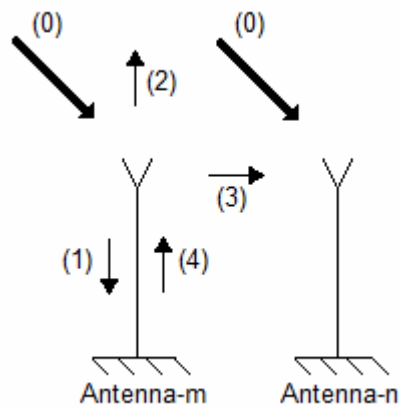


Figure 4.1 – Illustration of the Mutual Coupling Effect

The strength of the coupling decreases as the spacing between the antennas increases [28]. Considering the free space pattern of each element, if the elements are oriented such that they are illuminated by a pattern maximum then the coupling will be appreciable. If, on the other hand, the individual patterns exhibit a null in the direction of the coupled antennas, the coupling will be small [28]. Mutual coupling can be represented by an impedance, admittance, or scattering parameter matrix [31].

To observe the mutual coupling effect on the antennas of the system, scattering parameters, or S-parameters of the antennas are determined. Three antenna configuration shown in Figure 4.2, is characterized by the S-parameters [16].

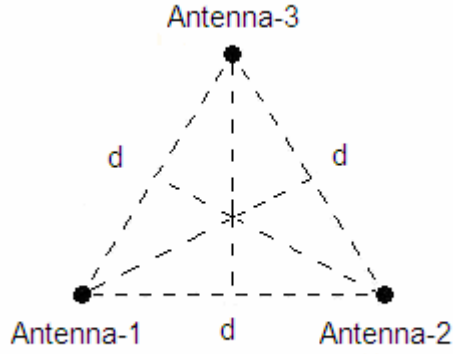


Figure 4.2 –Three Antenna Configuration

As it can be seen from Figure 4.2, antennas form equilateral triangle and d is the length of the antenna spacing.

The scattering matrix which is composed of the S-parameters relates the voltage waves incident on the ports to those reflected from the ports [32]. Scattering matrix of the three port network is determined from the relation,

$$\begin{bmatrix} V_1^- \\ V_2^- \\ V_3^- \end{bmatrix} = \begin{bmatrix} S_{11} & S_{12} & S_{13} \\ S_{21} & S_{22} & S_{23} \\ S_{31} & S_{32} & S_{33} \end{bmatrix} \begin{bmatrix} V_1^+ \\ V_2^+ \\ V_3^+ \end{bmatrix},$$

or

$$\mathbf{V}^- = \mathbf{S} \mathbf{V}^+, \quad (4.1)$$

where V_1^+ , V_2^+ and V_3^+ are the amplitudes of the voltage waves incident on the ports, V_1^- , V_2^- and V_3^- are the amplitudes of the voltage waves reflected from the ports, or, antennas. S_{11} is the antenna-1 reflection coefficient, S_{12} is antenna-2 to antenna-1 transmission coefficient, S_{13} is antenna-3 to antenna-1 transmission coefficient.

A specific element of the scattering matrix can be determined as [32],

$$S_{ij} = \left. \frac{V_i^-}{V_j^+} \right|_{V_k^+ = 0 \text{ for } k \neq j} \quad (4.2)$$

Equation (4.2) says that S_{ij} is found by driving port j with an incident wave of voltage V_j^+ , and measuring the reflected wave amplitude, coming out of port i . The incident waves on all ports except the j th port are set to zero, which means that all ports should be terminated in matched loads to avoid reflections [32].

For three ports network the impedance matrix \mathbf{Z} can be written as,

$$\begin{bmatrix} V_1 \\ V_2 \\ V_3 \end{bmatrix} = \begin{bmatrix} Z_{11} & Z_{12} & Z_{13} \\ Z_{21} & Z_{22} & Z_{23} \\ Z_{31} & Z_{32} & Z_{33} \end{bmatrix} \begin{bmatrix} I_1 \\ I_2 \\ I_3 \end{bmatrix},$$

or in matrix form as

$$\mathbf{V} = \mathbf{Z}\mathbf{I}, \quad (4.3)$$

where \mathbf{V} is the voltage matrix and \mathbf{I} is the current matrix of the ports.

Scattering matrix, \mathbf{S} , can be determined from the \mathbf{Z} matrix. First, it is assumed that the characteristic impedances of all the ports are identical and for convenience they can be set to 1 [32]. The relation between the \mathbf{S} and \mathbf{Z} matrices is [32],

$$\mathbf{S} = (\mathbf{Z} + \mathbf{U})^{-1} (\mathbf{Z} - \mathbf{U}), \quad (4.4)$$

where \mathbf{U} is the identity matrix.

To obtain S-parameters of the antenna system Agilent E5062A Network Analyzer is used. One of the antennas is excited and the coupled signals on the other two antennas are automatically measured by the network analyzer. Antennas are excited one

by one to calculate the S_{11} , S_{12} and S_{13} parameters of the antennas. Measurements are conducted separately when the distance between the antennas, d , is λ and $\lambda/2$.

Besides obtaining the S-parameters of antennas, VSWR and return loss characteristics of the antennas are also examined. The VSWR is calculated by [33],

$$VSWR = \frac{1 + \rho}{1 - \rho}, \quad (4.5)$$

where ρ is the magnitude of the reflection coefficient, S_{11} .

Another parameter is the return loss which is defined as [33],

$$Return Loss = -20 \log(\rho). \quad (4.6)$$

The S-parameters of the antennas for λ and $\lambda/2$ distances at 446MHz are given in Table 4.1.

Table 4.1 – S-parameters of the antennas

antenna distances s-parameters	λ	$\lambda/2$
S_{11}	$-0.429 + 0.047j$ $= 0.4532 \angle 174^\circ$	$-0.464 - 0.008j$ $= 0.4641 \angle -179^\circ$
S_{12}	$(-6.60 - 0.34j) \times 10^{-3}$ $= 6.6102 \times 10^{-3} \angle -177^\circ$	$(-6.75 - 0.23j) \times 10^{-3}$ $= 6.7621 \times 10^{-3} \angle -178^\circ$
S_{13}	$(-6.56 + 0.11j) \times 10^{-3}$ $= 6.5632 \times 10^{-3} \angle 179^\circ$	$(-6.63 - 0.46j) \times 10^{-3}$ $= 6.6514 \times 10^{-3} \angle -176^\circ$

The corresponding voltage standing wave ratio is 2.6598 for λ and 2.7371 for $\lambda/2$. The return loss is 6.878dB for λ and 6.654dB for $\lambda/2$. As it can be seen from Table 4.1, the imaginary parts of the S-parameters are remarkably smaller than the real parts.

The S-parameter matrix of the system for $\lambda/2$ antenna displacement can be written as,

$$S = \begin{bmatrix} -0.464 - 0.008j & (-6.75 - 0.23j) \times 10^{-3} & (-6.63 - 0.46j) \times 10^{-3} \\ (-6.63 - 0.46j) \times 10^{-3} & -0.464 - 0.008j & (-6.75 - 0.23j) \times 10^{-3} \\ (-6.75 - 0.23j) \times 10^{-3} & (-6.63 - 0.46j) \times 10^{-3} & -0.464 - 0.008j \end{bmatrix}. \quad (4.7)$$

The corresponding mutual coupling matrix (MCM) [34] is,

$$C = U - S. \quad (4.8)$$

By using (4.8), the C matrix of the system is found as,

$$C = \begin{bmatrix} 1.464 + 1.008j & (6.75 + 0.23j) \times 10^{-3} & (6.63 + 0.46j) \times 10^{-3} \\ (6.63 + 0.46j) \times 10^{-3} & 1.464 + 1.008j & (6.75 + 0.23j) \times 10^{-3} \\ (6.75 + 0.23j) \times 10^{-3} & (6.63 + 0.46j) \times 10^{-3} & 1.464 + 1.008j \end{bmatrix}. \quad (4.9)$$

When the C matrix is normalized with, $1.464 + 1.008j$, the matrix can be written in the form,

$$C = \begin{bmatrix} 1 & (3.20 - 2.04j) \times 10^{-3} & (3.21 - 1.90j) \times 10^{-3} \\ (3.21 - 1.90j) \times 10^{-3} & 1 & (3.20 - 2.04j) \times 10^{-3} \\ (3.20 - 2.04j) \times 10^{-3} & (3.21 - 1.90j) \times 10^{-3} & 1 \end{bmatrix}. \quad (4.10)$$

4.2 Gain-Phase Mismatch of the Receivers

In this part, the effect of gain-phase mismatch of the receivers is examined to improve the direction finding accuracy of the system. Since the receivers are not exactly matched in terms of the gain and the phase, DOA calculation errors are occurred in the system. To overcome the problem of the gain-phase mismatch, gain and phase differences of the receivers are determined and the system is calibrated.

To measure the gain-phase mismatch of the system, signal transmitter is located in front of the three antennas for three different cases as shown in Figure 4.3. The length of the antenna spacing is $\lambda/2$ and the distance of the transmitter to the center of the antennas, d , is equal to 5.5m (8.18λ). In each measurement case, the signal transmitter is located at a position where the transmitter has an equal distance with two antenna pairs. By this measurement configuration, equal phase and equal gain condition is satisfied for the antenna pairs. In the case-1, gain-phase mismatch of the antenna-1 and antenna-2, in the case-2, gain-phase mismatch of the antenna-2 and antenna-3 and in the case-3 gain-phase mismatch of the antenna-3 and antenna-1 is determined. In each case, phase and the amplitude of the received signals are determined for the antennas so that phase differences and amplitude ratios are obtained.

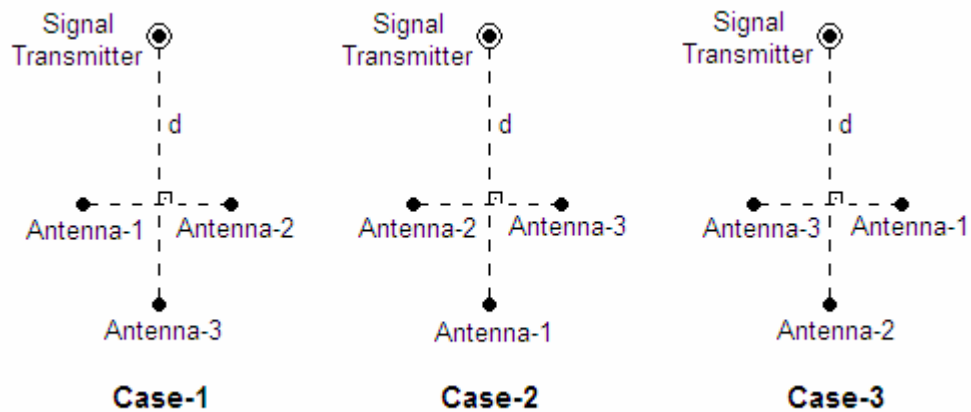


Figure 4.3 – Gain-Phase Mismatch Measurement Configuration

From the measurements phase difference and amplitude ratio of the antennas are determined as given in Table 4.2.

Table 4.2 - The gain-phase mismatch of the system antennas

gain/phase configuration	Phase Difference	Amplitude Ratio
Channel 1-2 (Case-1)	11°	0.961
Channel 2-3 (Case-2)	4°	1.019
Channel 1-3 (Case-3)	7°	0.981

4.3 Cramer Rao Bound Calculation

The Cramer-Rao bound (CRB) is a useful tool for assessing accuracy of parameter estimation methods, as it provides a lower bound on the accuracy of any unbiased estimator [34]. CRB gives the minimum value for the variance of an unbiased estimator [34].

For M-element circular array the CRB is represented [34] as,

$$CRB = \frac{\lambda^2}{8\pi^2 N SNR R^2 \overline{c^2(\phi)}}, \quad (4.11)$$

where N is the number of samples, λ is the wavelength of the signal and R is the radius of the circular array.

In (4.11), the term $\overline{c^2(\phi)}$ [34] is,

$$\overline{c^2}(\phi) = \sum_{m=1}^M \cos^2(\phi - \phi_m), \quad (4.12)$$

where M is the antenna number and θ_m is the angle of the antenna location on the circle.

For uniformly located circular three antenna system $\overline{c^2}(\phi)$ is equal to 1.5, number of the samples, N , is 250, SNR is 34 dB, λ is 0.672 m and R is 0.1939 m. By using (4.11), the CRB is calculated as 1.1933×10^{-5} in radians.

The lower bound for the RMSE of the azimuth angle can be found [34] as,

$$\text{Azimuth, RMSE (Lower Bound)} = \sqrt{\text{CRB}} \times \frac{180}{\pi}. \quad (4.13)$$

From (4.13), the lower bound of the RMSE of the azimuth angle is calculated as 0.198 degrees for the circular three antenna DF system.

CHAPTER 5

PERFORMANCE EVALUATION OF THE DIRECTION FINDING SYSTEM

In this part, the performance test results of the three channel direction finding system are explained and evaluated. Tests are based on finding the DOA by using three channel interferometer algorithm, correlative interferometer algorithm, LSE based correlative interferometer algorithm and MUSIC algorithm. Moreover DOA finding tests are repeated in the cases of multi signal source and reflection (multipath). Test results are evaluated by examining the RMSE of the DOA.

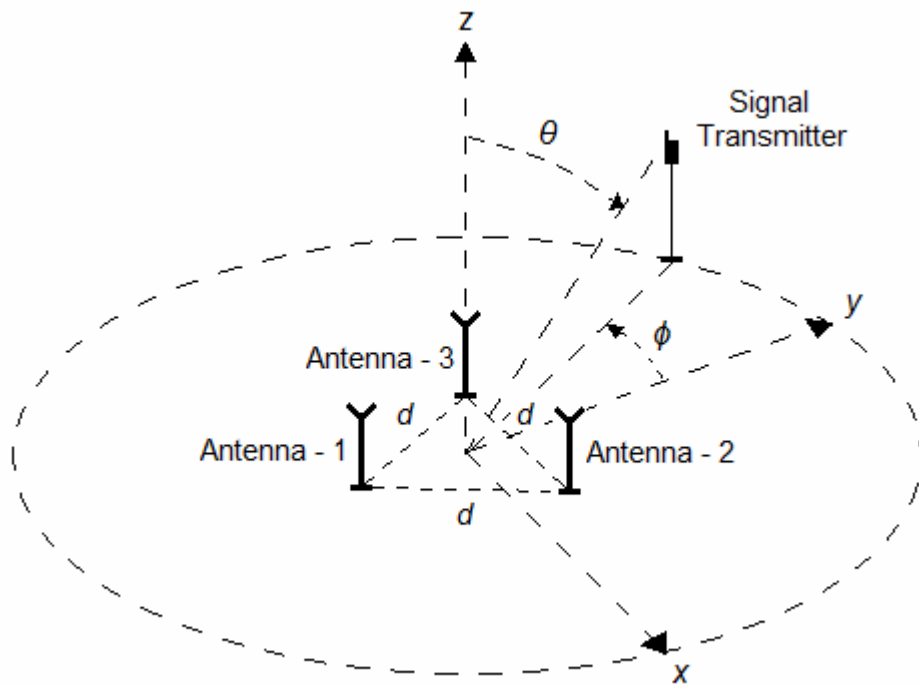
In the DF system, the MUSIC algorithm is realized by using MATLAB. The DF system sends the signal data to the computer so that signal data output of the DF system is processed in a MATLAB code which implements MUSIC algorithm to find the DOA.

Single transmitter test is described in Section 5.1, two transmitters case is explained in Section 5.2. The test results of the multipath case are given in Section 5.3.

5.1 Test Results of the Single Signal Transmitter Case

RMSE of the azimuth and the elevation angles of the DOA are determined in the case of a single transmitter for different algorithms. All of the tests are conducted in the open field area to avoid the environmental reflections. The RMSE of DOA tests and collecting the sample space data for correlative interferometer are realized as shown in Figure 5.1. First, the change in the RMSE of the azimuth and elevation angles of the

DOA is observed for different number of samples. Second, DF performance of the system is determined for different azimuth and elevation DOA angles. All of the tests are conducted for correlative interferometer algorithm, LSE based correlative interferometer algorithm, three channel interferometer algorithm, MUSIC algorithm and mutual coupling matrix (MCM) compensated MUSIC algorithm separately. The exact DOA of the signal is determined by using portable angle measurement apparatus as shown in Figure 5.2. The direction finding system test setup can be seen in Figure 5.3.



ϕ : azimuth angle
 θ : elevation angle
 d : length of the antenna spacing

Figure 5.1 – Test Setup of the Three Antenna DF System

While the sample space for the correlative interferometer algorithm is being formed, the transmitter is located at 5.5m (8.18 λ) far away from the origin of the

antennas and its frequency is 446MHz. The transmitter is moved with $\Delta\phi=5^\circ$ steps covering 360° azimuth angle and $\Delta\theta=7.5^\circ$ steps covering 15° elevation angle ranges, consequently, the sample space production process is realized in 216 steps.



Figure 5.2 – Three Antenna DF System with Angle Measurement Apparatus



Figure 5.3 – Three Antenna Direction Finding System and Signal Transmitter

In the first test, the transmitter is located 5.5m (8.18λ) away from the origin of the antennas to ensure far field. Azimuth and elevation angle values are calculated for different number of samples from 1 to 250 when the transmitter is placed at 0° azimuth and 90° elevation angle with respect to the origin axis of the system. RMSE values of the calculated azimuth and elevation angles are determined for all of the DF algorithms. By using the test results, the RMSE of the azimuth and elevation angles versus number of samples graphs are obtained. Azimuth and elevation RMSE versus number of samples test parameters are given in Table 5.1.

Table 5.1 – Angle RMSE versus number of samples test parameters

Transmitter Frequency	446MHz
SNR	34dB
Signal Source Distance	5.5m (8.18 λ)
Azimuth Angle	0°
Elevation Angle	90°

The RMSE of the azimuth angle versus number of samples graph is shown in Figure 5.4. As it can be seen from Figure 5.4, the azimuth error decreases and converges to a certain value when the number of the samples increases. Because of the mutual coupling effect, gain/phase mismatch of the receivers, non-ideal device accuracy and the signal reflections, the azimuth error does not drop under a certain value even if the number of the samples is increased above the value of 100.

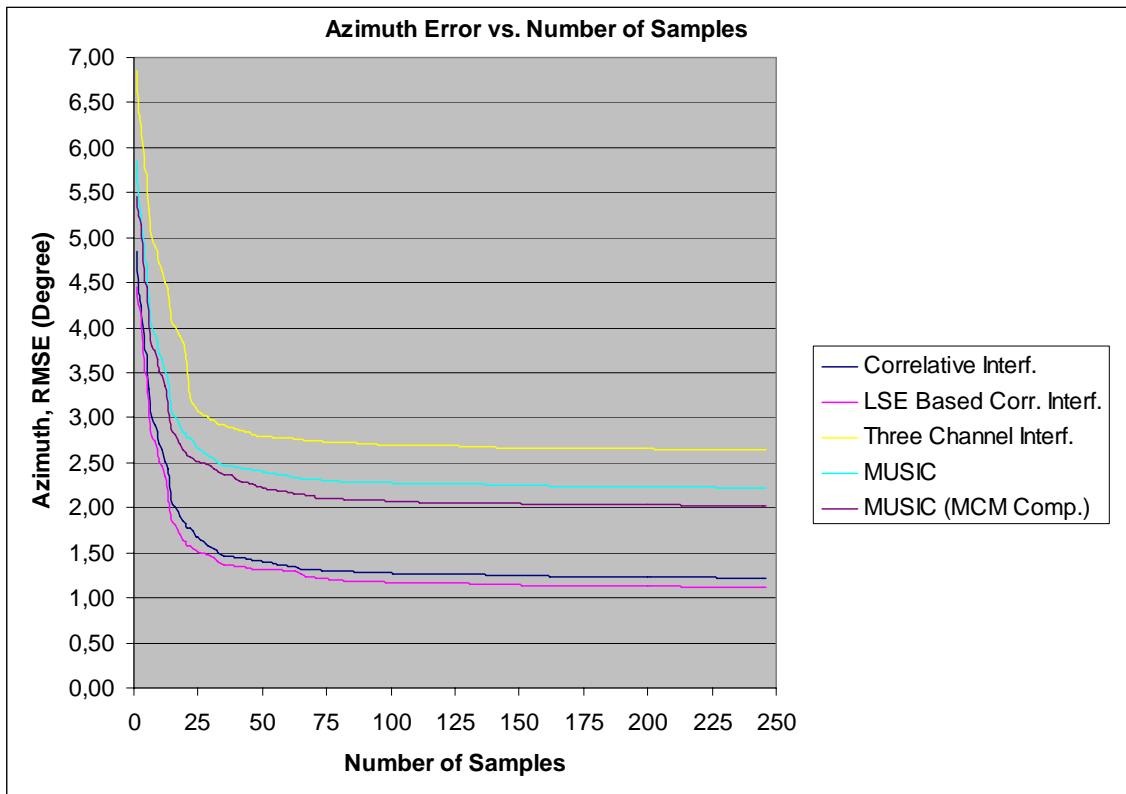


Figure 5.4 – RMSE of Azimuth Angle versus Number of Sample Graph

The RMSE of the elevation angle versus number of samples graph is shown in Figure 5.5. Similar to the azimuth angle error, the elevation error drops when the number of the samples is increased and the elevation error converges to a non-zero value.

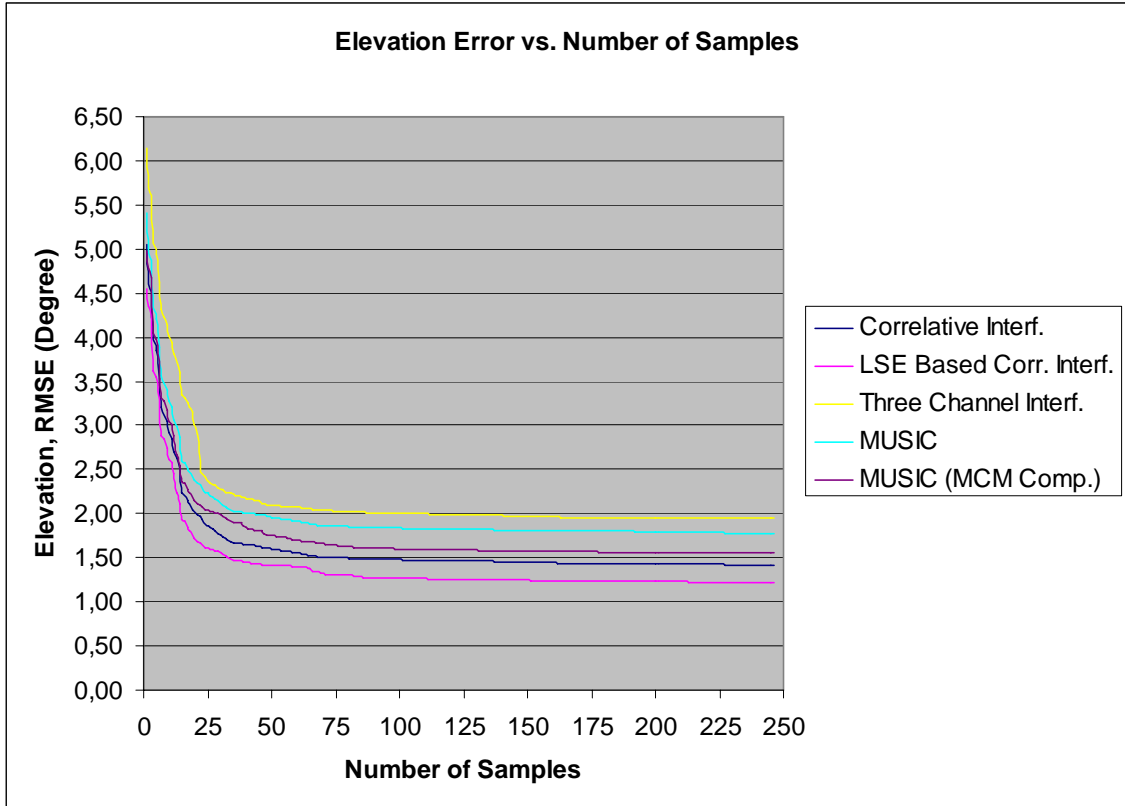


Figure 5.5 – RMSE of Elevation Angle versus Number of Sample Graph

In the second test, the placement of the transmitter is changed for different directions around the DF system. The distance of the transmitter to the system is 5.5m (8.18λ) away from the origin of the antennas. The transmitter is moved with 20° azimuth angle and 5° elevation angle steps for 0° - 360° azimuth and 90° - 70° elevation angle ranges respectively. In this test, it is aimed to observe the performance of the DF system for different azimuth and elevation angle values. Angle RMSE versus DOA test parameters are given in Table5.2.

Table 5.2 – Angle RMSE versus DOA test parameters

Transmitter Frequency	446MHz
SNR	34dB
Signal Source Distance	5.5m (8.18 λ)
Number of Samples	100

The RMSE of the azimuth angle versus DOA graph is shown in Figure 5.6. In this test, the elevation angle is 90° for the transmitter. As it can be seen from Figure 5.6, DF results of the correlative interferometer and the LSE based correlative interferometer algorithms are more accurate than the other algorithms. Although the accuracy of the correlative and LSE based correlative interferometer algorithms are close to each other, it is observed that the LSE based correlative interferometer algorithm is more accurate than the correlative interferometer algorithm. The DF error of the MCM compensated MUSIC algorithm is less than that of the uncompensated MUSIC algorithm because the effect of the mutual coupling is decreased in the MCM compensated MUSIC algorithm.

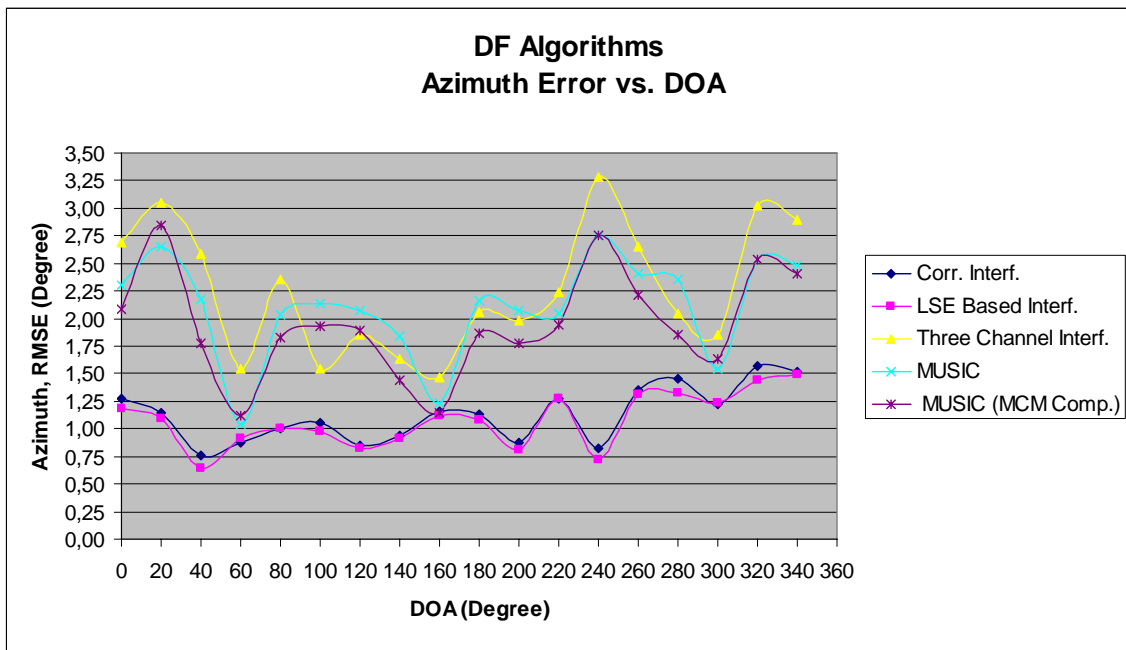


Figure 5.6 – RMSE of Azimuth Angle versus DOA Graph

The RMSE of the elevation angle versus DOA graph is shown in Figure 5.7. In this test, the azimuth angle of the transmitter is 0° . The elevation angle accuracy of the correlative interferometer and the LSE based correlative interferometer algorithm is higher than the that of other algorithms. Moreover, it can be seen that the elevation error of the MCM compensated MUSIC algorithm is slightly less than the uncompensated MUSIC algorithm at most of the azimuth points. However, it is observed that the mutual coupling compensation can not be achieved remarkably.

In the S-parameter method, the receiving or transmitting antenna array is modeled as an N-port network and the mutual coupling between antenna elements is modeled using scattering parameters [35]. Once the S-parameters are all determined, the decoupled signals can be computed from the coupled measurable terminals signals [35]. However, by using this method, only the transmitting array is modeled correctly with respect to the handling of the mutual coupling effect [35]. For a receiving array, because the definition of S-parameters requires that the antenna elements be driven by an active source connected at the terminals of one of the antennas array, it fails to correctly model the array whose antenna elements are all driven by an external source outside the array [35]. The consequence of this method is that the mutual coupling in the receiving array is independent of the external source which is incorrect [35]. Moreover, the S-parameter method does not take into account the terminal loads which actually affect the current distributions and which in turn affect the mutual impedance so calculated [36].

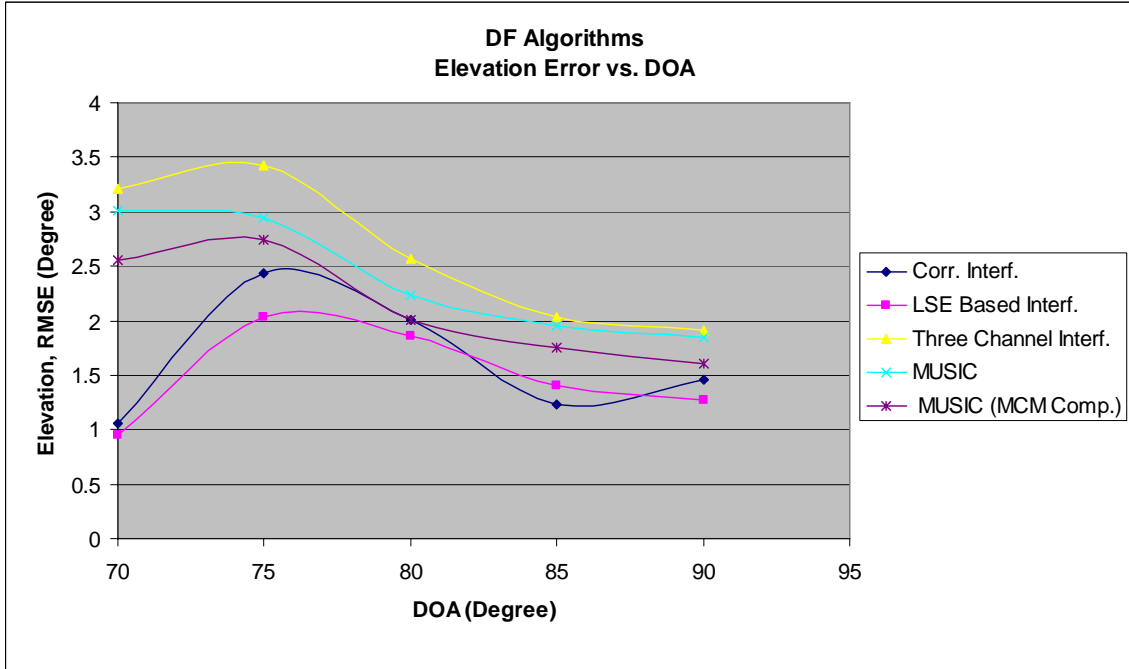


Figure 5.7 – RMSE of Elevation Angle versus DOA Graph

The performance of the correlative interferometer and the LSE based correlative interferometer DF algorithms are related to the number of sample space elements which is increased by interpolation. To observe the effect of the interpolation, the RMSE value of azimuth and elevation angles are determined for different interpolation values. For the 1° , 0.9° , 0.8° , 0.7° , 0.6° and 0.5° sample space angle steps, DF results of the correlative interferometer and LSE based correlative interferometer algorithm are calculated. Angle RMSE versus sample space angle step test parameters are given in Table 5.3.

Table 5.3 – Angle RMSE versus sample space angle step test parameters

Transmitter Frequency	446MHz
SNR	34dB
Signal Source Distance	5.5m (8.18λ)
Azimuth Angle	0°
Elevation Angle	90°

The RMSE of the azimuth angle versus sample space angle step graph is shown in Figure 5.8. When the sample space angle step is decreased, it is seen that the RMSE of the azimuth angle decreases. The accuracy of the sample space is increased when the sample space angle step is decreased so that the RMSE of the azimuth angle decreases. It is seen from Figure 5.8 that after the sample space angle step drops below the value of 0.8° , the RMSE of the azimuth angle reaches a value of 1.282° for the correlative interferometer algorithm and 1.194° for the LSE based correlative interferometer algorithm.

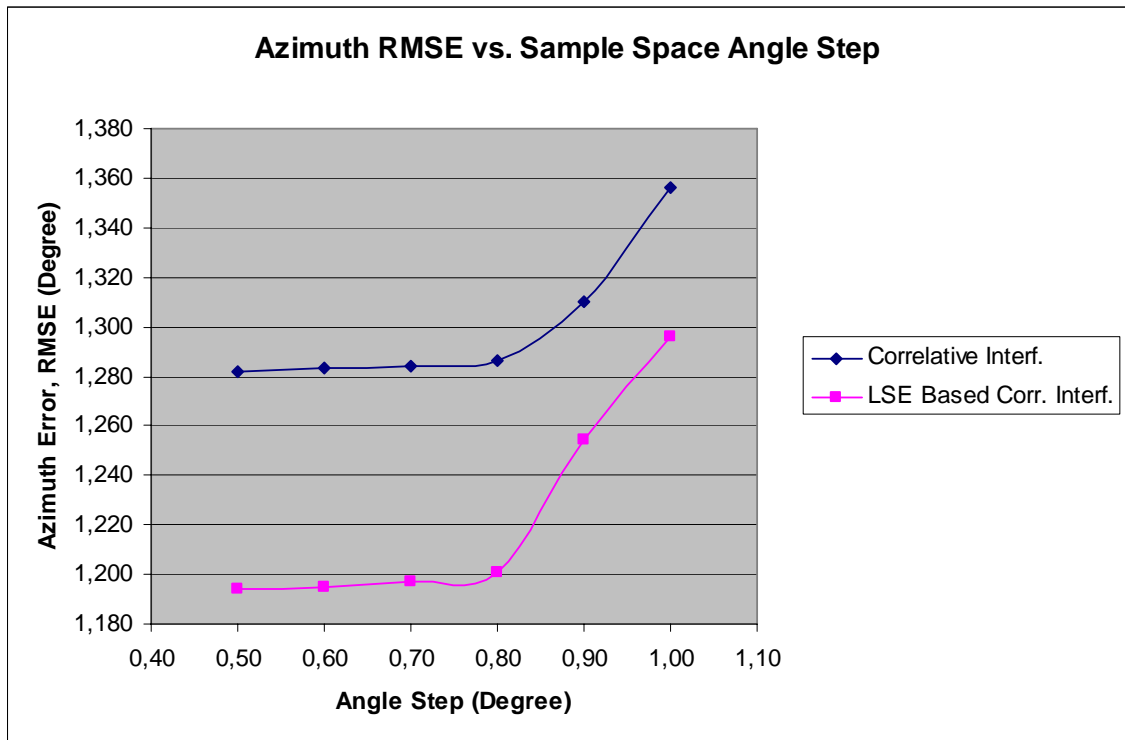


Figure 5.8 – RMSE of Azimuth Angle versus Sample Space Angle Step Graph

The RMSE of the elevation angle versus sample space angle step graph is shown in Figure 5.9. The RMSE of the elevation angle decreases when the number of elements in the sample space is increased. The drop in the RMSE of the elevation angle nearly stops when the sample space angle step is decreased below to the value of 0.8° .

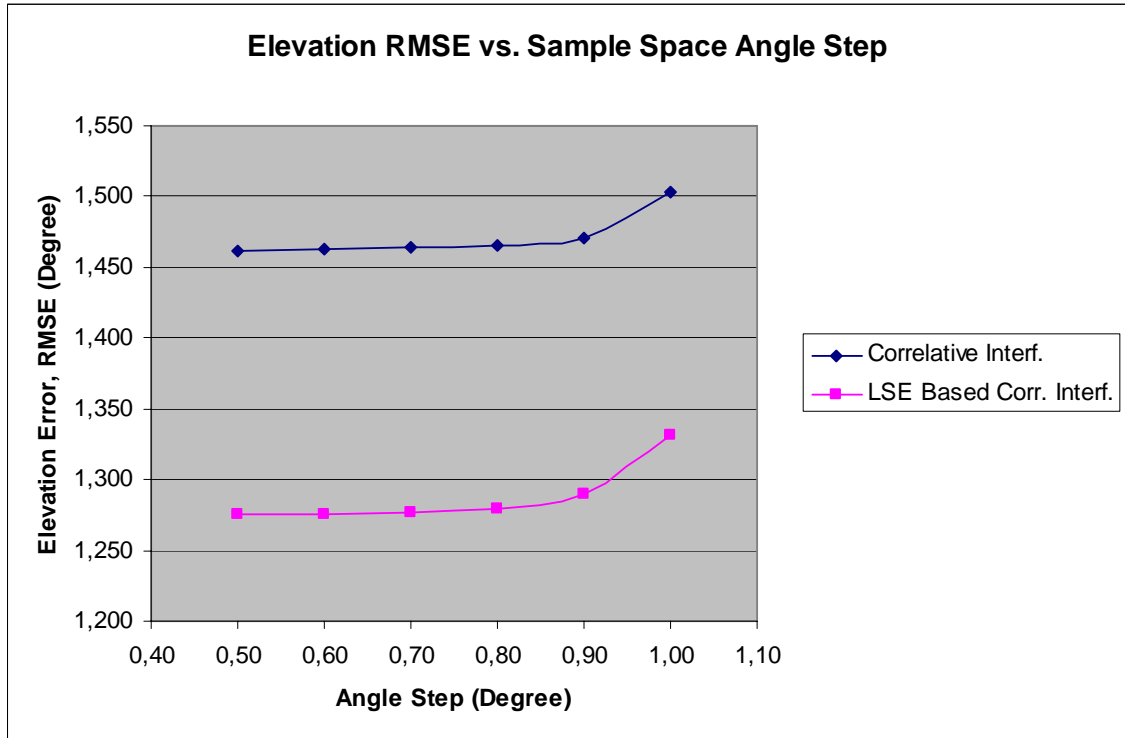


Figure 5.9 – RMSE of Elevation Angle versus Sample Space Angle Step Graph

From Figure 5.8 and Figure 5.9, it is seen that the interpolation improves the DF accuracy. The RMSE values of the azimuth and the elevation angles drop until the sample space angle step is decreased to the value 0.8° .

5.2 Test Results of Two Signal Transmitter Case

In the two signal transmitter case, changes in the direction finding performance of the algorithms are examined by using two transmitters. One of the transmitters is located at a fixed point and the other one is moved on the circle whose center is at the origin of the system. RMSE of direction of arrival for each algorithm is observed when there are two transmitters in the system.

First transmitter is placed at 0° azimuth and 90° elevation angle with respect to the origin of the system coordinates and the other transmitter is moved with 20° azimuth angle and 5° elevation angle steps for 0° - 360° azimuth and 90° - 70° elevation angle ranges respectively. The illustration of the two transmitters test is shown in Figure 5.10. The distance of the transmitters to the system is 5.5m (8.18λ) away from the origin of the antennas. Angle RMSE versus DOA test parameters for two transmitter case are given in Table 5.4.

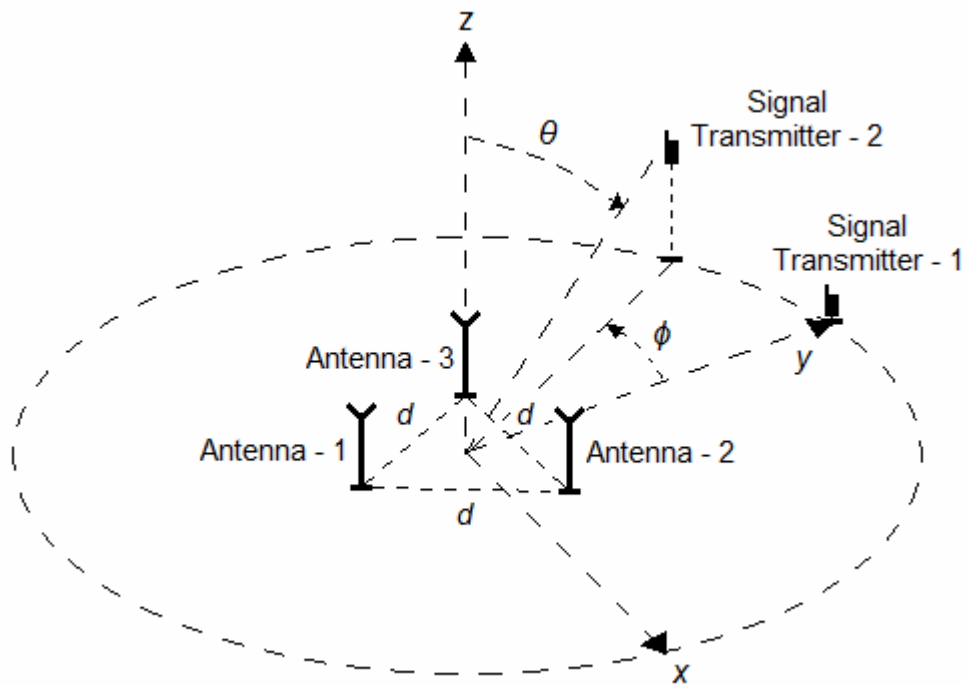


Figure 5.10 – Illustration of Two Transmitters Test Setup

Table 5.4 – Angle RMSE versus DOA test parameters for two transmitter case

Transmitter Frequency	446MHz
SNR	34dB
Signal Source Distance	5.5m (8.18 λ)
Number of Samples	100
Position of The First Transmitter	0° azimuth 90° elevation

The RMSE of the azimuth angle versus DOA graph is shown in Figure 5.11. In this test, the elevation angle of the transmitter is 90°. The MUSIC algorithm is more accurate than the other algorithms for the two transmitters case. MUSIC algorithm can indicate the locations of the transmitters. When the transmitters are close to each other, the RMSE of the azimuth angle decreases for the correlative interferometer algorithm, LSE based correlative interferometer algorithm and three channel interferometer algorithm.

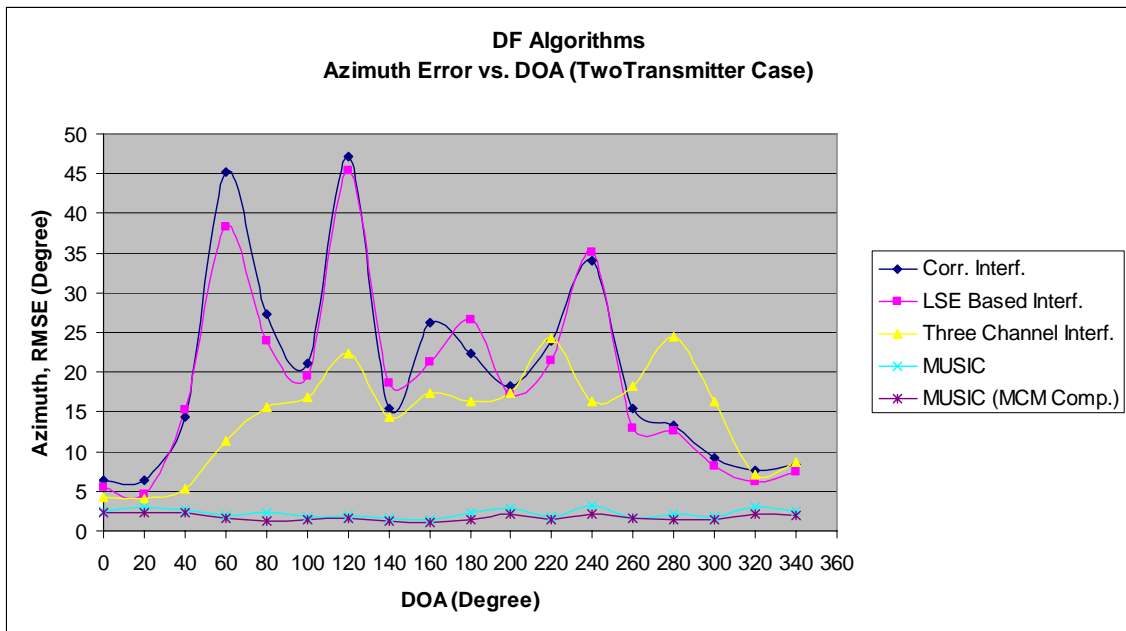


Figure 5.11 – RMSE of Azimuth Angle versus DOA Graph

The RMSE of the elevation angle versus DOA graph is shown in Figure 5.12. In this test, the azimuth angle of the transmitter is 0° . MUSIC algorithms have less RMSE of elevation angle than the other algorithms. MCM compensated MUSIC algorithm is the most accurate one. When the second transmitter becomes closer to the first transmitter at 90° elevation angle, the RMSE of the elevation angle decreases for the correlative interferometer algorithm, LSE based correlative interferometer algorithm and three channel interferometer correlative algorithm.

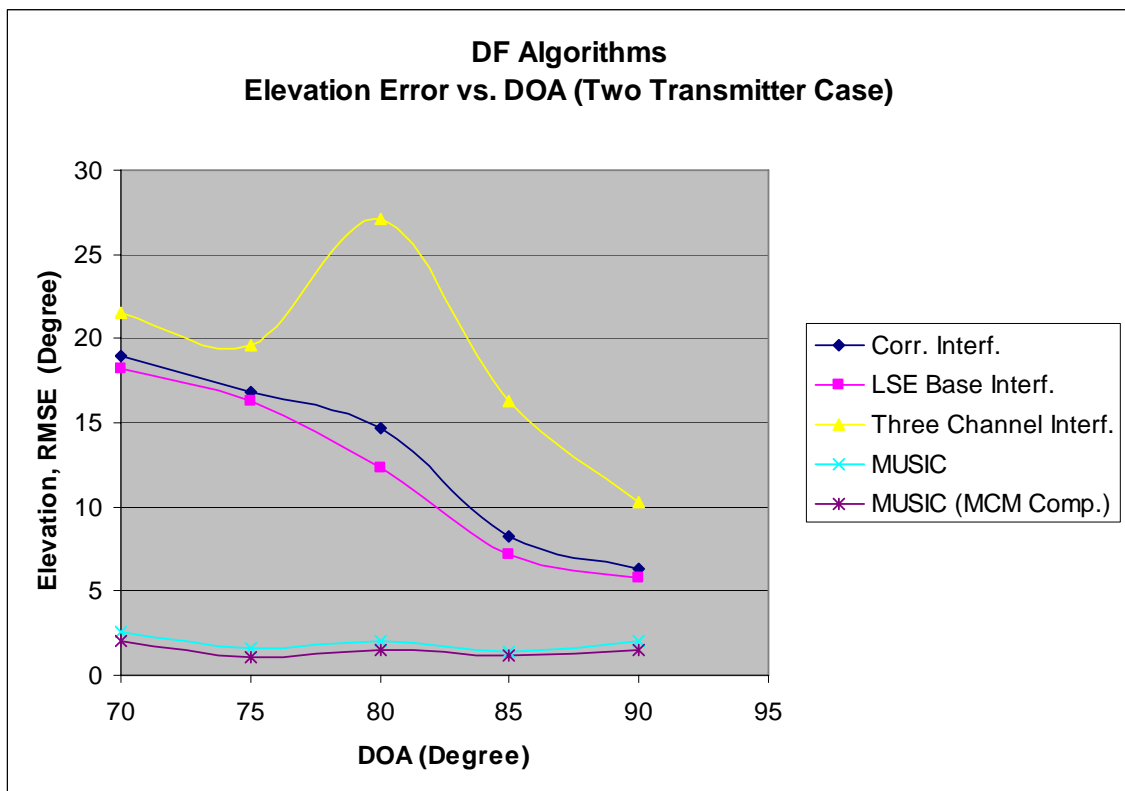


Figure 5.12 – RMSE of Elevation Angle versus DOA Graph

5.3 Test Results of Multipath Case

DOA tests are also conducted when there is a reflection in the system. As shown

in Figure 5.13, a metal plate is located near the system so that reflection signal path can be simulated. The differences in the DOA finding performance of the algorithms are examined by observing the RMSE of the DOA.

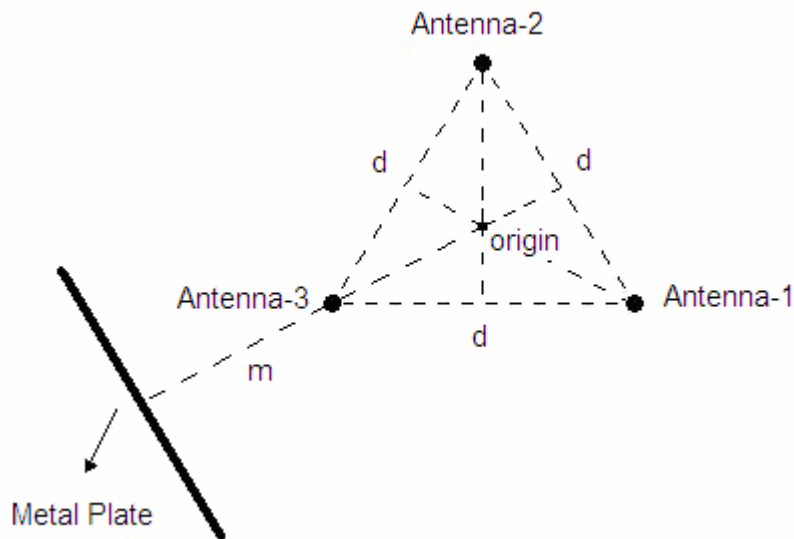


Figure 5.13 – Metal Plate Placement Near the Antennas

In Figure 5.13, m is the distance of the metal plate to the origin of the antennas. The dimension of the metal plate is 50cm x 50cm. The metal plate is placed at different m distance to observe the change in the DF performance of the system under the multipath effect. The plate is located at 80cm, 120cm, 160cm and 200cm distances so that the multipath sensitivity of the DF system can be determined for different steps. The plate is placed at 60° azimuth angle and 90° elevation angle with respect to the origin of the antennas. The illustration of the multipath signal test is shown in Figure 5.14. Angle RMSE versus DOA test parameters for multipath signal case are given in Table 5.5. In the azimuth angle graphs, the elevation angle of the transmitter is 90° . In the elevation angle graphs, the azimuth angle of the transmitter is 0° .

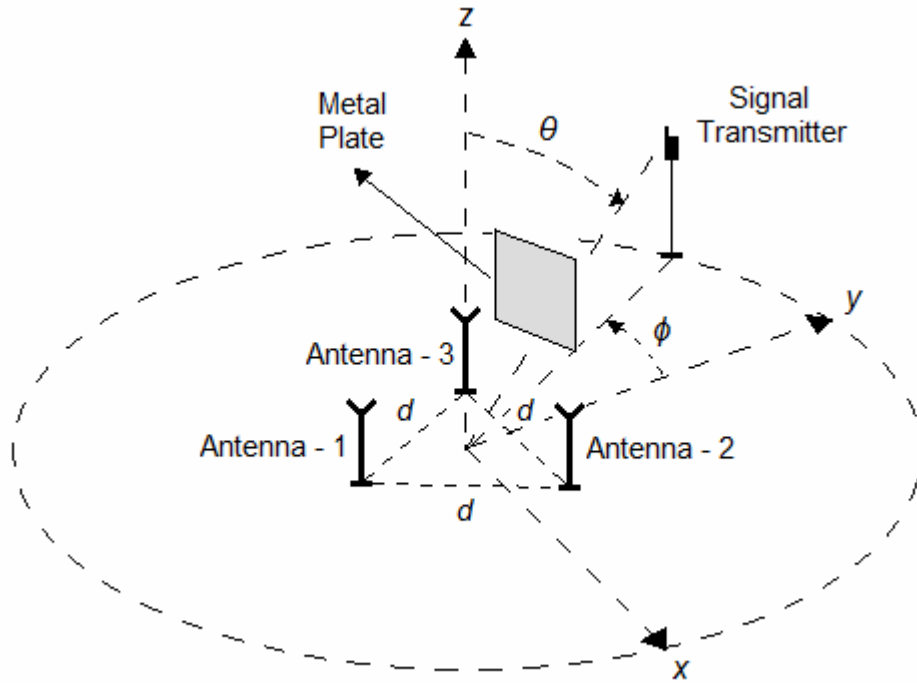


Figure 5.14 – The Illustration of the Multipath Signal Test Setup

Table 5.5 – Angle RMSE versus DOA test parameters for multi signal path case

Transmitter Frequency	446MHz
SNR	34dB
Signal Source Distance	5.5m (8.18 λ)
Number of Samples	100

The RMSE of the azimuth angle versus DOA and the RMSE of the elevation angle versus DOA graphs are shown in Figure 5.15 and Figure 5.16 respectively. In this case, the plate is located at 80cm far away from the origin ($m=80\text{cm}$). It is observed that the RMSE of the azimuth and the elevation angles increase drastically for all of the algorithms. Since the metal plate is located at 60° azimuth angle, the transmitter is placed at the backside of the metal plate when the DOA is 60° azimuth angle.

Consequently, it is seen that at that location of the transmitter, the RMSE of the azimuth angle for all the algorithms is higher than the azimuth angle error at other positions.

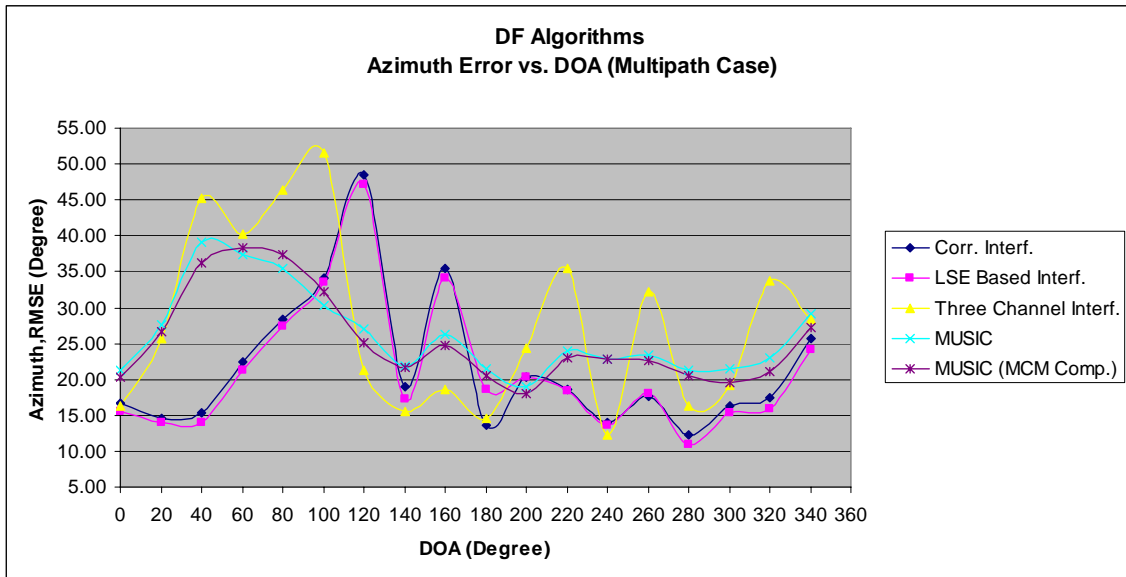


Figure 5.15 – RMSE of Azimuth Angle versus DOA Step-1 Graph

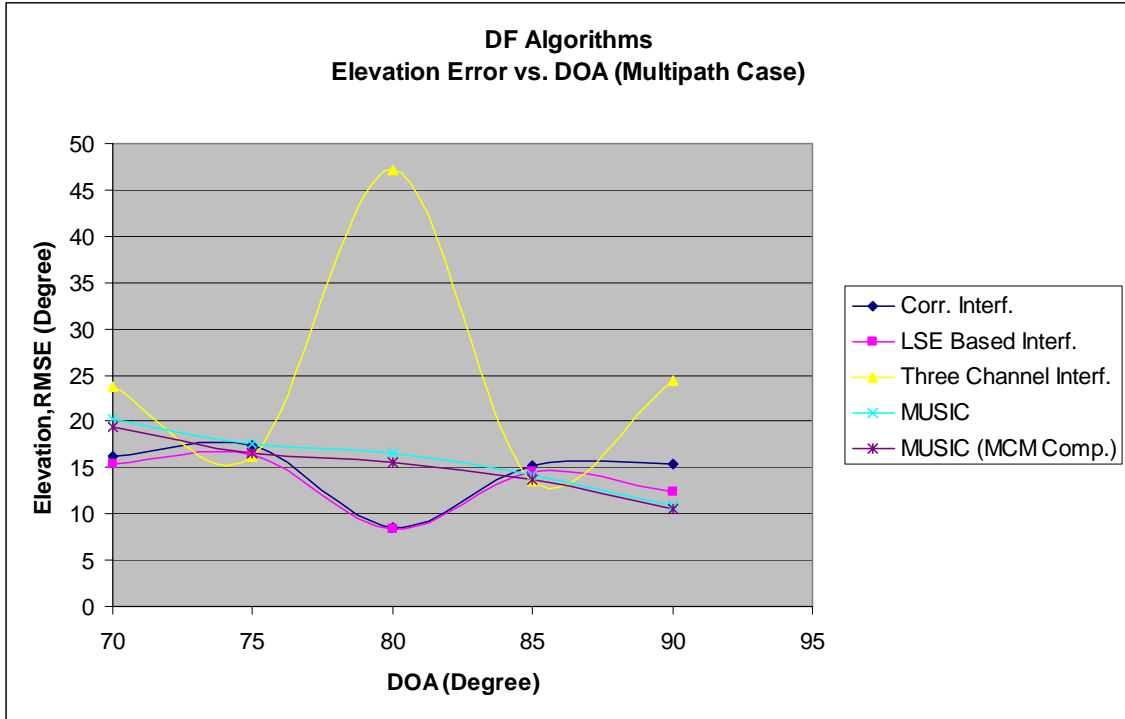


Figure 5.16 – RMSE of Elevation Angle versus DOA Step-1 Graph

When the plate is located at 120cm far away from the origin ($m=120\text{cm}$), the RMSE of the azimuth and the elevation angle decreases for all of the DF algorithms with respect to the previous step. The RMSE of the azimuth angle versus DOA and the RMSE of the elevation angle versus DOA graphs are shown in Figure 5.17 and in Figure 5.18.

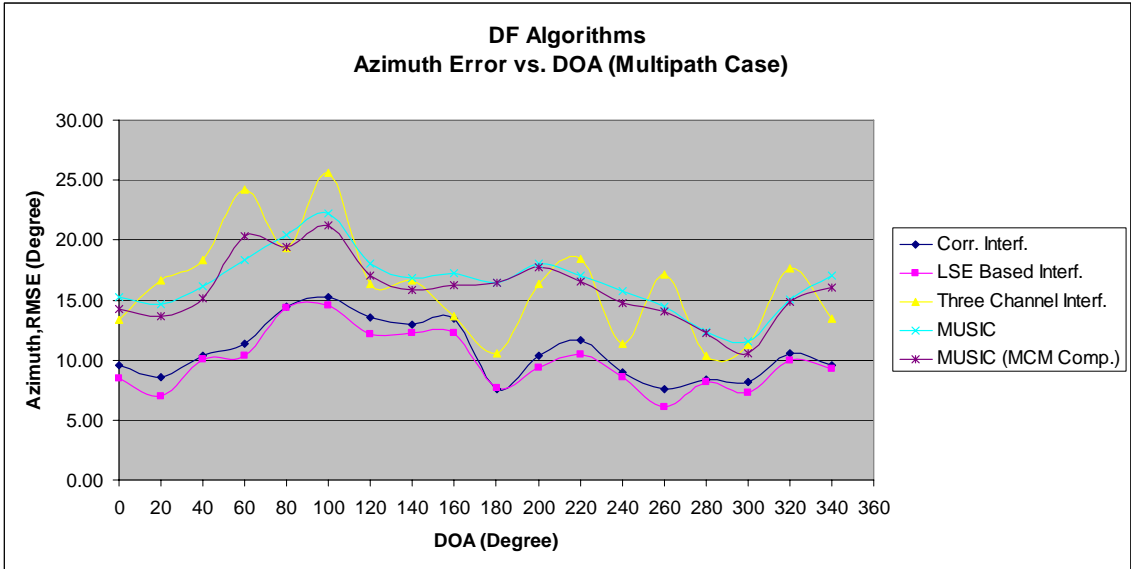


Figure 5.17 – RMSE of Azimuth Angle versus DOA Step-2 Graph

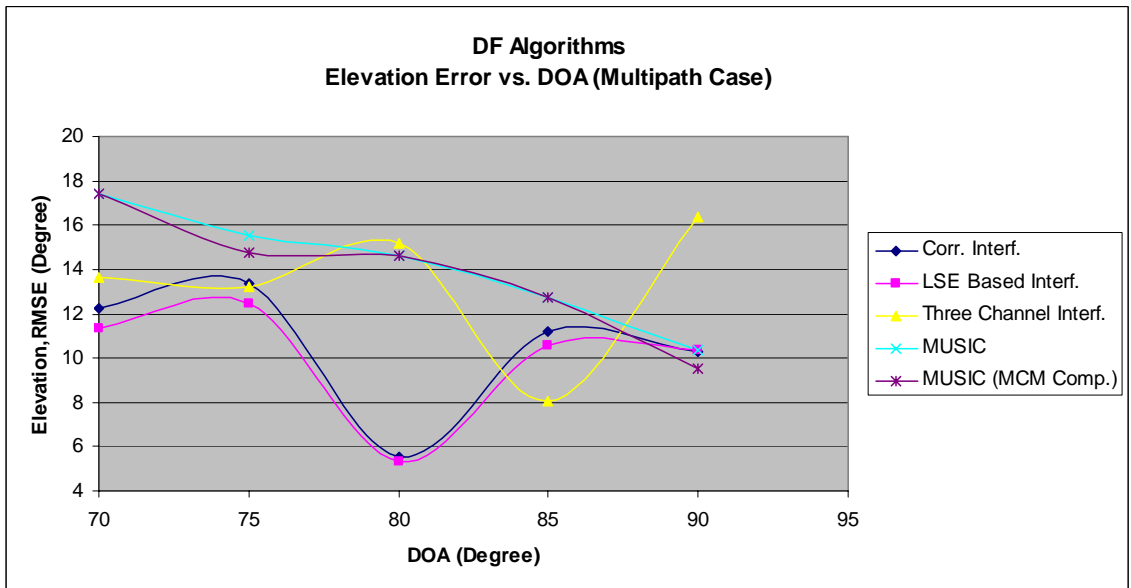


Figure 5.18 – RMSE of Azimuth Angle versus DOA Step-2 Graph

The RMSE of the azimuth angle versus DOA graph for $m=160\text{cm}$ is shown in Figure 5.19. In this step, it is seen that the RMSE of the azimuth and the elevation angle continues to decrease for the DF algorithms. Moreover, the effect of the metal plate at 60° azimuth angle is observed clearly especially for the correlative interferometer and

LSE based correlative interferometer algorithms. The RMSE of the elevation angle versus DOA graph is shown in Figure 5.20.

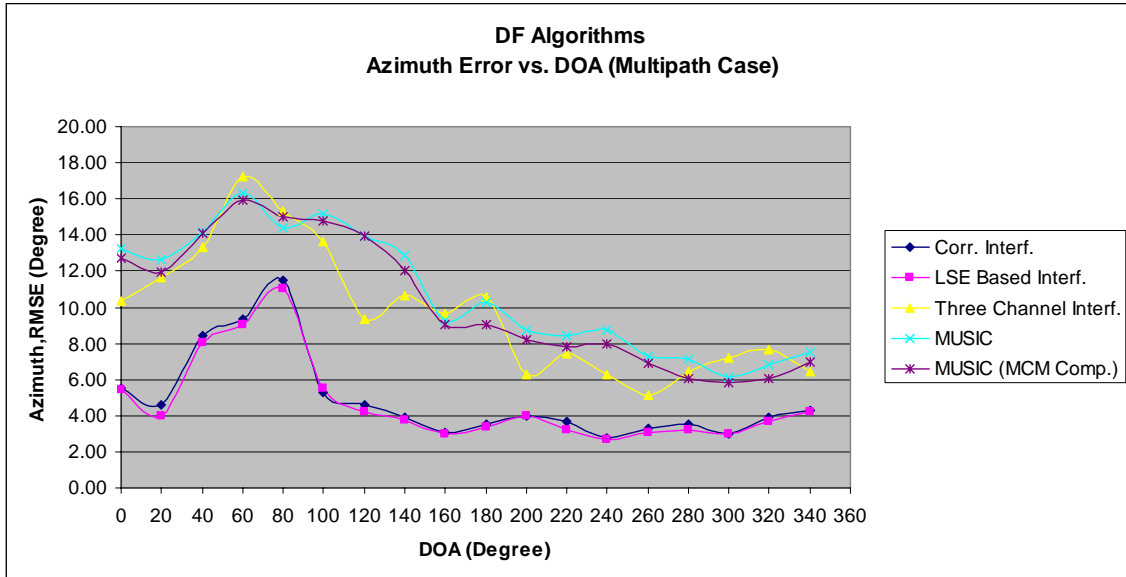


Figure 5.19 – RMSE of Azimuth Angle versus DOA Step-3 Graph

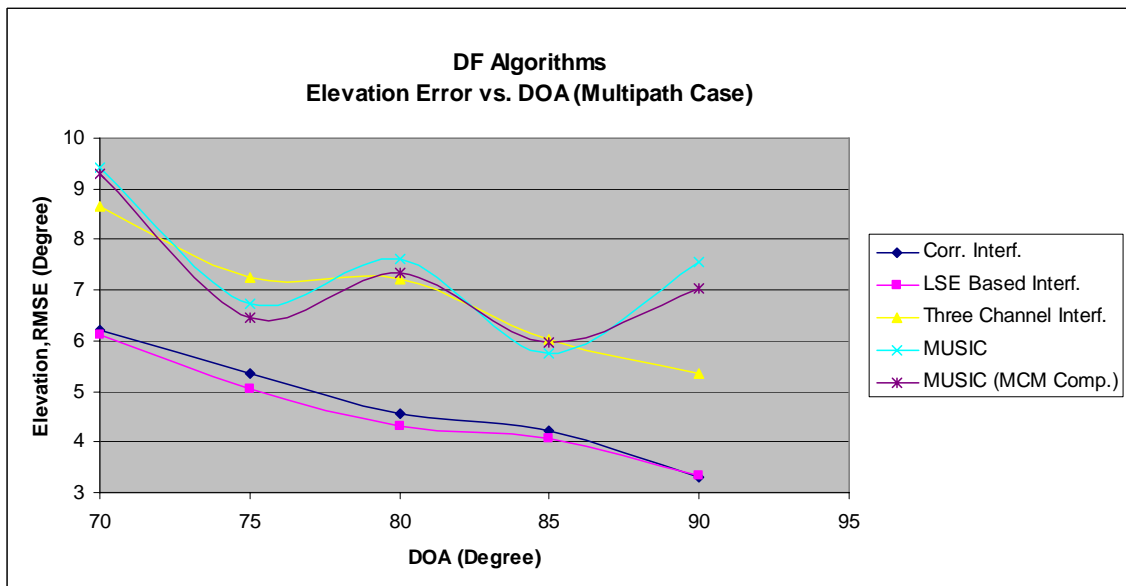


Figure 5.20 – RMSE of Elevation Angle versus DOA Step-3 Graph

When the plate is located at 200cm far away from the origin ($m=200\text{cm}$), the RMSE of the azimuth angle for the correlative interferometer and LSE based correlative

interferometer algorithms considerably drops except for the point where the azimuth angle of the transmitter is 60° . Similarly, the accuracy of the MUSIC and the three channel interferometer algorithms is increased remarkably. The RMSE of the azimuth angle versus DOA graph is shown in Figure 5.21.

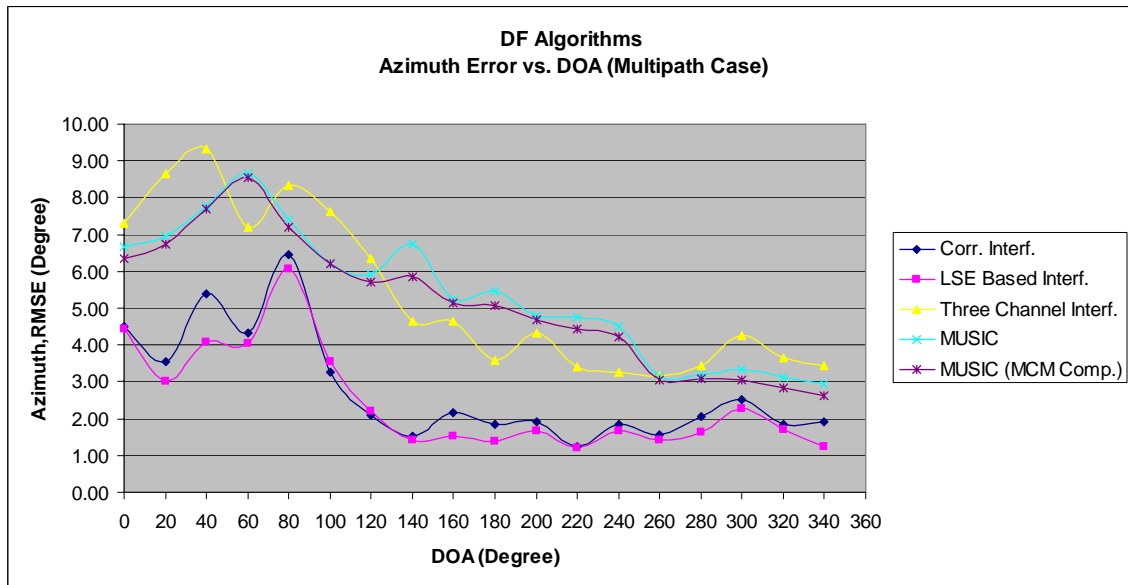


Figure 5.21 – RMSE of Azimuth Angle versus DOA Step-4 Graph

The RMSE of the elevation angle versus DOA graph is shown in Figure 5.22. The plate is located at 200cm far away from the origin ($m=200\text{cm}$). At this step, it is seen that the RMSE of the elevation angle drops for all the algorithms and RMSE values approach to the no reflection case.

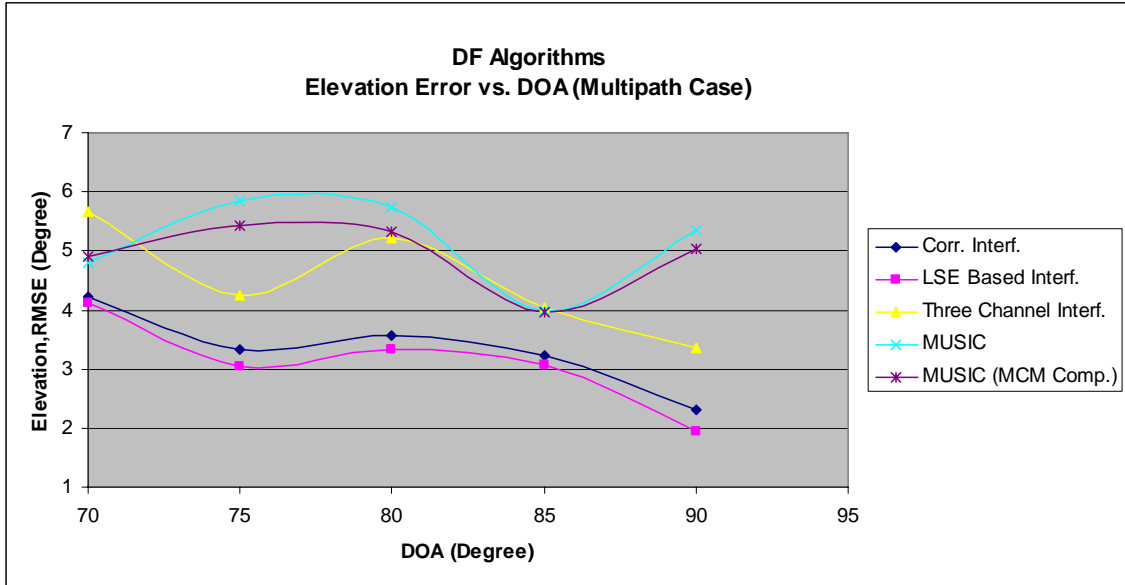


Figure 5.22 – RMSE of Elevation Angle versus DOA Step-4 Graph

From the multi signal path tests, it is determined that the accuracy of the DF system is affected from a metal plate signal reflector. When the metal plate approaches to the system, the RMSE of the calculated DOA angle gradually increases for the DF algorithms. The effect of the metal plate is considerably weakened when the plate is located at 200cm far away from the system origin.

Local reflections at the receiving site can produce a condition of coherence [37]. In this part, the simulation of the coherence condition is realized. It is observed that the MUSIC algorithm seriously affected from the coherency condition. The MUSIC algorithm does not work in the case of coherency. This is an expected result since the rank condition for the MUSIC algorithm no longer holds when coherent signals are received by the system [8]. Coherent signals are perfectly correlated in terms of amplitude and phase fluctuations [37]. Consequently, the full rank condition of the signal covariance matrix can not be satisfied and the MUSIC algorithm breaks down in the case of multi signal path [37].

CHAPTER 6

CONCLUSION

In this thesis, the implementation and performance evaluation of a three antenna direction finding system is considered. The system is tested by using different DF algorithms under the various environmental conditions.

Three channel interferometer, correlative interferometer, LSE based correlative interferometer and MUSIC algorithms are implemented in the DF system. The performance of the algorithms are determined and compared with each other. Performance tests are conducted when there are multiple sources and multipath signals.

The performance of the DF system is determined by obtaining RMSE in the azimuth and elevation angle of the DOA. The results are shown by investigating RMSE of the azimuth and elevation angle versus DOA angle graphs. RMSE of the azimuth and elevation angle versus number of sample graphs are also determined.

It is seen that the results of the correlative interferometer and the LSE based correlative interferometer algorithms are more accurate than the other algorithms in single transmitter and single signal path case. It is observed that the correlative interferometer and LSE based correlative interferometer algorithms have very similar DF results, although LSE based correlative interferometer algorithm gives better result. It is also seen that the results of the correlative interferometer and LSE based correlative interferometer algorithms are improved by applying interpolation technique to the sample space. The elements of the sample space is gradually increased and the effect of the interpolation on the DF system is observed by obtaining azimuth and elevation angle versus sample space angle resolution graphs.

In the multi transmitter case, it is determined that the results of the MUSIC algorithm are less affected than the other algorithm results which is expected. Since the DF system has three antennas, the MUSIC algorithm can work properly under the case of two transmitters. However the error in results of the other algorithms increases dramatically in multi transmitter case.

It is seen that the three antenna DF system can not work properly when there is a signal reflector near the antennas. To observe the effect of the reflector distance on the DF system, a metal plate is located at various points near the antennas. When the distance between the reflector and the antennas is less than 160cm, for the system parameters described in section 5.3 it is observed that the DF results of the algorithms are considerably affected. It is also determined that the MUSIC algorithm does not work in the case of coherent signals.

Mutual coupling effect on the three antenna DF system is investigated. Mutual coupling affects the system performance and causes error in DF results. To determine the mutual coupling, S-parameters of the antennas are obtained. The mutual coupling matrix is derived from the S-parameter matrix. The error in the MUSIC algorithm due to mutual coupling is compensated by using mutual coupling matrix. It is seen that the DF performance of the MUSIC algorithm is slightly improved when the mutual coupling is taken into account in the calculations. It is observed that the mutual coupling compensation of the MUSIC algorithm can not be realized efficiently because the method of S-parameters has deficiencies for modeling the mutual coupling.

The gain-phase mismatch of the receive channels in the DF system is determined. It is shown that the channels are not exactly matched in terms of gain and the phase. The DF system is calibrated according to gain-phase mismatch results and the matching is achieved in the receivers.

In conclusion, it is shown that three antenna direction finding system is affected by multi signal transmitter and multipath. The direction finding accuracy of the system

is seriously dropped in the cases of two signal transmitters and a signal reflector near the antennas. Moreover, mutual coupling causes errors in the DOA calculations. Although the mutual coupling effect can be decreased by using mutual coupling matrix in the MUSIC algorithm, it has still considerable effect on the performance of the system.

6.1 Future Work

The number of the antennas in the system can be increased to observe the performance of the DF system under the condition of multi signal transmitter. It is expected that the accuracy of the DF results are increased and direction of more than two different signals can be determined.

The direction finding tests can be conducted by using signal source with variable frequency to determine the ambiguities in the direction of the signal calculations related to antenna location and transmitter frequency.

The mutual coupling can be calculated precisely enough and it can be used efficiently to improve the accuracy of the DF system.

REFERENCES

- [1] John L. Volakis, "Antenna Engineering Handbook", Fourth Edition, McGraw Hill.
- [2] Y. T. Lo, S. W. Lee, "Antenna Handbook: Theory, Applications, and Design", Van Nostrand Reinhold Company, 1988.
- [3] Friedlander, B.; Weiss, A.J. "Direction finding in the presence of mutual coupling" *Antennas and Propagation, IEEE Transactions on* Volume 39, Issue 3, Mar 1991 Page(s):273 - 284.
- [4] I. J. Gupta and A.A.Ksienski, "Dependence of adaptive array performance on conventional array design," *IEEE Trans. Antenna. Propagation*, Vol. 30, July 1982, pp.549-553.
- [5] I. J. Gupta and A. A. Ksienski, "Effect of mutual coupling on the performance of adaptive arrays," *IEEE Transactions on Antenna. Propagation*, Vol. 31 September 1983, pp.785-791.
- [6] Tongtong Zhang, Hon Tat Hui "Simultaneous estimation of mutual coupling matrix and DOA's using structured least square method", *Proceedings of the Second IASTED International Conference, Antennas, Radar, and Wave Propagation*, July, 2005, pp.277-280.
- [7] An Xiabo, Feng Zhenghe, "A single Channel Correlative Interferometer Direction Finder Using VXI Receiver", 2002 3rd International Conference on Microwave and Millimeter Wave Technology Proceedings.
- [8] Petre Stoica, Randolph L. Moses, "Introduction to Spectral Analysis", Prentice Hall, 1997.
- [9] Herndon H. Jenkins, "Small Aperture Radio Direction Finding", Artech House, 1991.
- [10] Cheol-Sun Park, Dae-Young Kim, "The Fast Correlative Interferometer Direction Finder Using I/Q Demodulator".
- [11] S.Drabowitch, A.Papiernik, H.D. Griffiths, J.Encinas, B.L.Smith "Modern Antennas", Second Edition, Springer.

- [12] Francis Castanie, "Spectral Analysis Parametric and Non-Parametric Digital Methods", ISTE 2006.
- [13] Simon R. Saunders, "Antennas and Propagation for Wireless Communication Systems", Second Edition, John Wiley & Sons.
- [14] Lal Chand Godara, "Handbook of Antennas in Wireless Communicaitons", CRC Press, 2002.
- [15] Rodney Vaughan, Jorgen Bach Andersen, "Channels Propagation and Antennas for Mobile Communications", The Institution of Electrical Engineers, 2003.
- [16] Yi Huang, Kevin Boyle, "Antennas: From Theory to Practice" John Wiley & Sons, Inc, 2008.
- [17] Rodney Vaughan, Jorgen Bach Andersen, "Channels Propagation and Antennas for Mobile Communications", The Institution of Electrical Engineers, 2003.
- [18] MAXIM, "MAX1449EHJ Analog to Digital Converter Datasheet", Literature Number: 19-4802, October 2000.
- [19] Proakis, "Digital Communications", Third Edition McGraw Hill.
- [20] Alan V. Oppenheim, Alan S. Willsky, "Signal and Systems", Second Edition, Prentice Hall.
- [21] XILINX, "Using Block RAM in Spartan-3 Generation FPGAs", Literature Number: XAPP463 (v2.0), March 2005.
- [22] D. Sclitharle, "Digital Filters Basics and Design", Springer, 2000.
- [23] Sen M. Kuo, Woon-Seng Gan, "Digital Signal Processors Architectures, Implementaions, and Applications", Pearson Prentice Hall, 2004.
- [24] B.A. Sheno, "Introduction to Digital Signal Processing and Filter Design", Wiley-Interscience, 2005.
- [25] Monson H. Hayes, "Digital Signal Processing", Second Edition, Mc Graw-Hill.
- [26] Mark Balch, "Complete Digital Design", McGraw Hill, 2003.
- [27] Paul A. Lynn, Wolfgang Fuerst, "Introductory Digital Signal Processing with Computer Applications", Second Edition, John and Wiley Sons.
- [28] Warren L. Stutzman, Gary A. Thiele, "Antenna Theory and Design", John Wiley & Sons, Inc Second Edition.

- [29] B.Allen, M.Dohler,E.E.Okon, “Ultra-wideband Antennas and Propagation”, John Wiley & Sons,Inc, 2007.
- [30] Constantine A. Balanis, “Antenna Theory Analysis and Design”, John Wiley & Sons,Inc Second Edition.
- [31] Thomas A. Milligan, “Modern Antenna Design”, John Wiley & Sons,Inc Second Edition.
- [32] David M. Pozar, “Microwave Engineering”, Addison-Wesley Publishing Company, September, 1993.
- [33] Joseph J. Carr, “Practical Antenna Handbook”, Mc Graw-Hill, Fourth Edition.
- [34] Engin Tuncer, Benjamin Friedlander, “Classical and Modern Direction-of-Arrival Estimation”, Academic Press, 2009.
- [35] Non Tat Hui, “Decoupling Methods for the Mutual Coupling Effect in antenna Arrays: A Review ”, Recent Patents on Engineering 2007, 1, pp. 187-193.
- [36] Non Tat Hui, “A New Definition of Mutual Impedance for Application in Dipole Receiving Antenna Arrays”, IEEE Antennas and Wireless Propagation Letters, Vol. 3, pp. 364-367.
- [37] P.J.D. Gething, “Radio Direction Finding and Superresolution”, Peter Peregrinus Ltd., 1991.

APPENDIX A

CIRCUIT DIAGRAMS OF THE PROCESSING BOARD

The regulators which are used for voltage production in the processing board can be seen in Figure A.1 and in Figure A.2.

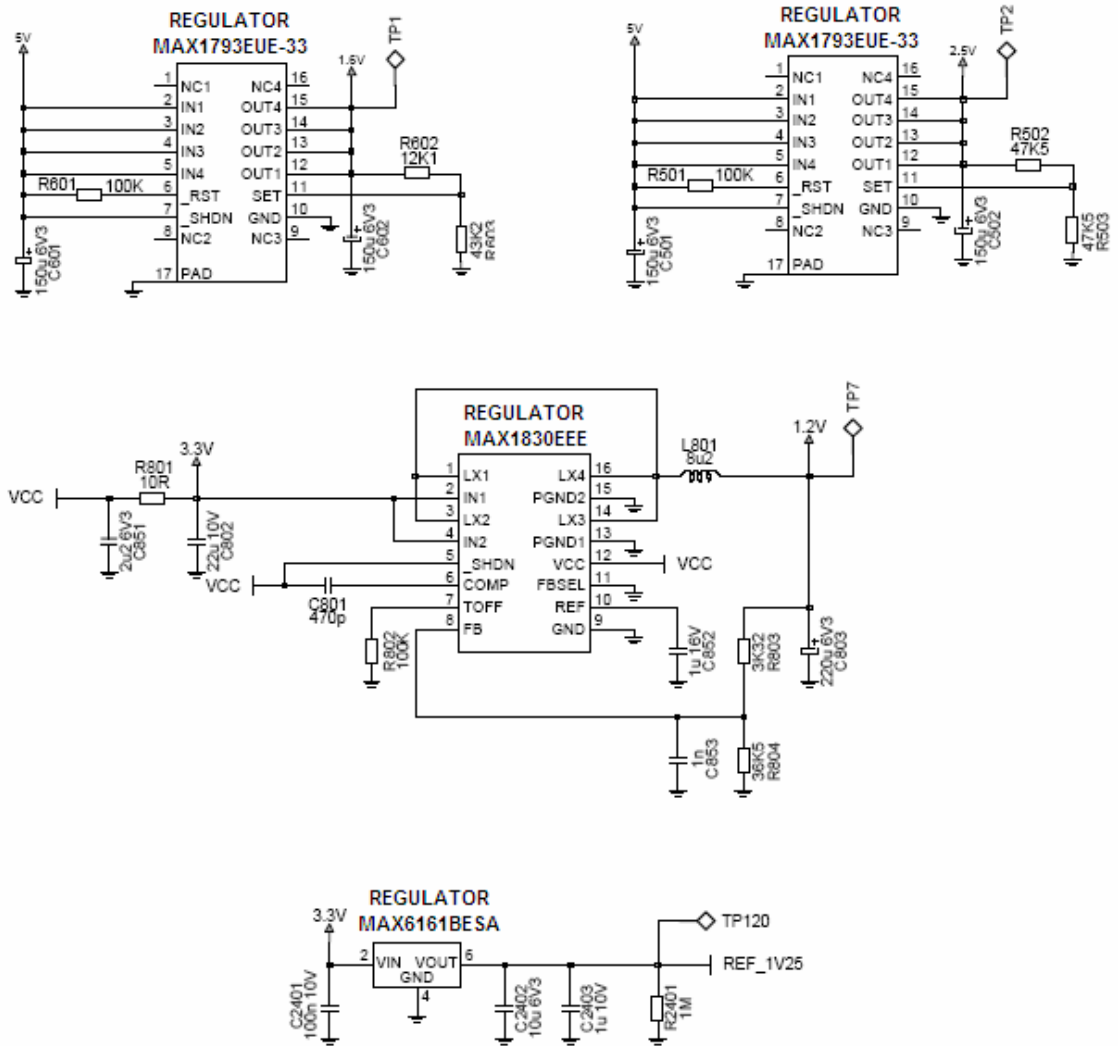


Figure A.1 – First Voltage Production Circuit

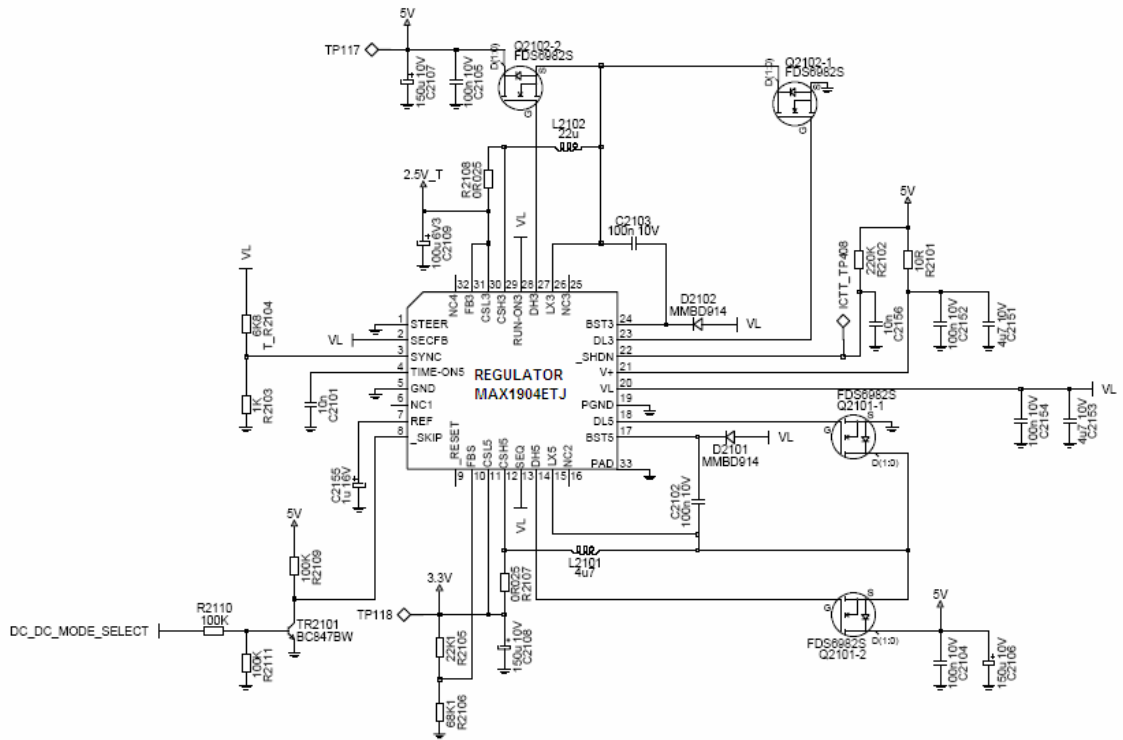


Figure A.2 – Second Voltage Production Circuit

The reset circuit of the board is shown in Figure A.3.

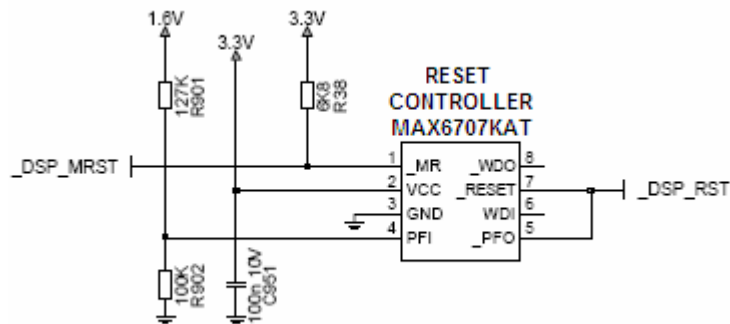


Figure A.3 – Reset Circuit

The interface of one ADC and the FPGA is shown in Figure A.5. In the processing board there are totally three ADC and FPGA interfaces as shown in Figure A.5 for each receive channels.

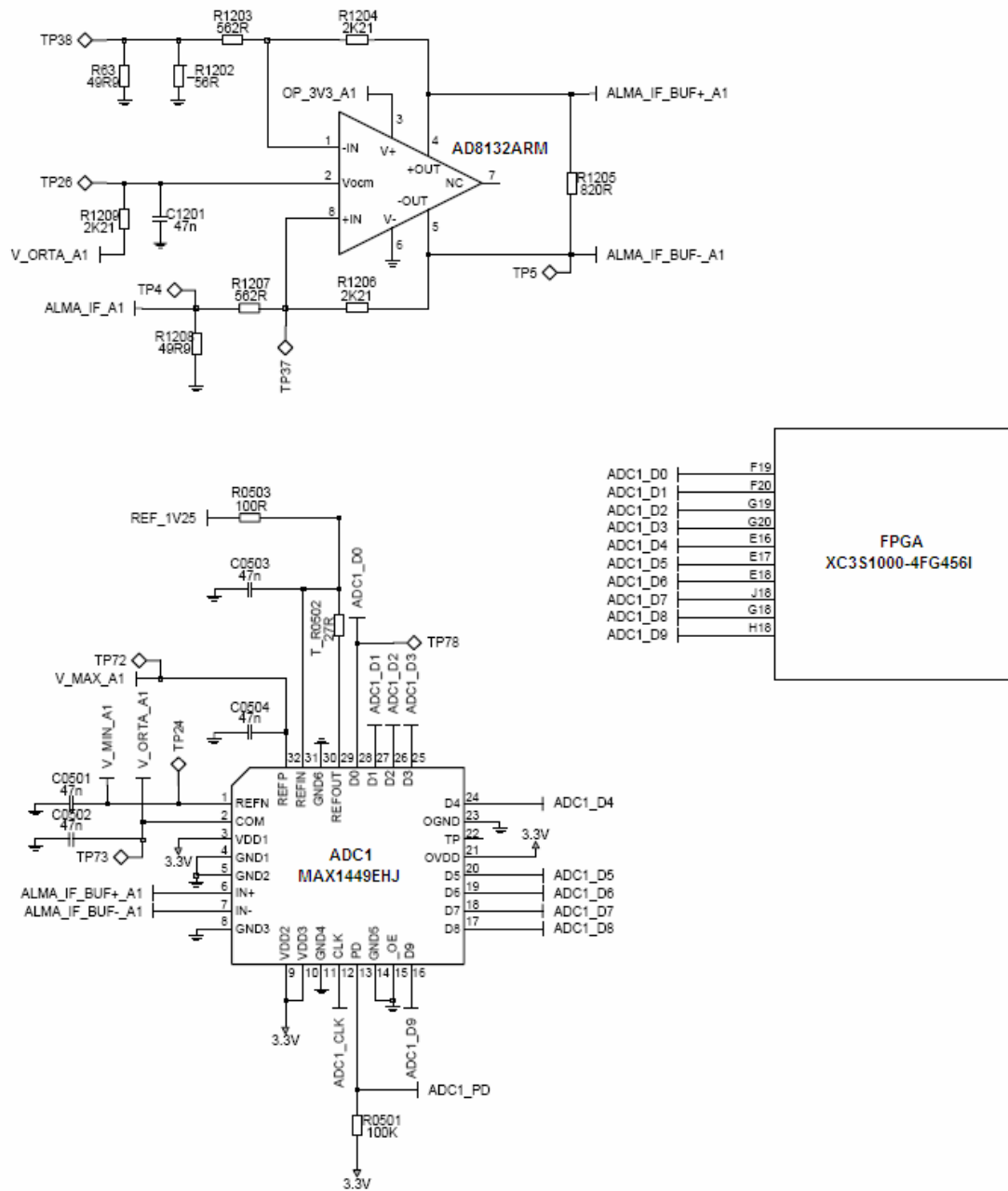


Figure A.5 – ADC and FPGA Data Interface Circuit

The circuit of the FPGA and the PROM interface is shown in Figure A.8.

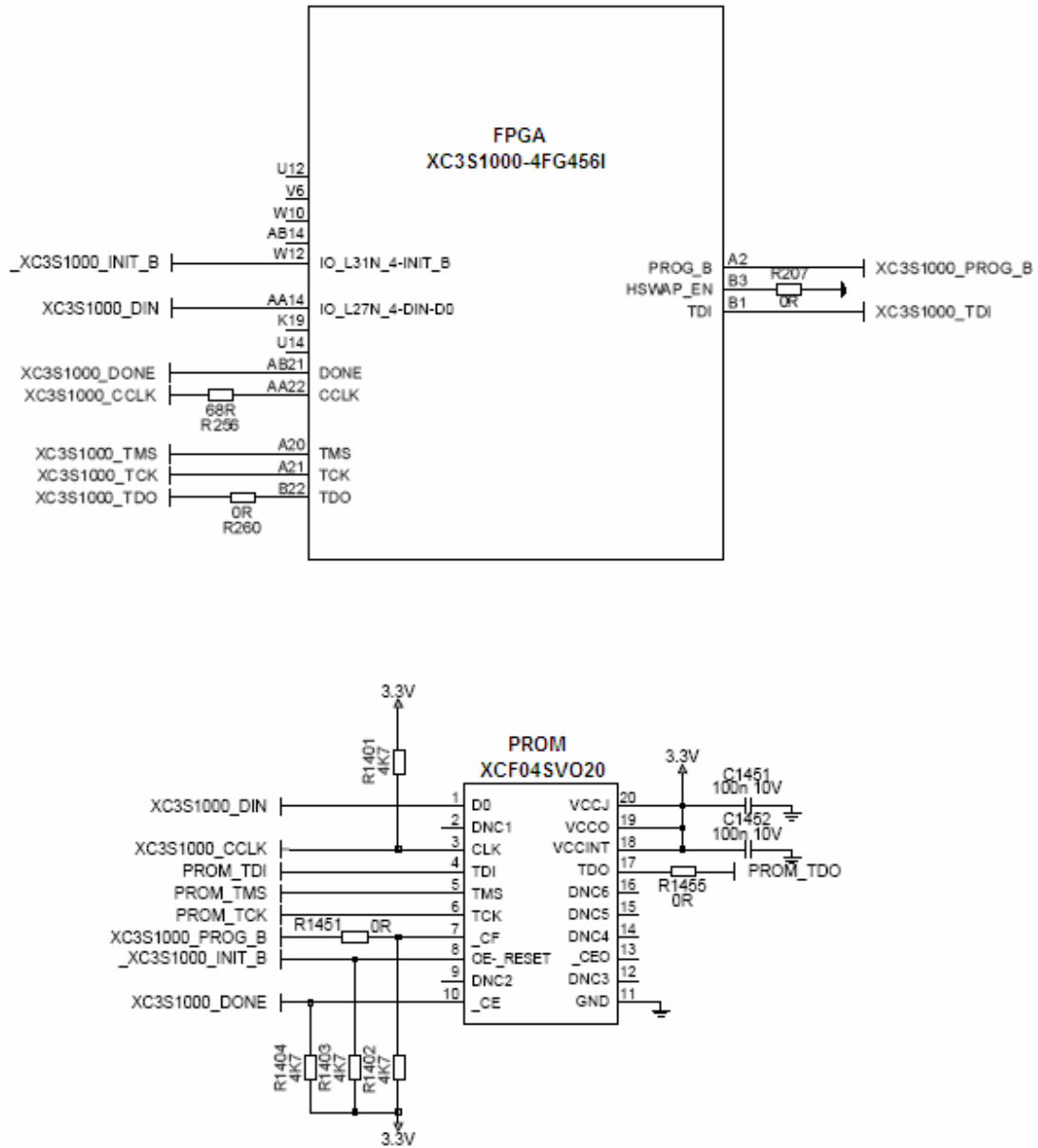


Figure A.8 – FPGA and the PROM Interface Circuit

The circuit of the DSP and the UART transceiver interface is shown in Figure

A.9.

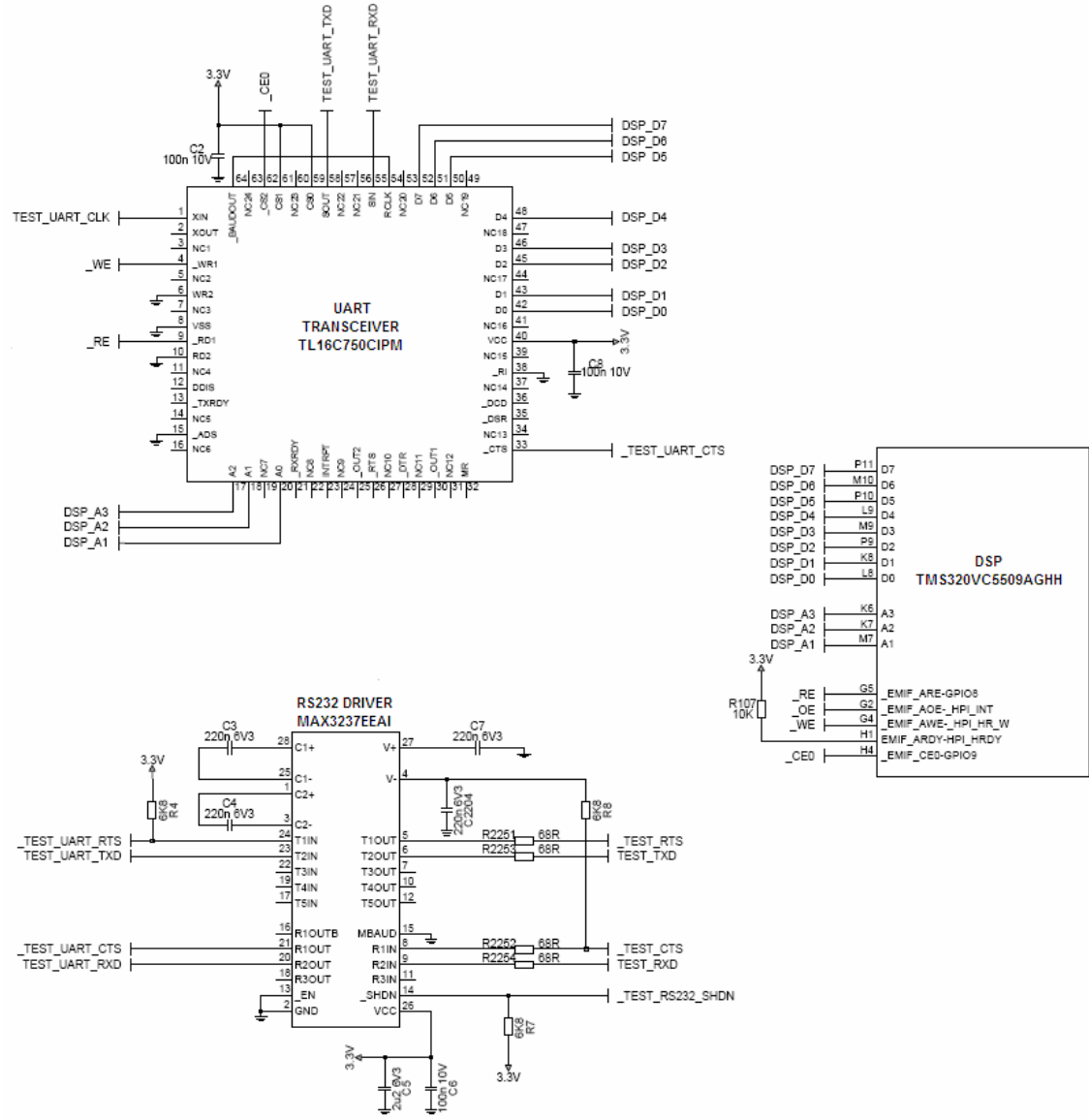


Figure A.9 – DSP and UART Transceiver Interface Circuit

APPENDIX B

LAYOUT AND ROUTING OF THE PROCESSING BOARD

Three RF front-end connectors, FPGA, DSP and clock oscillator are placed at the front side of the processing board. ADC's, clock buffer and the UART transceiver are located at the backside of the processing board.

The layout and routing of front and backside of the processing board can be seen in Figure B.1 and in Figure B.2, respectively.

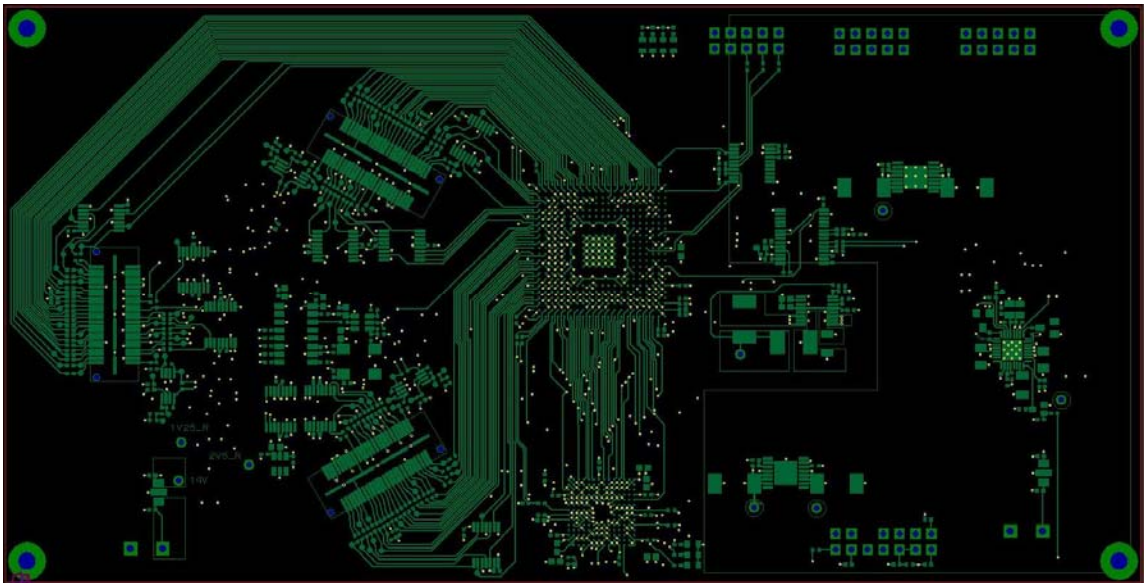


Figure B.1 – Front Side of the Processing Board

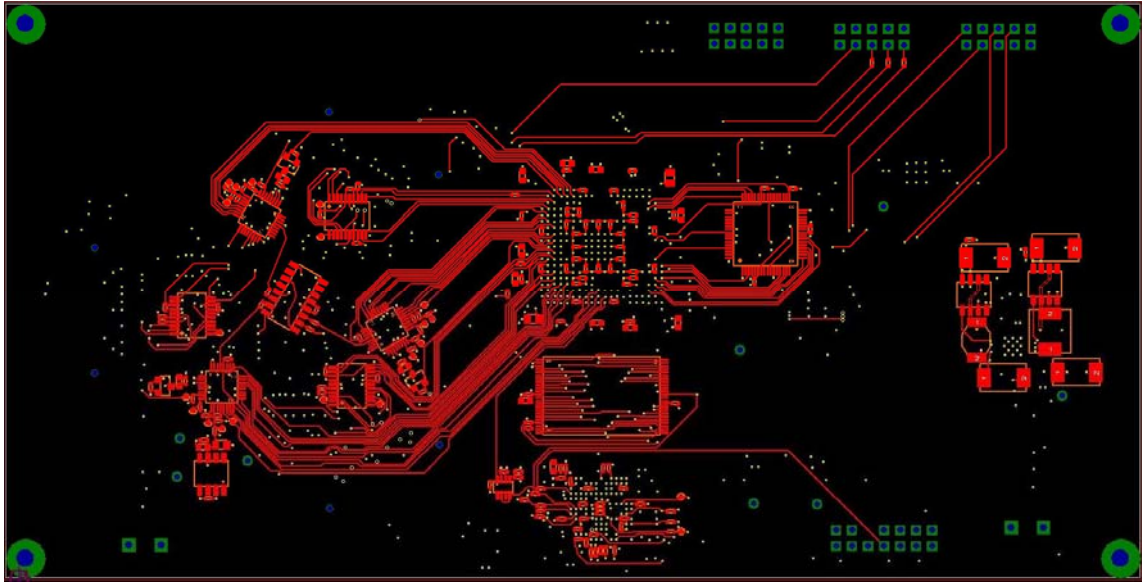


Figure B.2 – Back Side of the Processing Board

Clock buffer, ADC's and clock signal routing of the ADC's are shown in Figure B.3. Clock routes of the ADC's are placed identically for all the ADC's as it can be seen in Figure B.3.

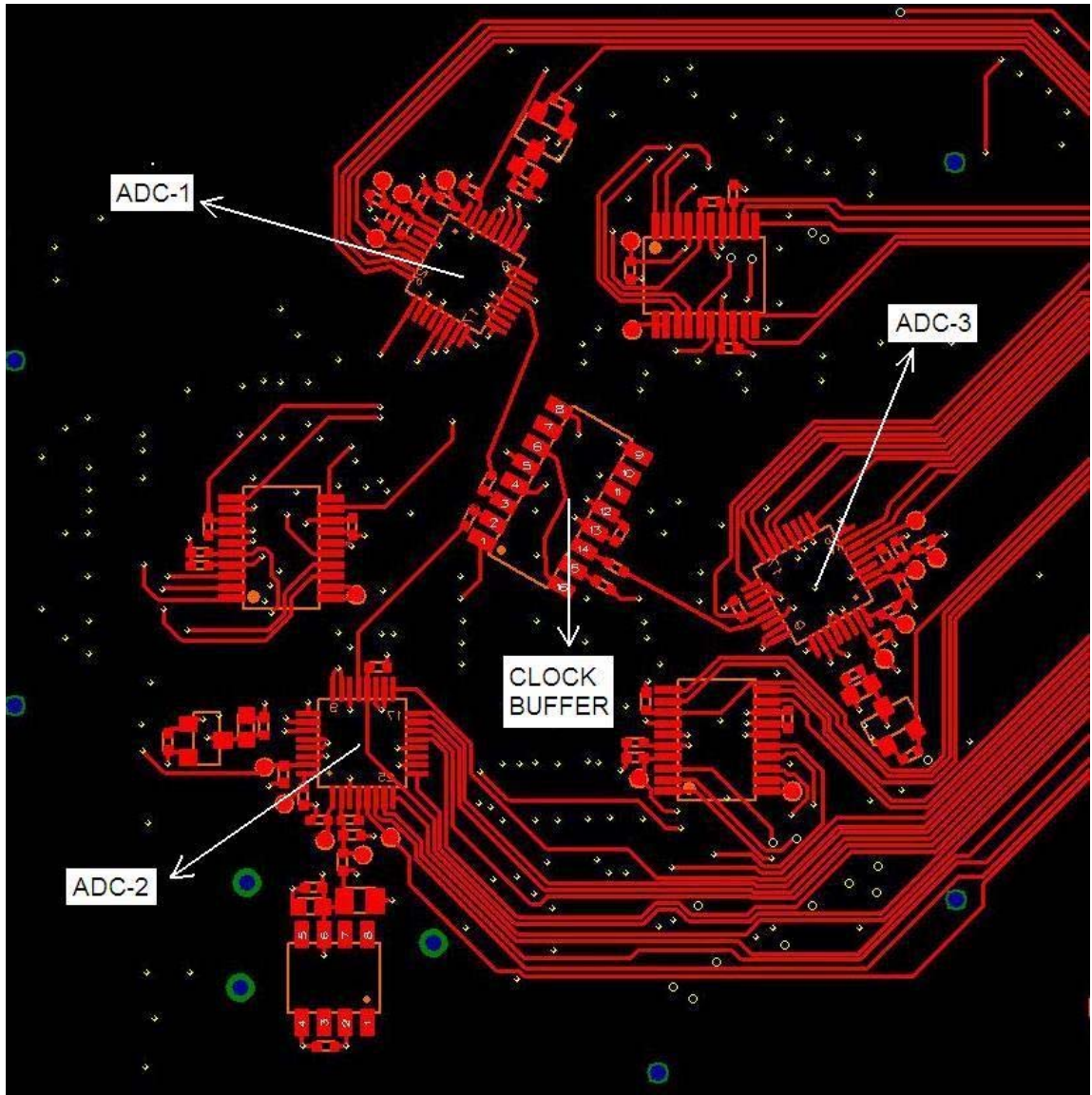


Figure B.3 – Clock Buffer and ADC's

APPENDIX C

GRAPHICAL USER INTERFACE

The three antenna DF system is connected to a computer via RS232 communication standard with a cable. Monitoring and algorithm selection of the DF system is controlled by a graphical user interface (GUI) which is installed in a computer. The GUI includes a screen part which shows the azimuth DOA of the signal with an arrow and a result part which shows the azimuth and elevation angle values of the DOA. The DF algorithms selection buttons are located at the left side of the GUI screen. The GUI of the DF system can be seen in Figure C.1.

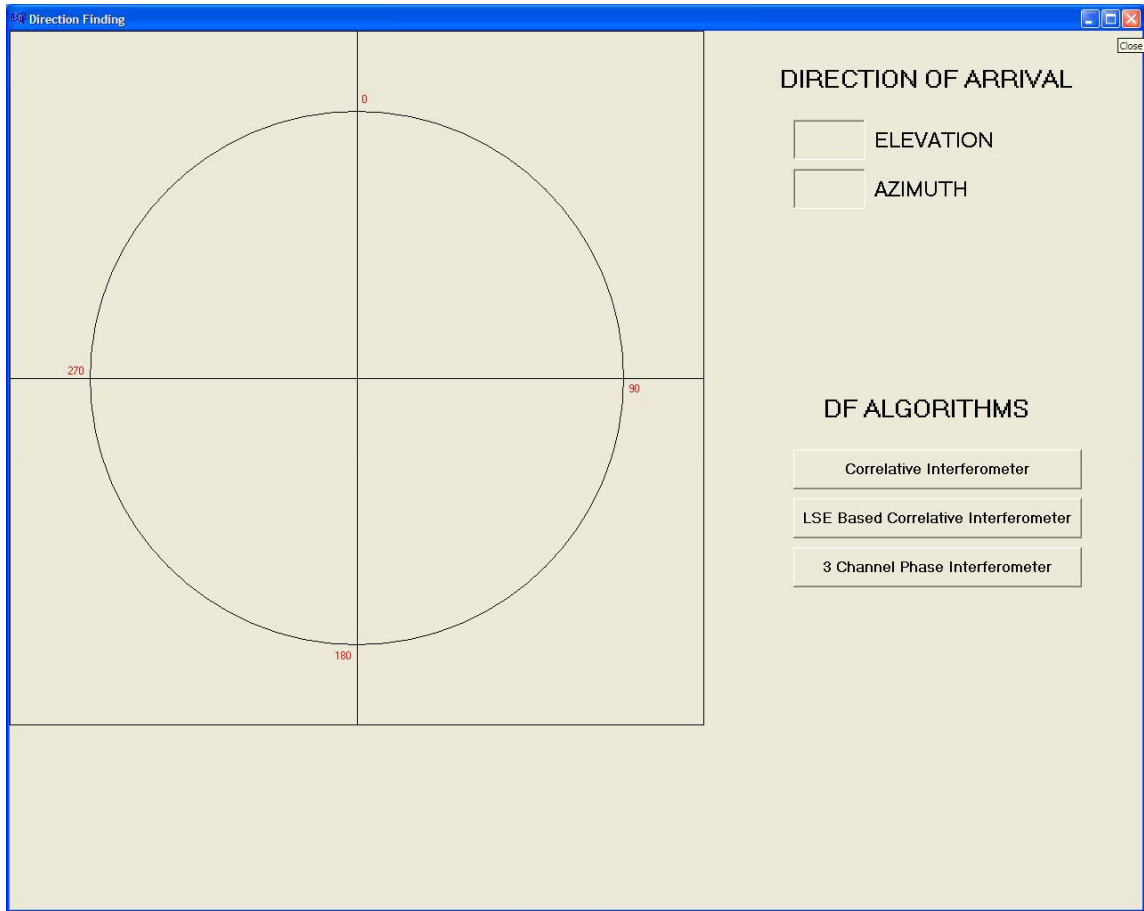


Figure C.1 – GUI of the DF System

When the algorithm selection buttons are clicked, the GUI program starts to send related algorithm type command to the processing board and the selected algorithm starts to run in the system. When the user selects the type of the DF algorithm, the system implements the selected algorithm in the DSP to find the DOA and the red arrow shows the result in the screen part of the GUI. The GUI of the system during the run-time of the DF processing is shown in Figure C.2.

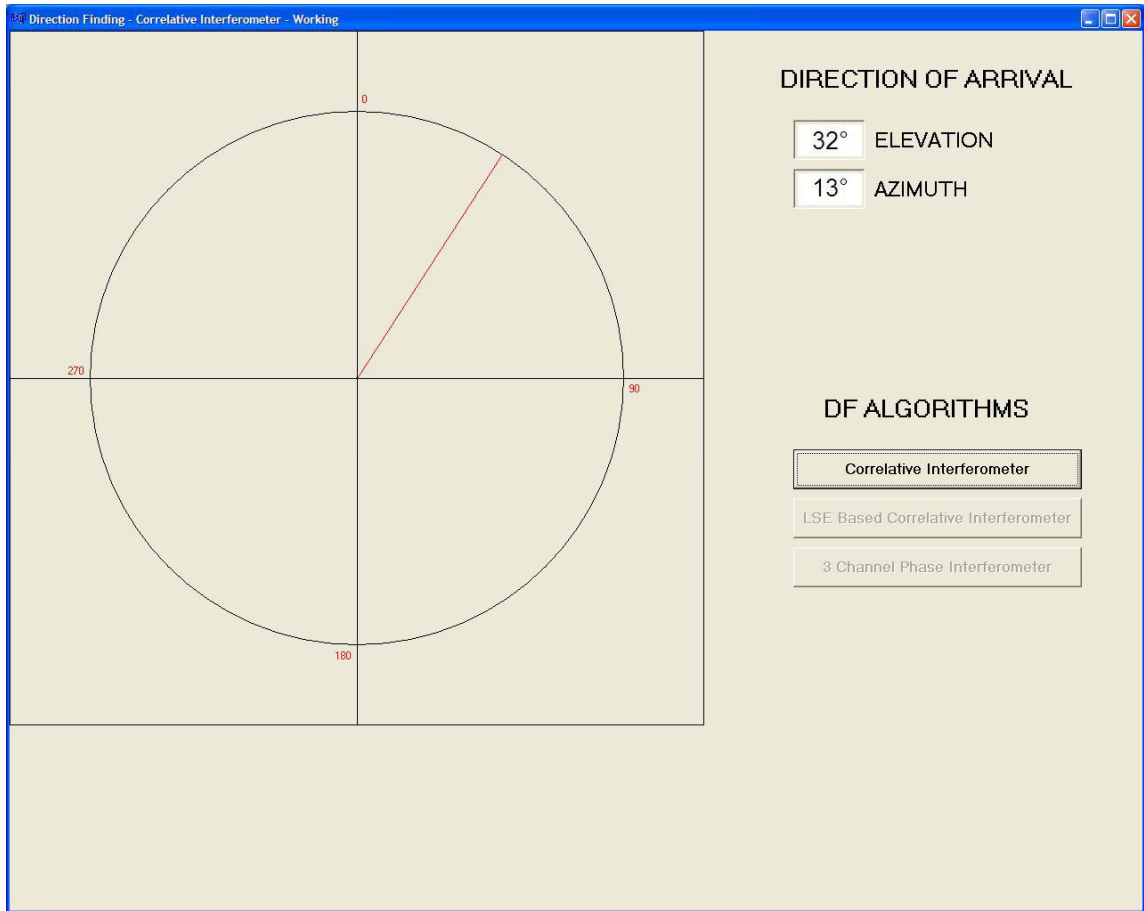


Figure C.2 – View of the GUI During the Program Run-Time